Distribution Agreement

In presenting this thesis or dissertation as a partial fulfillment of the requirements for an advanced degree from Emory University, I hereby grant to Emory University and its agents the non-exclusive license to archive, make accessible, and display my thesis or dissertation in whole or in part in all forms of media, now or hereafter known, including display on the world wide web. I understand that I may select some access restrictions as part of the online submission of this thesis or dissertation. I retain all ownership rights to the copyright of the thesis or dissertation. I also retain the right to use in future works (such as articles or books) all or part of this thesis or dissertation.

Signature:

_____ _____

Juan D. Rodriguez Date

ECTOPIC TRANSCRIPTION DUE TO INAPPROPRIATELY INHERITED HISTONE METHYLATION MAY INTERFERE WITH THE ONGOING FUNCTION OF TERMINALLY DIFFERENTIATED CELLS.

By

Juan D. Rodriguez
Doctor of Philosophy

Graduate Division of Biological and Biomedical Science
Genetics and Molecular Biology

_____
David J. Katz, PhD
Advisor

_____
Guy Benian, PhD
Committee Member

_____
Dorothy Lerit, PhD
Committee Member

_____
William Kelly, PhD
Committee Member

_____
Victor Corces, PhD
Committee Member

Accepted:

_____
Kimberly Jacob Arriola, Ph.D.
Dean of the James T. Laney School of Graduate Studies

_____
Date

Ectopic transcription due to inappropriately inherited histone methylation may interfere with the ongoing function of terminally differentiated cells

By Juan D. Rodriguez, MS

Advisor: David J. Katz

An abstract of A dissertation submitted to the Faculty of the James T. Laney School of Graduate Studies of Emory University in partial fulfillment of the requirements for the degree of Doctor of Philosophy in Genetics and Molecular Biology, 2023

Ectopic transcription due to inappropriately inherited histone methylation may interfere with the ongoing function of terminally differentiated cells

By Juan D. Rodriguez, MS

Many human neurodevelopmental disorders are caused by *de novo* mutations in histone modifying enzymes. These patients have craniofacial defects, developmental delay, intellectual disability and behavioral abnormalities, but it remains unclear how the mutations lead to such developmental defects. Here we take advantage of the invariant *C. elegans* lineage, along with a unique double mutant in the H3K4me1/2 demethylase SPR-5/LSD1/KDM1A, and the H3K9 methyltransferase MET-2/SETDB1 to address this question. We demonstrate that *spr-5; met-2* double mutant worms have a severe chemotaxis defect that is dependent upon the ectopic expression of germline genes in somatic tissues. In addition, by performing single-cell RNAseq, we find that germline genes begin to be ectopically expression widely in *spr-5; met-2* embryos. However, surprisingly we found that *spr-5; met-2* mutants have no somatic lineage defects p to the 200-cell stage of embryogenesis. This suggests that the altered chemotaxis behavior may be due to ongoing defects in terminally differentiated cells rather than a defect in development. To test this directly, we used RNAi to shut off the ectopic expression of germline genes in L2 *spr-5; met-2* larvae, which have a fully formed nervous system. Remarkably, we find that shutting off the ectopic germline expression rescues normal chemotaxis behavior in the same adult worms that previously had a chemotaxis defect at the L2 stage. This suggests that ongoing ectopic transcription can block normal behavior in a fully intact nervous system. These data raise the possibility that intellectual disability and altered behavior in neurodevelopmental syndromes, caused by mutations in histone modifying enzymes, could be due to ongoing ectopic transcription and may be reversible.

Ectopic transcription due to inappropriately inherited histone methylation may interfere with the ongoing function of terminally differentiated cells

By Juan D. Rodriguez, MS

Advisor: David J. Katz

A dissertation submitted to the Faculty of the James T. Laney School of Graduate Studies of Emory University in partial fulfillment of the requirements for the degree of Doctor of Philosophy in Genetics and Molecular Biology, 2023

Acknowledgments

I want to thank many people that helped me and supported me during this journey. My family, friends, and professors from Inter-American University, Kennesaw State and Emory University. I am so grateful for their wonderful support. However, I want to focus and dedicated this dissertation to the woman that raised me and the person that I loved with all my heart, my grandma, Tina Figueroa. She passed away in my fourth year as a graduate student. Her death showed that life is so short and most of the time we are so busy with stuff that steal our time from the peoples that we love more. I would love to see her on my defense. My grandma only have a third grade of school, but she was the smarter person that I ever met. Abuelita, te dedico todo este esfuerzo y gracias por formar la persona que soy hoy en día. Todo lo que aprendí de ti, de no rendirme, ser dedicado, agradecido y ayudar a los demás, fueron las herramientas que necesité para lograr mi doctorado. Love you y sigue cuidándonos desde el cielo, gracias Abuelita!

Table of Contents

CHAPTER 1 Introduction:

Histone Modifications and Chromatin Remodeling Proteins

1. Histone modifications

The nucleosome is composed of four histones, H3, H4, H2A, H2B and is assembled in an octamer manner, with two copies of each core histone (*Marino-Ramirez et al., 2005*). The nucleosome is a structure where 147 base pairs of DNA is wrapped around a core of histone proteins. This structure is referred to as chromatin. Chromatin is thought to enable DNA to be packaged into the nucleus. This structural arrangement also provides a dynamic environment for diverse remodeling factors that need to interact with the chromatin. In addition to the core histones, there are variants of these histones, such H2A.Z, H2A.X, and H3.3. All these histones are highly conserved in all eukaryotic organisms, including the linker histone H1, which binds to the nucleosomal core to protect the free linker DNA (*Hergeth et al., 2015*)

Histone phosphorylation

Histone modifications can regulate gene expression post-translationally (PTMs). Like all the modifications, histone phosphorylation is highly dynamic. The amino acids on the histone that can be phosphorylated are Serine (S), Threonine (Thr) and Tyrosine (Y). Phosphorylation takes place on the N-terminal of the histone tail. The addition of a phosphoryl group (PO3) adds a negative charge, resulting in more open chromatin. Phosphorylation of H2A.X plays an important role during DNA Damage repair (*Firsanov et al., 2011*). For this and other reasons, it is very important that histone modifications can be dynamically regulated, particularly during development.

Histone methylation

Histone methylation can alter the chromatin structure, changing the chromatin to open or more compact. The addition of methyl group occurs on the Lysine(K) or Arginine

(R) of the histone N-terminal tail. Methylation alters chromatin through the binding of readers (see below). The methylation could be mono-, di-, or trimethylation. H3K4 methylation is associated with active chromatin. Monomethylation of H3K4 is often associated with enhancers, promoters and at the transcription start site (TSS), where it is thought to help with transcription initiation (*Pekowska et al., 2011*). H3K4 methylation is facilitated by the COMPASS complex which is recruited to genes by RNA polymerase II. As a result, H3K4 methylation is thought to be transcription-coupled. This makes it a good candidate to be functioning as an epigenetic memory of transcription (see below). Consistent with H3K4 methylation being transcriptionally coupled, the pattern of H3K4 methylation matches RNA polymerase II occupancy. Trimethylation on H3K4 is primarily enriched at transcriptional start sites (TSSs), while di-methylation extends into the gene body (*Pekowska et al., 2011*). In addition, a small peak of monomethylation is also found at the end of genes, presumably due to polymerase stalling prior to falling off DNA. On the other hand, a methyl group on H3K9 tends to be associated with repressed chromatin, which is referred to as heterochromatin (*Padeken et al., 2022*). H3K9 methylation is found primarily at transposable elements, satellite repeats and telomeres, where transcription silencing is necessary. In addition, H3K9 methylation is also found at some genes that are transcriptionally repressed. Another repressive histone modification is H3K27 methylation. For example, in *C. elegans* MES-2 is an H3K27 methyltransferase. The MES proteins are part of a protein family, with MES 2,3 and 6 forming the highly conserved Polycomb repressive protein complex. H3K27 methylation is required for normal germline development in *C. elegans* (*Holdeman et al 1998*).

Histone acetylation

Histones can also be acetylated. The amino acid that can be acetylated is Lysine (K). The addition of an acetyl group by histone acetyltransferase (HAT) can partially neutralize the positive charge of histones, resulting in more open chromatin. An acetyl group can also be removed by a histone deactylase (HDAC). For example, in *C.elegans* the NURD complex, composed of MEP-1, LET-418 and HAD-1, regulates the somatic pattern of gene expression by removing an acetyl group (*Unhavaithaya et al., 2002*). The dynamic of addition and removal of the acetyl group is also required for the proper development of the zygote.

Histone ubiquitination

Histones ubiquitination is primarily thought to occur on H2A and H2B. The ubiquitination of H2A and H2B is in transcription regulation, chromatin maintenance, and DNA repair. The H2Aub is normally associated with gene silencing, while H2Bub is associated with transcription activation. Chromatin immunoprecipitation (ChIP) experiments have shown that this histone ubiquitination is primarily found in the satellite regions of the genome, and in the gene body of transcriptionally active genes (*Cao et al., 2012*).

2. Chromatin

Cellular differentiation is controlled by temporal gene expression and epigenetics factors. The epigenetic state will regulate the expression of genes. In eukaryotic chromosomes, genes can be transcriptionally inactive or active. Under a closed or compacted chromatin state, the transcription is mostly silenced or lowered in expression. This state of chromatin is known as heterochromatin. This state also protects the DNA, which can be access by the chromatin remodeling machinery. Heterochromatin has been

categorized into two types, facultative and constitutive heterochromatin. Constitutive heterochromatin is a persistent repressed state of chromatin. Constitutive heterochromatin can be found in the telomeres of the chromosomes where the genes are be expressed (*Saksouk et al., 2015*). Facultative heterochromatin refers to the chromatin state where genes have been silenced but can switch to an active state during development. Euchromatin is transcriptionally active, which results in an open chromatin state making it accessible to transcription initiation factors.

Chromatin remodeling complexes

DNA stores all the genetic information, and epigenetics provides an additional layer of regulation. Chromatin modifying proteins interact with histones to change or maintain the chromatin state. For example, the chromatin remodeling complex SWI/SNF uses ATP to push away and separate the nucleosomes, making the chromatin accessible for the activation or inactivation of genes (*Tang et al., 2010*). The SWI/SNF ATP-dependent complex is highly conserved through all eukaryotes. Once the nucleosomes are pushed apart, one of the complexes that can access the chromatin is the COMPASS complex. The COMPASS complex functions in gene activation by adding an active modification, methylation of lysine 4 on histone H3 (H3K4me). The addition of methyl groups to this histone correlates with the elongation of RNA polymerase. In *C. elegans* the core COMPASS subunit WDR-5 works together with the H3K4 methyltransferase SET-2 to enable RNA polymerase elongation (*Wood et al., 2007*).

On the other hand, some protein complexes can repress and block transcription. For example, the highly conserved protein Heterochromatin protein 1 (HP1), binds to

lysine 9 of histone H3 (H3K9me) to facilitate gene repression (*Eskeland et al., 2007*). Once HP1 binds H3K9 methylation, the methyltransferase adds additional H3K9 methylation to spread gene repression. In humans, one of the H3K9 methyltransferases is SETDB1. In *C. elegans* the ortholog of SETDB1 is MET-2 (*Delaney et al., 2022*). In *C. elegans* there are two additional H3K9 methyltransferases SET-25 and SET-32 (*Woodhouse et al., 2018*).

Chromatin proteins are characterized into three categories: readers, writers and erasers. An example of a reader protein, is the protein HP1 which recognizes a histone that has been methylated at H3K9. A writer protein will add a new modification to the histone. Examples of writer proteins are histone methyltransferases (HMTs) which add a methyl group and histone acetyltransferases (HATs) which add an acetyl group. An eraser protein will remove a modification from a histone. For example, the Jumonji family proteins can remove a methyl group from a histone. Another example of an eraser in *C. elegans* is SPR-5, which is a demethylase protein (HDMs) that can remove mono or di-methylation from H3K4. I will discuss SPR-5 and MET-2 more deeply later in this introduction. What makes the difference in the function of these three groups of chromatin proteins is their protein domains. The readers use a PHD zinc finger motif, Bromodomain, Chromodomain or Tudor domain to recognize a specific histone modifications locus. This helps to recruit other factors, such as chromatin remodeling enzymes. The methyltransferase writer proteins (i.e.MET-2) use a SET domain to add a methyl group. The SPR-5 demethylase (eraser) contains an amine oxidase demethylase domain, as well as TOWER and SWIRM domains that help SPR-5 interact with other proteins and access chromatin respectively (*Eimer et al., 2002*).

2.3 Epigenetic regulation during development

Chromatin remodeling mechanisms are essential for the proper development of the zygote. Modifications like methylation can be added to DNA or histones and can be read, written, and erased by other proteins to control the accessibility of genes to the transcription machinery. This is required throughout the development of multicellular organisms for proper gene expression in different cells. In multicellular eukaryotes, heterochromatin serves two main functions; it silences the transcription of satellite repeats and transposons and it silences tissue-specific genes during development (*Methot et al., 2021*). In contrast, euchromatin allows the transcription machinery to transcribe genes. During development, histone modifications change to create a balance between gene activation and gene repression. In addition, during development, some genes contain both the activating modification H3K4me3 and the repressive modification H3K27me3. Genes containing both modifications are known as bivalent. Bivalent chromatin is crucial during stem cell differentiation, which works as a safeguard for the appropriate differentiation of stem cells (*Bernstein et al., 2006*). Upon differentiation, bivalent chromatin converts to either active or repressed to help drive differentiation.

During *C. elegans* embryogenesis, chromatin helps to specify the germline. For example, H3K36me that is added during the transcription of germline genes in the mother, is maintained in the early embryo by the transcription-independent H3K36 methyltransferase MES-4. H3K36me serves as a “bookmark” for those germline genes which are in a quiescent state in the embryo, but will be expressed at the larvae stage (*Furuhashi et al 2010*). Another method of regulation is the control of germline gene

expression in somatic lineages. In *C. elegans* mutation of *lin-35,* a conserved member of the DREAM complex, results in ectopic expression of germline genes in somatic lineages (*Goetsch et al 2017*). This suggests that LIN-35 normally represses the expression of germline genes in the soma. This is an example of how repressive chromatin helps to specify cell fate.

2.4 Histone methylation as a transcriptional memory

Histone methylation can act as an epigenetic memory, which can be passed to the next generation. For example, the Gurdon laboratory showed during Somatic Cell Nuclear Transfer (SCNT), that genes expression in the donor nucleus can continue to be expressed in the recipient embryos and that this epigenetic memory of transcription is dependent upon Lysine 4 of Histone H3. High levels of H3K4me in the embryo are retained at genes that were transcriptionally active in the donor nucleus. Reducing the levels of H3K4me results in an improvement in obtaining cloned animals from SCNT. A similar scenario has been shown in different organisms. This suggests that H3K4me is a major barrier that limits proper nuclear transfer and transcriptional reprogramming (*Ng and Gurdon et al., 2008*).

In *C. elegans* the P lineage (blastomere) contains high levels of H3K4me2. However, after P4 divides, the primordial germ cells Z2 and Z3 rapidly lose H3K4me2 (*Furuhashi et al 2010*). The lack of H3K4me2 is conserved in the *Drosophila* germline in pole cells (*Schaner et al., 2003*). This conserved mechanism suggests that the absence of H3K4me2 and transcriptional repression is necessary for the proper maintenance of primordial germ cell fate. In *C. elegans,* when there is a failure to erase H3K4me at

fertilization, it can be inherited and accumulate throughout many generations (*Katz et al., 2009*). Eventually after many generations, this results in the inappropriate retention of H3K4me2 in the primordial germ cells and sterility. This is consistent with H3K4me2 erasure being required for fertility.

3. Suppressor of presenilin (SPR) rescue of the egg-laying phenotype

Interactions between genes can be identified through genetic suppressor screens. The suppressor of presenilin (SPR) genes, were identified in a suppressor screen for an egg-laying defect, caused by a mutation of the presenilin gene, *sel-12* (*Jarriault and Greenwald et al., 2002*). Each of the five genes discovered can rescue the egg-laying defect, including *spr-5*, which is expressed in the germ line. SPR-5 has an amine oxidase domain that can regulate transcription by removing mono and dimethylation from the H3K4. SPR-5 is an ortholog of human KDM1A (LSD1). SPR-5 interacts with SPR-1 which is the *C. elegans* ortholog of the human CoREST, which acts as the core component of a corepressor complex with histone deacetylase enzymatic activity (*Eimer et al., 2002*).

spr-5 mutants show a progressive sterility phenotype over generations, referred to as germline mortality. This sterility phenotype correlates with the misregulation of spermatogenesis genes across generations due to the transgenerational accumulation of H3K4me2 (*Katz et al., 2009*). This suggests H3K4me2 can function as an epigenetic memory. SPR-5 suppresses the loss of the presenilin *sel-12* by causing a second presenilin gene *hop-1,* which is functionally redundant to *sel-12,* to be ectopically expressed in the vulva. *Hop-1* is normally only expressed in the germline. But when *spr-*

5 is mutant, transgenerationally inherited H3K4me2 allows *hop-1* to be expressed somatically.

3.1 The methyltransferase MET-2 is a regulator of vulval cell-specification

In *C. elegans,* loss of the H3K9 methyltransferase MET-2, a homolog of the human SETDB1, results in a multivulval phenotype and a germline mortality phenotype that is highly similar to *spr-5* mutants (*Andersen and Horvitz et al., 2007*). This suggested that SPR-5 and MET-2 might synergistically cooperate to reestablish the epigenetic ground state at fertilization (*Kerr et al., 2014*). Our lab showed that *spr-5; met-2* mutants have a synergistic maternal-effect sterility phenotype due to the inheritance of inappropriate H3K4me2 and loss of H3K9me2, which results in the ectopic expression of germline genes. MET-2 can also regulate vulval cell fate specification by repressing the expression of the *lin-3* gene, which induces vulval development (*Andersen and Horvitz et al., 2007*). This function of MET-2 may occur directly in somatic lineages or indirectly through transgenerational inheritance.

Summary

In this dissertation, we investigated how chromatin enzymes could affect cell specification. We know that the chromatin state could influence in transcription. During these chapters, we investigated how histone methyltransferases and histone demethylases interact together. We have shown in *C. elegans* that SPR-5 and MET-2, work synergistically to reset epigenetic ground state, thus the zygote can develop properly. However, how SPR-5 and MET-2 can regulate cell specification is not well known. The main chapter 4, addressed this question, using the unique tool of the invariant

cell lineage of *C.elegans*. In the absence of SPR-5 and MET-2, we have shown that a group of germline genes express ectopically (Carpenter *et al.,* 2021). However, we don't know how the cell responds to this scenario. I have shown that cell lineage is resistant to this ectopic expression but is affecting the function of the fully differentiated cell, such as neurons. My work could provide a hint about some human diseases syndrome. For example, Kabuki syndrome is caused by a mutation in chromatin-modifying enzymes. The development of these children could have no defects but the function of their nervous system could be compromised and affect their function. As I showed with the worms, knocking down the ectopic expression of those upregulated genes in the fully developed worms, results in the rescue of the phenotype. With the Kabuki syndrome patients could be the same mechanism, the ectopic expression of certain genes could be affecting the function of the fully differentiated cells.

Chromatin modifiers proteins, Mammals and *C. elegans* names			
Enzymatic activity	**Mammals name**	***C. elegans* name**	**References**
HMT H3K4m2/3	Setd1b	*set-2*	Brici *et al.* (2017), Caron *et al.* (2022)
HMT H3K4me2/3	Kmt2d, MII2,MII4	*wdr-5*(part of the MLL3/4 complex, COMPASS complex), *set-2*	Andreu-Vieyra *et al.* (2010), Lee *et al.* (2019)
HMT H3K36me3	Setd2	*met-1*	Xu *et al.* (2019), Cockrum *et al.* (2022)
HMT H3K9me1/2	G9a, Ehmt2,Kmt1c	*met-2, set-25*	Zylicz *et al.* (2018), Andersen *et al.* (2004)
HMT H3K9me	Setdb1	*met-2, set-25*	Kim *et al.* (2016), Andersen *et al.* (2004)
HMT H3K27me2/3	Ezh2 (PRC2)	*mes-2, mes-3* and *mes-6* (part of the PcG complex)	Erhardt *et al.* (2003), Strome *et al.* (1994)
KDM H3K4me1/2	Kdm1a	*spr-5, amx-1, lsd-1*	Wasson *et al.* (2016), Katz *et al* (2009)
KDM H3K4me1/2	Kdm1b	*spr-5, amx-1, lsd-1*	Stewart *et al.* (2015), Katz *et al* (2009)
KDM H3K27me3	KDM6A, utx	*jhdm-1, utx-1*	Yang *et al.* (2016), Cockrum *et al.* (2022)
Chromatin remodeler	Brg1(SWI/SNF)	*swsn-1, swsn-9*	Bultman *et al.* (2006), Mathies *et al.* (2020)
Chromatin remodeler (repress complex)	Co-REST	*spr-1*	Carpenter and Scott *et al.* (2023), Jarriault *et al.* (2002)

HMT= Histone methyltransferase, KDM=Lysine demethylase

REFERENCES

Adam Wood, Abhijit Shukla, Jessica Schneider, Jung Shin Lee, Julie D. Stanton, Tiffany Dzuiba, Selene K. Swanson, Laurence Florens, Michael P. Washburn, John Wyrick, Sukesh R. Bhaumik & Ali Shilatifard (2007) Ctk Complex-Mediated Regulation of Histone Methylation by COMPASS, Molecular and Cellular Biology, 27:2, 709-720, DOI: 10.1128/MCB.01627-06

Andersen, E. C., & Horvitz, H. R. (2007). Two *C. elegans* histone methyltransferases repress lin-3 EGF transcription to inhibit vulval development. Development, 134(16), 2991–2999. https://doi.org/10.1242/dev.009373

Bernstein, B. E., Mikkelsen, T. S., Xie, X., Kamal, M., Huebert, D. J., Cuff, J., … Lander, E. S. (2006). A Bivalent Chromatin Structure Marks Key Developmental Genes in Embryonic Stem Cells. Cell, 125(2), 315–326. https://doi.org/10.1016/j.cell.2006.02.041
Cao, J., & Yan, Q. (2012). Histone ubiquitination and deubiquitination in transcription, DNA damage response, and cancer. Frontiers in Oncology, 2(MAR), 1–9. https://doi.org/10.3389/fonc.2012.00026

Delaney, C. E., Methot, S. P., Kalck, V., Seebacher, J., Hess, D., Gasser, S. M., & Padeken, J. (2022). SETDB1-like MET-2 promotes transcriptional silencing and development independently of its H3K9me-associated catalytic activity. Nature Structural and Molecular Biology, 29(2), 85–96. https://doi.org/10.1038/s41594-021-00712-4

Eimer, S., Lakowski, B., Donhauser, R., & Baumeister, R. (2002). Loss of spr-5 bypasses the requirement for the C.elegans presenilin sel-12 by derepressing hop-1. EMBO Journal, 21(21), 5787–5796. https://doi.org/10.1093/emboj/cdf561

Eskeland, R., Eberharter, A., & Imhof, A. (2007). HP1 Binding to Chromatin Methylated at H3K9 Is Enhanced by Auxiliary Factors. Molecular and Cellular Biology, 27(2), 453–465. https://doi.org/10.1128/mcb.01576-06

Firsanov, D.V., Solovjeva, L.V. & Svetlova, M.P. H2AX phosphorylation at the sites of DNA double-strand breaks in cultivated mammalian cells and tissues. *Clin Epigenet* **2**, 283–297 (2011).

Furuhashi, H., Takasaki, T., Rechtsteiner, A., Li, T., Kimura, H., Strome, S., & Kelly, W. G. (2010). Trans-generational epigenetic regulation in *C. elegans* primordial germ cells. Developmental Biology. https://doi.org/10.1016/j.ydbio.2010.05.363

Goetsch, P. D., Garrigues, J. M., & Strome, S. (2017). Loss of the Caenorhabditis elegans pocket protein LIN-35 reveals MuvB's innate function as the repressor of DREAM target genes. PLoS Genetics, 13(11), 1–25. https://doi.org/10.1371/journal.pgen.1007088

Hergeth SP, Schneider R. The H1 linker histones: multifunctional proteins beyond the nucleosomal core particle. EMBO Rep. 2015 Nov;16(11):1439-53. doi: 10.15252/embr.201540749. Epub 2015 Oct 15. PMID: 26474902; PMCID: PMC4641498.

Holdeman R, Nehrt S, Strome S. MES-2, a maternal protein essential for viability of the germline in Caenorhabditis elegans, is homologous to a Drosophila Polycomb group protein. Development. 1998 Jul;125(13):2457-67. doi: 10.1242/dev.125.13.2457. PMID: 9609829.

Jarriault, S., & Greenwald, I. (2002). Suppressors of the egg-laying defective phenotype of sel-12 presenilin mutants implicate the CoREST corepressor complex in LIN-12/Notch signaling in *C. elegans*. Genes and Development, 16(20), 2713–2728. https://doi.org/10.1101/gad.1022402

Katz, D. J., Edwards, T. M., Reinke, V., & Kelly, W. G. (2009). A *C. elegans* LSD1 Demethylase Contributes to Germline Immortality by Reprogramming Epigenetic Memory. Cell, 137(2), 308–320. https://doi.org/10.1016/j.cell.2009.02.015 evelopmental Cell, 5(5), 747–757. https://doi.org/10.1016/S1534-5807(03)00327-7

Kerr, S. C., Ruppersburg, C. C., Francis, J. W., & Katz, D. J. (2014). SPR-5 and MET-2 function cooperatively to reestablish an epigenetic ground state during passage through the germ line. Proceedings of the National Academy of Sciences, 111(26), 9509–9514. https://doi.org/10.1073/pnas.1321843111
Mariño-Ramírez L, Kann MG, Shoemaker BA, Landsman D. Histone structure and nucleosome stability. Expert Rev Proteomics. 2005 Oct;2(5):719-29. doi: 10.1586/14789450.2.5.719. PMID: 16209651; PMCID: PMC1831843.

Methot, S. P., Padeken, J., Brancati, G., Zeller, P., Delaney, C. E., Gaidatzis, D., … Gasser, S. M. (2021). H3K9me selectively blocks transcription factor activity and ensures differentiated tissue integrity. Nature Cell Biology, 23(11), 1163–1175. https://doi.org/10.1038/s41556-021-00776-w

Ng., R. K., & Gurdon, J. B. (2008). Epigenetic memory of an active gene state depends on histone H3.3 incorporation into chromatin in the absence of transcription. Nature Cell Biology, 10(1), 102–109. https://doi.org/10.1038/ncb1674

Padeken, J., Methot, S. P., & Gasser, S. M. (2022). Establishment of H3K9-methylated heterochromatin and its functions in tissue differentiation and maintenance. Nature Reviews Molecular Cell Biology, 23(9), 623–640. https://doi.org/10.1038/s41580-022-00483-w

Pekowska A, Benoukraf T, Zacarias-Cabeza J, Belhocine M, Koch F, Holota H, Imbert J,

Andrau JC, Ferrier P, Spicuglia S. H3K4 tri-methylation provides an epigenetic signature of active enhancers. EMBO J. 2011 Aug 16;30(20):4198-210. doi: 10.1038/emboj.2011.295. PMID: 21847099; PMCID: PMC3199384.

Saksouk, N., Simboeck, E., & Déjardin, J. (2015). Constitutive heterochromatin formation and transcription in mammals. Epigenetics and Chromatin, 8(1), 1–17. https://doi.org/10.1186/1756-8935-8-3

Schaner, C. E., Deshpande, G., Schedl, P. D., & Kelly, W. G. (2003). A conserved chromatin architecture marks and maintains the restricted germ cell lineage in worms and flies.

Seydoux, G., Mello, C. C., Pettitt, J., Wood, W. B., Priess, J. R., & Fire, A. (1996). Repression of gene expression in the embryonic germ lineage of *C. elegans*. Nature, 382(6593), 713–716. https://doi.org/10.1038/382713a0

Tang, L., Nogales, E., & Ciferri, C. (2010). Structure and function of SWI/SNF chromatin remodeling complexes and mechanistic implications for transcription. Progress in Biophysics and Molecular Biology, 102(2–3), 122–128. https://doi.org/10.1016/j.pbiomolbio.2010.05.001

Unhavaithaya, Y., Shin, T. H., Miliaras, N., Lee, J., Oyama, T., & Mello, C. C. (2002). MEP-1 and a homolog of the NURD complex component Mi-2 act together to maintain germline-soma distinctions in *C. elegans*. Cell, 111(7), 991–1002. https://doi.org/10.1016/S0092-8674(02)01202-3

Woodhouse, R. M., Buchmann, G., Hoe, M., Harney, D. J., Low, J. K. K., Larance, M., … Ashe, A. (2018). Chromatin Modifiers SET-25 and SET-32 Are Required for Establishment but Not Long-Term Maintenance of Transgenerational Epigenetic Inheritance. Cell Reports, 25(8), 2259-2272.e5. https://doi.org/10.1016/j.celrep.2018.10.085

CHAPTER 2

Lineage Tracing and Single-Cell RNA-seq in *C. elegans* to Analyze Transgenerational Epigenetic Phenotypes Inherited from Germ Cells

Chapter 2. Lineage Tracing and Single-Cell RNA-seq in *C. elegans* to Analyze Transgenerational Epigenetic Phenotypes Inherited from Germ Cells

Juan D. Rodriguez[1] and David J. Katz[1*]

[1]Department of Cell Biology, Emory University School of Medicine, Atlanta GA 30322, USA.

*corresponding author:
David J. Katz
Associate Professor
Department of Cell Biology
Room 443, Whitehead Biomedical Research Building
Emory University School of Medicine
Atlanta, GA 30322, USA
Phone: (404) 727-3403
djkatz@emory.edu

*Accepted publication Springer Science 2023

Abstract The last several years have seen an increasing number of examples of transgenerational epigenetic inheritance, in which phenotypes are inherited for three or more generations without changes to the underlying DNA sequence. One model system that has been particularly useful for studying transgenerational epigenetic inheritance is *C. elegans*. Their short generation time and hermaphroditic reproduction have allowed multiple transgenerational phenotypes to be identified, including aging, fertility, and behavior. However, it is still not clear how transgenerational epigenetic inheritance from the germline affects embryogenesis. Fortunately, the *C. elegans* embryo has a unique property that makes it ideal for addressing this question: they develop via an invariant lineage, with each cell undergoing stereotypical cell divisions to adopt the same cell fate in every individual embryo. Because of this invariant cell lineage, automated lineage tracing and single-cell RNA-seq can be employed to determine how transgenerational epigenetic inheritance from the germline affects developmental timing and cell fate. Unfortunately, difficulties with these techniques have severely limited their adoption in the community. Here, we provide a practical guide to automated lineage tracing coupled with single-cell RNA-seq to facilitate their use in studying transgenerational epigenetic inheritance in *C. elegans* embryos

Key words: *C. elegans*, Lineage tracing, Single-cell RNAseq, Epigenetic transgenerational inheritance, Germ cells

INTRODUCTION

The germline is a highly specialized tissue that produces gametes by the specialized cell division of meiosis. Gametes serve as the repository of all information that will be passed from one generation to the next. Predominantly, this information is encoded genetically in DNA. However, over the last few years, there have been an increasing number of examples of transgenerational epigenetic phenotypes not encoded by changes in the DNA sequence itself. This much rarer mode of inheritance has been documented in organisms ranging from yeast to humans and has been proposed to occur via mechanisms like small non-coding RNAs, DNA methylation, and histone modifications [1, 2]. Studying epigenetic transgenerational inheritance is difficult in systems with a slow generational time, because of the time and effort it takes to monitor multiple generations. Studying epigenetic transgenerational inheritance can also be complicated by genetic variation, which can contribute to phenotypes not directly caused by transgenerational inheritance. One model organism that avoids these complications is the nematode *Caenorhabditis elegans* (*C. elegans*). *C. elegans* has a short generation time of 3 days and reproduces as self-fertilizing hermaphrodites, which limits genetic variation [3]. Partially as a result of these advantages, a large number of epigenetic transgenerational phenotypes have been observed in worms, including those that affect lifespan, fertility, and behavior [4, 5, 6, 7, 8]. Despite the examples of epigenetic transgenerational inheritance that have been identified, it remains unknown how heritable epigenetic transgenerational information causes phenotypes in resulting offspring. Fortunately, *C. elegans* has a unique property that makes it highly suitable for addressing this question. As originally identified by John Sulston, the *C. elegans*

embryonic lineage is invariant [9], which means that the timing, cell movement, and cell fate of every cell remains the same between individual embryos, allowing the full lineage to be characterized. Because of this unique property, *C. elegans* can be used to investigate transcriptional and cell lineage defects at the single-cell level in the embryo [10]. In order to identify cell lineage defects, an automated cell tracking pipeline has been developed: StarryNite and AceTree [11]. These programs can be used to track each cell within an embryo and curate the cell lineage by utilizing live confocal imaging to follow mCherry- or GFP-labeled nuclei. By examining the cell lineage from mutant worms and comparing it with Wild Type (N2), it is possible to identify any defects in cell timing, cell migration, and inappropriate cell death, during all stages of embryogenesis. In addition, cell fate transformations can be identified by lineage conversion, as shown by the example reproduced from work by Boyle et al. [12] (Fig. 1). Along with automated lineage tracing, single-cell transcriptomics have been performed on N2 *C. elegans* embryos at all stages [13, 14, 15]. These experiments have defined the transcriptome of each cell in the *C. elegans* embryo, facilitating the identification of defects by comparison to N2.

2. MATERIALS

2.1 Growing worms

1. Agar plates: 1 L Nematode Growth Media (NGM): 3 g NaCl , 20 g Agar, 2.5 g Bacto peptone dissolved in 975 mL with diH O. The remaining ~25 mL will be added after autoclaving. Be sure to add a stir bar to the solution before autoclaving. Autoclave for 1 h. Cool the flask by stirring on a heat/stir plate until the flask is ~55 °C (cool enough to briefly touch) and add the rest of the reagents: 25 mL of 1 M KPO buffer pH 6.0 (108.3 g KH PO , 35.6 g K HPO in a total of 1 L H O, autoclaved) (25 mM final), 1 mL 1 M MgSO (1 mM final), 0.5 mL of 1 M CaCl (0.5 mM final), 1 mL of 5 mg/mL Cholesterol (0.005 mg/mL final). Continue to stir and heat using a heat/stir plate while pouring into the 60 mm Petri dishes. The heating will prevent the agar from solidifying. It is recommended to use a plate pouring machine so that plates are all the same height, which eliminates the need to refocus when looking through multiple plates. Leave the plates lid-side up to dry for 2–4 days, then store lid-side down at 4 °C. Plates can be stored for several months.

2. Seeding the agar plates with bacteria for worm growth. Make Luria Broth (LB), which is used to grow E. coli (OP50 strain) that *C. elegans* feed upon. 1 L LB: 10 grams of Tryptone, 10 g of NaCl, and 5 g of yeast extract. Dissolve in distilled water, up to 1 L, and split into 10 glass flasks; each one should have approximately 100 mL. Autoclave. Inoculate 100 mL of LB media with a single colony of E. coli OP50 obtained from the Caenorhabditis Genetics Center (CGC); incubate overnight at 37 °C. From this culture, spot three OP50 drops onto each 60 mm NGM plate using a 5 mL serological pipette. The OP50 culture can be stored at 4 °C and used for several weeks.

2.2. **scRNA-seq**

1. M9 buffer: 22 mM KH PO , 42 mM Na HPO , 86 mM NaCl, and 1 mM MgSO (store at room temperature). Prepare 1 L. Sometimes the MgSO will precipitate out after autoclaving. In this case, an alternative approach is to add the MgSO after autoclaving.

2. Embryo collection: Bleach solution: M9 buffer containing 20% Bleach and 10 M NaOH (store at 4 °C). Prepare 500 mL. The bleach solution can be stored for up to 1 month. After this, the bleach solution should be remade from bleach stock purchased at least every 6 months to prevent a loss of efficacy. Note: the anti-splash additive now included in many commercial bleaches is not good for bleaching worms, so do not use bleach containing anti-splash additive.

3. Egg Buffer: 118 mM NaCl, 48 mM KCl, 3 mM CaCl , 3 mM MgCl , 5 mM HEPES pH 7.2 (store at room temperature). Prepare 2 L, then add BSA to 100 mL, stored in 50 mL conical tubes (Egg Buffer +1% BSA, store at −20 °C).

4. 60% sucrose in H O (store at 4 °C). Prepare 100 mL and store in a sterilized container.

5. PBS (Corning 21-040-CV) (store at room temp).

6. Egg Buffer +1% BSA (−20 °C).

7. Chitinase (Sigma Aldrich C6137-5UN, ≥200 units/g solid) stored at −20 °C.

8. Pronase (Sigma Aldrich-10165921001, 1G) stored at 4 °C.

9. RNAse Zap (Thermofisher AM9782).

10. Autoclaved sterile glass Pasteur pipettes.

11. Individual sterile plastic transfer pipet.

12. 3 cc syringe and 21½ G needle.

13. 10 μM filter.

14. Trypan Blue.

15. Glass hemocytometer.

2.3. Preparation of Solutions and Equipment for Microscopy

1. Boyd's buffer with methylcellulose: 60 mM NaCl, 32 mM KCl, 3 mM Na HPO , 2 mM MgCl, 2 mM CaCl ; 5 mM Hepes, 0.2%

Glucose, 1% methylcellulose. This buffer can be used when dissecting worms and to make the 20 μm beads dilution. Prepare 1 L(store at 4 °C).

2. M9 buffer (see Subheading 3.1).

3. Frosted microscope slides 25 × 75 × 1.0 mm (Fisherbrand: 12-550-15).

4. Coverslip 18 mm × 18 mm (sigma Aldrich: 12-548-A).

5. Two 25G × 5/8 Needles (BD:305122).

6. 10 well-cutting glass plate (Fig. 4).

7. 20 μm beads (5 mL from Polyscience, 18329).

8. Confocal microscope (Zeiss LSM 510, or other) equipped with temperature-controlled stage (Brook Industries, Lake Villa IL).

Setting the temperature-controlled stage at 20 °C mimics standard laboratory conditions for *C. elegans*.

9. Petroleum jelly (1.75 ounce jar of Vaseline brand purchased from a drug store).

10. Mouth pipette with a capillary glass tube (VWR 51608) Length 75 mm ±0.05, Column 75μL.

2.4. Website to Download Lineage Program Software

1. StarryNite launcher: Integration of StarryNite and AceTree: https://waterston.gs.washington.edu/ [11] (see Note 1).

2. StarryNite: https://wormguides.org/starry-nite/

3. AceTree: https://github.com/zhirongbaolab/AceTree [11].

3. METHODS

3.1. Cell Isolation for scRNA-seq

For scRNA-seq cell isolation, you will perform 3 separate synchronization steps. First, you will roughly synchronize the first generation. Second, you will collect their progeny for more precise synchronization. Finally, you will collect young embryos at the desired stage for performing scRNA-seq. For complete resuspension of the chitinase enzyme, please see Note 2.

1. Grow worms on 20 plastic 60 mm petri dishes, seeded with OP50 bacteria (see Subheading 2): place 3 L4-stage worms per plate (1 on each drop). All worms are grown in a 20 °C incubator. 20 plates of N2 will ultimately yield approximately 29,000 embryos at the ~100 cell stage (2.9 × 10 total cells). Certain mutants may be less fertile than N2 and will require starting with a larger number of worms.

2. Wait until each plate is confluent with gravid adults (worms containing two rows of embryos), but not starved (~3–4 days for N2, but the timing may be different in mutants). Using a plastic transfer pipet, rinse worms off plates with M9 buffer (by squirting onto a tilted plate ~10–20 mL for 20 plates). Collect the worms into a 50 mL conical tube, and let worms settle to the bottom by gravity (~10 min). Wash with M9 three times by removing the supernatant with a 50 mL plastic transfer pipet and adding 50 mL of M9 each time.

3. After the last wash, carefully pipet out most of the M9 with a plastic transfer pipet and add 25–30 mL of bleach solution. Place the tube onto a platform rocker and monitor degradation by looking in the tube under a dissecting light microscope (under 3–5× magnification) until most of the carcasses first disappear and embryos remain (~10 min, but this varies widely depending on the bleach, concentration of worms, etc.). Be careful not to let the embryos sit excessively in bleach as this will damage them.

4. After only embryos remain, bring the volume to 50 mL with M9 and centrifuge for 1 min at 450 rcf (Eppendorf Centrifugation 5810 R table top centrifuge). Carefully remove the supernatant using a serological pipet but leave a little bit of volume so the pellet won't be discarded by accident. Resuspend pelleted worms by bringing the volume to 50 mL with Egg Buffer and gently mix by inversion. Centrifuge for 2 min at 450 rcf. During this time prepare a 15 mL conical tube with 5 mL of 60% sucrose (stored at 4 °C). After centrifugation is completed, discard the supernatant using a 50 mL plastic serological pipet.

5. Resuspend the embryos with 5 mL of Egg Buffer by pipetting up and down with a 5 mL plastic transfer pipet and transfer to a 15 mL conical tube with the 60% sucrose; vortex for 5 s and centrifuge for 5 min at 3220 rcf.

6. After centrifugation, two layers will form. The embryos will be in the top layer. Transfer the embryos to a 50 mL conical tube by using a glass Pasteur pipette (do not use plastic because the embryos and cells will stick to the plastic). Bring the volume to 40 mL with Egg Buffer and centrifuge for 2 min at 1260 rcf. Remove the supernatant with a 50 mL plastic serological pipet, leaving 2 4 2 2 6 a little bit behind so the embryo pellet won't be discarded by accident. Resuspend in 1–1.5 mL of Egg Buffer (final

volume, ~2 mL total). Then transfer the resuspended embryos onto 8–10 60 mm unseeded plates with a glass Pasteur pipette.

7. Allow the embryos to hatch overnight at 20 °C on unseeded plates. Without food, worms arrest at the L1 larval stage, so hatching onto unseeded plates synchronizes L1 larvae. After hatching overnight on unseeded plates move the synchronized L1 larvae to seeded plates by rinsing off the plates by squirting ~1–2 mL M9 per plate onto a tilted plate, using a glass Pasteur pipette.

8. Following the first L1 larval synchronization, proceed with a second synchronization. This second synchronization limits the number of worms you will obtain, but is necessary to make the synchronization tighter. Allow the L1 larvae to grow at 20 °C for approximately 46 h. This produces young adult worms with the first embryos in the gonad. After 46 h (this time may differ for mutant strains), repeat the bleach synchronization starting at step 2 of Subheading 3.2

3.2. Staging Worms and Collecting ~100 Cell Embryos

1. To obtain worms at approximately the 100-cell stage, allow the twice-synchronized L1 larvae to grow at 20 °C for approximately 46 h. This produces young adult worms with the first embryos in the gonad.

2. Pick individual young adults with the first embryos in the gonad onto a 60 mm plate containing a single OP50 drop from a 5 mL serological pipet. Even though the worms have been synchronized twice, picking worms is necessary to get the correct stage. It is important to pick all of the young adults within 1 h. scRNA-seq requires 10,000 cells, which generally requires starting the process with 14,000 cells. Therefore, if embryos

are at the ~100 cell stage, you will need 140 embryos. Obtaining ~140 embryos generally requires starting from 20 or more 60-mm plates of confluent worms.

3. Rinse plates with ~1–2 mL M9 (for 20 plates) by squirting onto a tilted plate with a plastic transfer pipet and collect worms into a 15 mL conical tube. Let the worms sink in the conical tube by gravity (~10 min) and wash the worm pellet with M9 three times by removing the supernatant with a 10 mL plastic serological pipet and adding 10 mL of M9 each time. The liquid should become clearer with each wash as the bacteria is removed.

4. After removing the last wash, add 7–10 mL of bleach solution, vortex for 20-s and place the 15 mL conical tube on a platform rocker for ~10 min. Monitor the worm degradation with a dissecting light microscope (3–5× magnification), vortexing occasionally, until at least 80–90% of embryos have been released and the carcasses disappear.

5. After confirming that embryos are released, bring the volume to 50 mL with M9 and centrifuge for 1 min at 450 rcf. After centrifugation is completed, carefully remove supernatant, but leave some volume behind so that the pellet won't be discarded by accident. Resuspend the pellet by bringing the volume to 50 mL with Egg Buffer and centrifuge for 2 min at 450 rcf. During this time, prepare a 15 mL tube on ice and add 5 mL of cold 60% sucrose solution. After the centrifugation is complete, discard the supernatant using a 50 mL plastic serological pipet.

6. Resuspend embryos with 5 mL of Egg Buffer and transfer to the 15 mL conical tube containing cold 60% sucrose. Vortex for 5 s to mix, then centrifuge for 5 min at 3220 rcf. The embryos should be in the top layer.

7. Transfer the embryos from the top layer to a 50 mL conical by with a glass Pasteur pipette. Bring the volume to 40 mL with Egg Buffer. At this point, you can let the embryos develop in Egg Buffer until the target cell stage is reached (see Note 3).

8. Once the target stage is reached, centrifuge for 2 min at 450 rcf., remove the supernatant using a 50 mL plastic serological pipet and resuspend the embryos in 1–1.5 mL Egg Buffer. Transfer the resuspended embryos to a 12-well plastic cell culture plate with a glass Pasteur pipette, then proceed with the cell membrane and cell isolation step.

3.3. Eggshell Removal and Single-cell Suspension

1. Add a ratio of 1 mL chitinase (1 U/mL) to 0.5 mL embryo suspension and incubate at room temperature for 20–30 min (if the desired embryos are greater than the 300-cell stage, see Note 4). Monitor eggshell removal under a dissecting light microscope (3.5–55×). It is very important to keep monitoring the cell suspension during the incubation time to observe the removal of the eggshell, so that the reaction does not proceed past the removal of the eggshell. Proceeding past the initial removal of the eggshell can result in damage to the individual cells. In the meantime, thaw the Egg Buffer with 1% BSA (stored @ −20 °C) and place a new 15 mL conical tube on ice for step 4.

2. Optional: Another way to confirm eggshell disruption is to place 2 μL of the sample on a slide with a 2% agarose pad and examine under differential interference contrast (DIC) microscopy at 40× to verify the single-cell isolation (see Fig. 2). If there are still clumps of cells, pass the suspension through the 21½G needle again multiple times. Clumps can clog the 10× Chromium capture mixer (10× Genomics) and/or result in cell doublets within a single GEM droplet.

3. After confirmation of the disruption of the eggshell, pass the embryos repeatedly through a 21 G needle ~20 times to generate a single-cell suspension in one well of a 12-well cell culture plate. Incubate at room temperature for 5 min. The 12-well plate makes it easier to pass through the syringe multiple times and to monitor the single-cell isolation under a dissection light 1/2 microscope (10–20×). Then move to step 5 if the embryos are less than the 300-cell stage. If the desired embryonic stage is greater than 300 cells, proceed with the Subheading 3.3 , step 4. Place 10 μL of the single-cell suspension on a 2% agarose pad and look under the DIC microscope at 40–100× to

verify the single-cell isolation (see Fig. 2). If there are still clumps of cells, pass the suspension through the 21½G needle again multiple times. Clumps can clog the 10× Chromium capture mixer (10× Genomics) and/or result in cell doublets within a single Gel bead in EMulsion (GEM) droplet.

4. Stop the enzymatic reaction by adding 3–4 mL of Egg Buffer with 1% BSA (thawed in step 1) to the well of the 12-well plate.

5. Transfer to a chilled 15 mL tube by passing the cells through a 10 μm filter on a 3 cc syringe. Filtering through the 10 μm filter on a 3 cc syringe removes almost all of the debris and intact embryos, while all of the single cells pass through. As a result, this filtering step should be included.

6. Centrifuge at 2500 rcf for 5 min at 4 °C. The cells will be in the pellet. In the original protocol, this centrifugation was performed at a slower speed to pellet the debris. However, after a slow speed spin, many single cells were found in the pellet with the debris and were lost during this step. The inclusion of the filtering in step 6 makes pelleting the debris unnecessary. As a result, a slightly stronger spin (2500 rcf for 5 min at 4 °C) can be used to pellet all of the single cells in this step.

7. Using a glass Pasteur pipette, carefully remove the supernatant and wash the pellet 3× by centrifuging at 2500 rcf for 3 min. Resuspend pellet in 1 mL Egg Buffer with 1% BSA by pipetting up and down with a glass Pasteur pipette. After the first resuspension, transfer to a nonstick polypropylene Eppendorf tube for the second and third washes (see Note 5).

8. Following the final wash, remove most of the supernatant and add 1 mL of Egg Buffer with 1% BSA. Then centrifuge at 4 °C at 2500 rcf for 5 min.

9. Using a glass Pasteur pipette, carefully remove the supernatant and resuspend the pellet by adding 100 µL of ice-cold Egg Buffer and pipetting up and down with a glass Pasteur pipette. Then proceed with cell counting (see Note 6).

10. Following resuspension, count the number of cells using a hemocytometer (Fig. 3). During the counting, keep the resuspended cell on ice all the time. Clean the glass hemocytometer and coverslip with clean ethanol. Place the coverslip onto the hemocytometer, the coverslip should cover both chambers. Gently flick the Eppendorf tube that has the cells. Then take 10 µL and apply it into the loading area of the hemocytometer, underneath the coverslip. Wait around 30–60 s for the cells to settle. Finally, count the cells at 10× or 20× magnification using a phase contrast microscope. The cells can be counted by quadrant. For example, you could count the four outside edge quadrants and the one in the center. Then the formula that would apply to the cell counting is: number of cells counted in each quadrant multiplied by the dilution factor (if you diluted the cells, i.e., with Trypan blue – see Note 7) equals the number of cells 10× cells/mL, divided in the # of quadrants, in this example the # of quadrants is 5. This information will be important for the 10× Genomics protocol. During the cell counting process, keep cells on ice and proceed directly, as quickly as possible, to the 10× Genomics protocol for RNA isolation, cDNA conversion, library preparation, and sequencing guidelines (see Note 8).

11. After counting, immediately follow the 10× Genomics protocol for RNA isolation, cDNA conversion, library preparation and sequencing. Details related to the 10× Genomics protocol are not included here because the 10× Genomics protocols are constantly changing. However, it should be noted that for troubleshooting and smaller

samples, currently it is recommended to use the Chromium Next GEM Single Cell 3′ LT v3.1 low throughput kit (PN-1000325). For full samples, use the Chromium Next GEM Single Cell 3′ LT v3.1 kit (PN-1000128).This kit is more expensive but the cell recovery is much higher. In addition, more cells can be analyzed in a single assay using this kit.

3.4. Synchronization and Worm Dissection to Obtain 2-Cell Embryos for Lineage Tracing

1. The automated lineage tracing was designed for use with the Zeiss LSM 510 microscope. It may be possible to use other confocal microscopes, but we encountered difficulty when we tried to use a Leica SP8 (see Note 9).

2. Embryos should start to be imaged at the 2–4-cell stage, to allow the tracking software to function correctly. The program to track the cells is StarryNite (see Note 10).

3. Pick around 20–30 L4 worms and place them on a seeded plate (see Note 11). Use the JIM113 strain: ujIs113 [pie1p::mCherry::H2B::pie-1 3'UTR + nhr-2p::his-24::mCherry::let-858 3'UTR + unc-119(+)]. The goal is to compare Wild Type to certain mutants, so mutations will need to be crossed into the JIM113 genetic background.

4. After 20–24 h, worms should have the first embryos in the uterus.

5. Prepare the imaging setup prior to placing the worms into the cutting glass plate (see Note 12). Place 3–4 worms into one well of a 10-well-cutting glass plate (Fig. 4) filled approximately half way with M9. Move the worms into a new well 3× to rinse and remove the bacteria.

6. Cut the worms by using two needles and slicing the worm at the boundary between the uterus and the gonad (approximately in the middle of the worm).

7. Using a mouth pipette, move ~4–6 (as many as you can find) 2–4 cell embryos into a new well of a 10-well-cutting glass plate containing M9. This helps to reduce any remaining bacteria contamination. It is best if the embryos are at the 2-cell stage or even the occasional fertilized egg at the 1-cell stage.

8. Create the bead mount: Place 3 μL of 1:20 dilution of 20 μm beads in Boyd's buffer (final concentration of beads, 1 μM) onto a microscope slide and mouth pipet 2–4 embryos from the 10-well-cutting glass plate at the 2–4 cell stage (pick the earliest staged embryos available). Using a worm pick, gently lower the coverslip onto the embryos to avoid damaging them.

9. Seal the edges of the coverslip with enough petroleum jelly to cover the edges using a brush (e.g., a cleaned nail polish brush). Sealing the coverslip prevents evaporation. Do not use nail polish, as the acetone in the nail polish can kill the embryos (see Note 13).

10. Place the slide into the previously prepared temperature-controlled stage and start live-imaging with a Zeiss LSM 510 (see Note 14).

11. Live imaging must start with 2 or 4 cell-stage embryos and 200 min is typically sufficient to reach the 100 cell-stage. It requires ~13 h to image until the embryo hatches. At the earlier stages (2–16 cell-stage), the laser power can be high (>80). However, as cells start to divide, the signal intensity increases as nucleus size decreases, which makes it difficult for StarryNite to track the cells. As a result, the StarryNite program makes more mistakes, which requires extensive manual correction. Murray and colleagues [11] suggest setting the software to automatically adjust the laser power and other parameters in different time blocks during the imaging, but some

versions of the ZEN software for running the Zeiss LSM 510 lack that option. If automatically changing the laser power and other parameters is not an option, the laser can be adjusted manually by decreasing the laser power by 20–40% after 1–2 h of live imaging. Images should be collected using a 63×, 1.4NA oil Plan-APOCHROMAT objective (see Notes 15 and 16).

12. When using the Zeiss LSM 510, follow the microscope settings and parameters listed in Murray et al. 2006 [11]. Images should be exported in the 8-bit TIFF format. The confocal generates individual images for every focal plane at every time point. In order to run the images on StarryNite, they must be grouped by timepoints. Murray and colleagues [11] suggest using Matlab to group the images. However, an alternative way to create folders with images grouped by timepoints is to use a Mac command. To do this use a command written in AWK to compile each image by timepoint, and group each timepoint in a separate folder (see Note 17). When images are grouped by timepoints, use an ImageJ macro command to compress all of individual Z-stacks into a single 8-bit TIFF file, which can then be imported to StarryNite (see Note 17).

13. StarryNite produces multiple outputs. Open the XML file (contained in the ZIP file) in AceTree.

14. AceTree is used to visualize the lineage and can be used to manually correct any cell division mistakes or add any cells that failed to be tracked. The most common error made by StarryNite is missing a daughter cell from the previous division. To correct this error in AceTree, click on the “edit” option and select “edit tools.” This step opens two new windows, “Edit Tracks” and “Adjust or Delete Cells.” Select the mother cell by right-clicking on the cell in the embryo image window that contains the error, then click on

use active cell from the “Edit Track” window. In the “Edit Track” window, check the box that says “is early set correctly?” Then move to the next timepoint by clicking on the forward arrow in the embryo image window and click on the unlabeled daughter cell that the software has failed to track. A new circle will form around the cell. Finally, click “use active cell” and “apply” from the “Edit Track” window. Now the two daughter cells will be linked to their mother cell (Fig. 5 for an example of this common mistake). Until you fix the tracking errors, AceTree will show many untracked cells as Nuc# instead of as the correct cell lineage name. Once you correct the error, AceTree will automatically assign the correct Sulston lineage name to the fixed cell.

4. NOTES

1. Initially, SNlauncher software downloaded from the original website (Subheading 2.1 , item 1) did not function. After communication with Bao lab members, an alternative version of AceTree was obtained (Subheading 2.4, item 2) and this version was successfully installed on a Mac OS version 12.2.1. Therefore, if SNlauncher downloaded from Subheading 26.42, item 1 does not work, try downloading from Subheading 1.3, item 2 as an alternative.

2. The chitinase purchased from Sigma Aldrich often does not dissolve completely, leaving very small particles that can only be observed under phase-contrast microscopy. The remaining small particles interfere with the single-cell experiment by replacing actual cells in the single GEM droplet during 10× Genomics RNA isolation. To avoid this problem, perform an ultracentrifuge step to separate the chitinase enzyme from the solid undissolved particles. Centrifuge for 30 min at 48,000 rpm at 4 °C. After

centrifugation, remove the supernatant containing the particle-free chitinase enzyme and transfer to a new tube for use.

3. It typically takes ~40 min to isolate embryos via bleaching and pelleting over the sucrose cushion. To target the ~100-cell stage, let the embryos develop in Egg buffer for an additional 30–45 min. The amount of time has been empirically determined by monitoring under a dissecting light microscope (10–20× magnification) for N2 at room temperature. As a result, the amount of time will need to be separately determined for every mutant strain. This is the step before the chitinase process (Subheading 3.3).

4. If the desired embryos are greater than the 300-cell stage: The original protocol for isolating single cells from the *C. elegans* embryo incorporated both a chitinase and Pronase step. However, if targeting an embryonic cell stage of less than 300 cells, only the chitinase step is necessary, because using both chitinase and Pronase on embryos at earlier stages affects the viability of the cells. If the desired embryos are greater than the 300-cell stage, use Pronase to remove the vitelline layer of the eggshell: Add 100 µL per mL of 15 mg/mL Pronase (final concentration 1.5 mg/mL) to the sample. Using a 3 cc syringe, pass embryos repeatedly through a 21½ G needle ~20 times to generate a single-cell suspension in one well of a 12-well cell culture plate. Incubate at room temperature for 5 min. The 12-well plate makes it easier to pass through the syringe multiple times and to monitor the single-cell isolation under a dissection light microscope (10–20×).

5. Pay attention to the pellet because cells can stick to the tube. If you find that the cells are sticking to the tube, you can try centrifuging for a shorter amount of time (e.g., 30–60 s).

6. Do not use an automated cell counter instrument because the cell counting is likely to be very inaccurate. These kinds of instruments are typically designed for mammalian cells. The *C. elegans* embryonic cells are very small, often resulting in the instrument counting incorrectly. Instead, use a traditional hemocytometer to count the cells manually at 20× magnification or greater (Fig. 3).

7. Trypan blue dye is used to determine the viability of cells because dead cells take up the dye. For 10× Genomics, it is highly recommended to start with a cell population with viability of >90%, because transcripts tend to be degraded in dead cells.

8. Additional reagents not provided by the 10× Genomics kit will be needed. It's recommended that all the additional reagents be made fresh on the day of the protocol.

9. It may be possible to use a confocal other than a Zeiss LSM 510. For example, automated lineage tracing has been published using a Leica SP5 [16]. However, the StarryNite program failed to track early cell divisions from Z-stack time series generated with a Leica SP8. This may be due to differences with the metadata or with StarryNite parameters.

10. The first cell divisions in the *C. elegans* embryo occur approximately every 15 min. To slow down this process, store the buffer M9 and cutting glass at 4 °C. This will provide more time for the embryo cell stage selection, slide preparation and the microscope setup. 11. Picking L4 larvae 20–24 h prior to dissection of the adults will increase the number of worms that have 2–4 cell stage embryos 20–24 h later. 12. The temperature stage should be prepared prior to the cutting of the worms by filling the tank with distillated water and setting the temp to 20 °C. 13. Seal the slide with warm petroleum jelly. Warm petroleum jelly can be maintained permanently by storing in a

glass test tube in a heat block at >65 °C. 14. Sometimes embryos will settle during the live-imaging process, which changes the focal plane and disrupts StarryNite's ability to track the lineage. If this happens, consider the following solutions: (a) Setup additional Z-stacks beyond the 3 recommended by Murray and colleagues [11]. (b) Use a modified agar plate to prevent embryos from sinking: Using an empty 60-mm plastic petri dish, make a small opening with a heated surgical blade (sigma Aldrich:2976, No. 11) on the bottom of the plate; embryos will be placed on the exposed agar in the opening (Fig. 6). Then add 10–15 mL of hot NGM agar. Place the hole over a coverslip when pouring the NGM to prevent leakage (10–15 mL is more than needed to fill the plate, in case of leakage). Let the NGM agar solidify overnight on the bench and use the next day. If you are using this technique, mouth pipette the embryos into the hole (instead of onto a slide AQ3 , Subheading 63.34, step 7) and gently cover embryos with a glass coverslip; use a worm pick to gradually lower the coverslip at a diagonal. Note, when using this technique, there are no beads and no liquid on the agar. Seal the coverslip with enough petroleum jelly to prevent airflow (identical to Subheading 3.4 , step 8). Place the plate on the temperature stage to start live imaging (a video link showing this process is provided in Video 1). 15. Use an upright confocal microscope rather than an inverted microscope to prevent embryos from settling out of the focal plane when inverted. 16. Any 63× objective (including oil, glycerol, or water) can be used for imaging. However, the standard 63× oil lens yielded a weaker signal. Signal intensity was improved slightly by a glycerol lens. However, a strong signal was only obtained by using the Zeiss CApochromat 63×/1.20 W Corr UV-VIS-IR water objective. Poor signal prevents StarryNite from correctly assigning cell fate, which greatly

increases the amount of time that will be needed for manual correction. 17. The script used for image grouping is included in Fig. 7 (AWK code in Linux). The ImageJ macro for formatting the images prior to running StarryNite is included in Fig. 8 .

FIGURES AND FIGURES LEGENDS

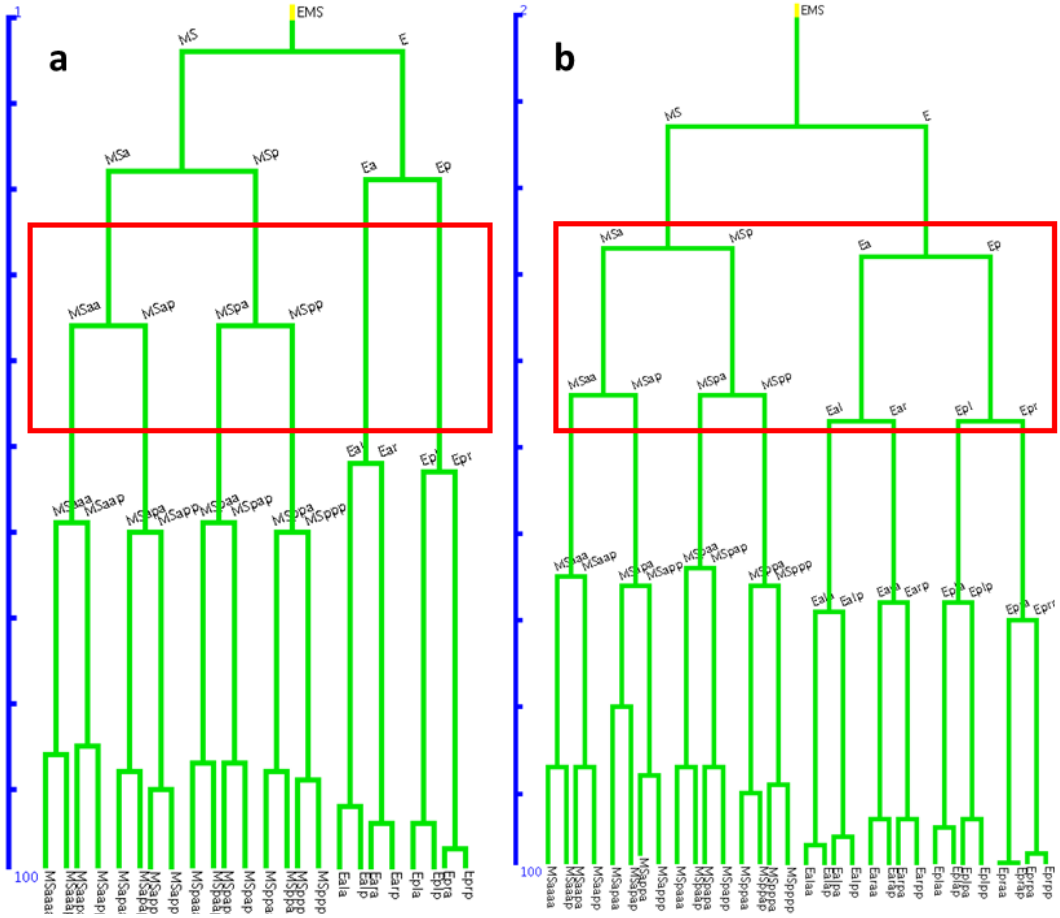

Fig. 1 Example of a lineage conversion. (a) the Wild Type (N2) and (b) the *lit-1*(*RNAi)* EMS sub-lineage. Red squares highlight difference in cell division timing between the MS (muscle) and E (intestine) lineages which are eliminated in *lit-1(RNAi)* animals. This result suggests that the E lineage adopted the cell fate of the MS. This result was previously shown by Boyle *et al* 2006 and colleagues, and is useful as a positive technical control[1].

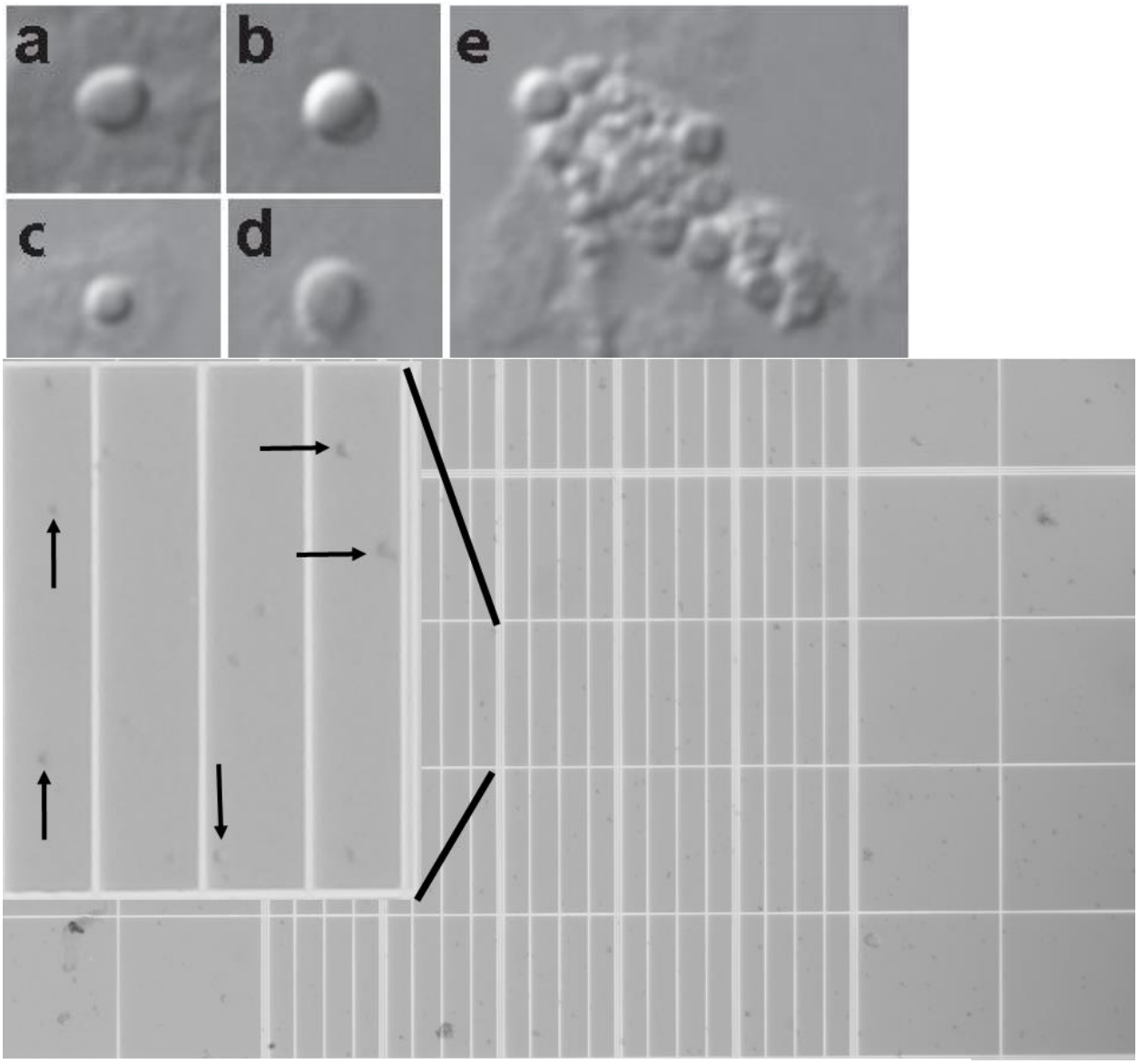

Fig. 3 Cell counting. A volume of 10 µL was loaded into the hemacytometer. The boxed inset shows a zoom in of the region of the hemacytometer that is circled. The arrows point to isolated cells. Image was taken at 20X

Fig. 4 A 10-well glass plate. This plate can be used to clean the worms and perform the dissection

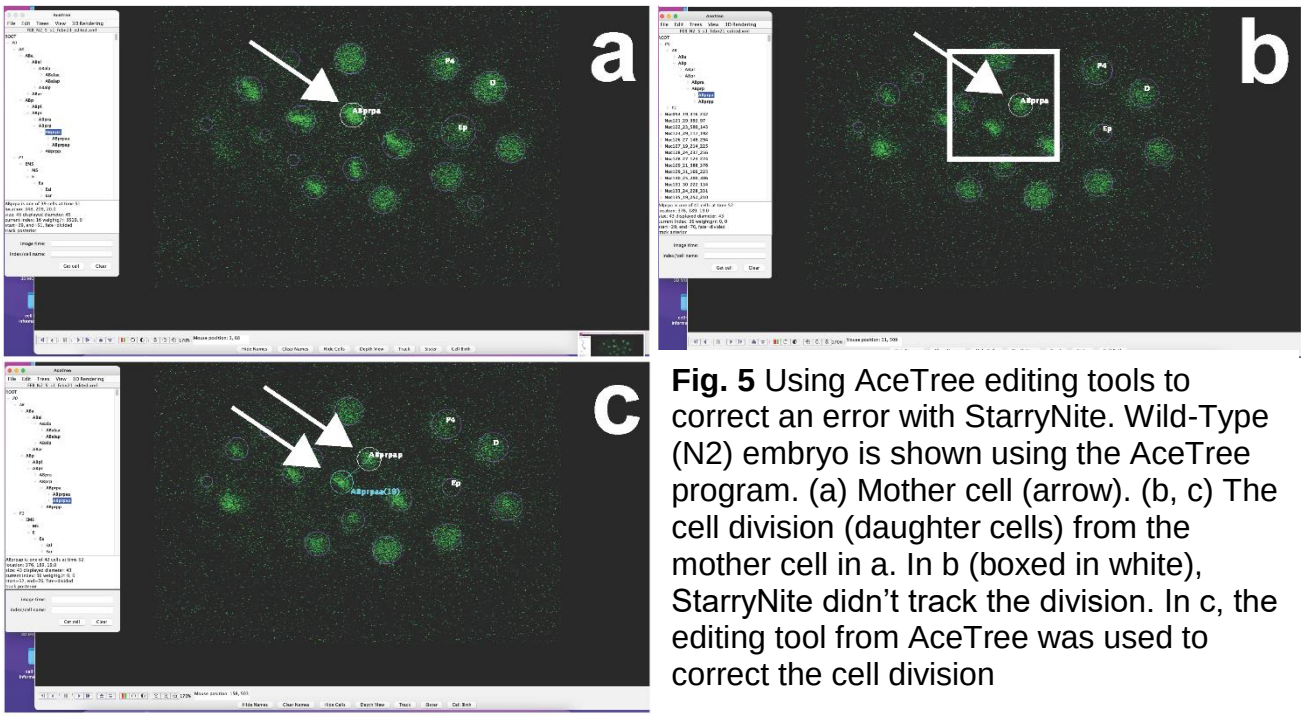

Fig. 5 Using AceTree editing tools to correct an error with StarryNite. Wild-Type (N2) embryo is shown using the AceTree program. (a) Mother cell (arrow). (b, c) The cell division (daughter cells) from the mother cell in a. In b (boxed in white), StarryNite didn't track the division. In c, the editing tool from AceTree was used to correct the cell division

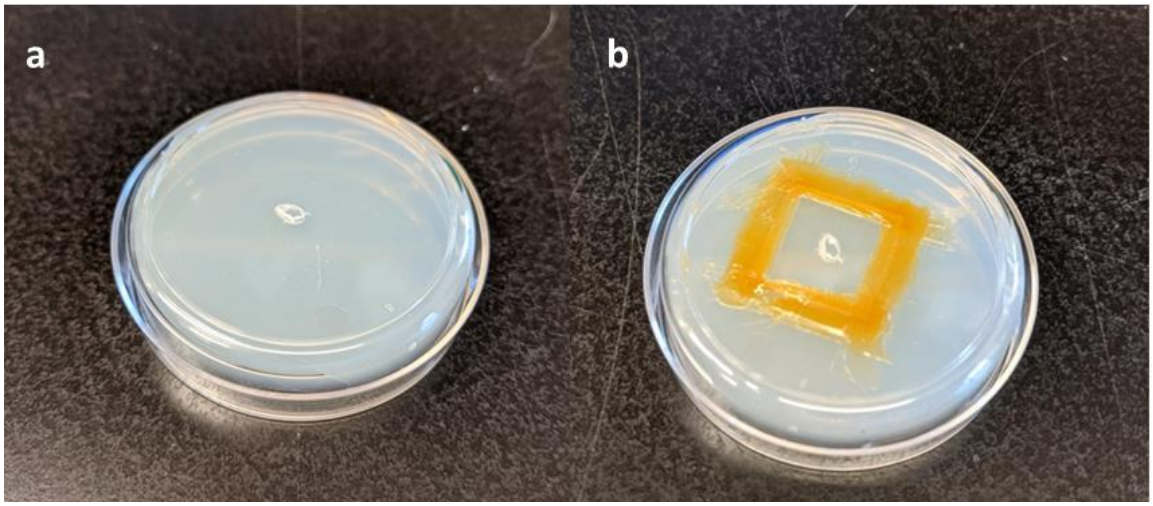

Fig. 6 Alternative method to prevent the embryo from settling during live imaging. Plate designed to prevent settling (sinking) of embryos. (**a**) NGM plate with hole where embryos will be placed. (**b**) Plate after the coverslip has been added and sealed with petroleum jelly (for details, see video link: https://www.youtube.com/watch?v=q9GlxGfvEiQ)

```
ls -lt > qc1

ls -1 | sed 's/.tif//g' | sed 's/_/ _/g' | awk '{print $6}' | sed 's/_/
sort -k 1,1 | uniq | grep -v "(" | grep t | awk '{print "mkdir "$1}' >
directory.sh

sh directory.sh

ls -lt > qc2

ls -1 | grep tif | sed 's/_/ /g' | sed 's/.tif/ .tif/g'| awk '{print
$6"\t"$7}' | sort -k 1,1 | uniq | awk '{print "mv *"$1$2" "$1"/"}' > mv

sh mv.sh
```

Fig. 7 This Linux AWK command can be used to group images by each timepoint.

```
/*
 * Macro template to process multiple images in a folder
 */

#@ File (label = "Input directory", style = "directory") input
#@ File (label = "Output directory", style = "directory") output
#@ String (label = "File suffix", value = ".tif") suffix

// See also Process_Folder.py for a version of this code
// in the Python scripting language.
setBatchMode(true);
processFolder(input);

// function to scan folders/subfolders/files to find files with correct suffix
function processFolder(input) {
	list = getFileList(input);
	list = Array.sort(list);
	for (i = 0; i < list.length; i++) {
		if(File.isDirectory(input + File.separator + list[i]))
			processFolder(input + File.separator + list[i]);
		if(endsWith(list[i], suffix))
			processFile(input, output, list[i]);
	}
}

function processFile(input, output, file) {
	// Do the processing here by adding your own code.
	// Leave the print statements until things work, then remove them.

	print("Processing: " + input + File.separator + file);
  open(input + File.separator + file);
	outfile = output + File.separator + file;
	ofile="[" + outfile + "]";

	run("Image... ", "outputfile=&ofile display=&ofile");
	//run("Image... ", "outputfile=[&outfile] display=&file"); only does 1
	print("file:" + file);
	close();
}
setBatchMode(false)
```

Fig. 8 ImageJ macro for formatting the images prior to running on StarryNite

References

1. Fitz-James MH, Cavalli G (2022) Molecular mechanisms of transgenerational epigenetic inheritance. Nat Rev Genet 23(6):325–341
2. Miska EA, Ferguson-Smith AC (2016) Transgenerational inheritance: models and mechanisms of non-DNA sequence-based inheritance. Science 354:59–63
3. Brenner S (1974) The genetics of Caenorhabditis elegans. Genetics 77:71–94
4. Greer EL, Maures TJ, Ucar D et al (2011) Transgenerational epigenetic inheritance of longevity in Caenorhabditis elegans. Nature 479:365–371
5. Katz DJ, Edwards TM, Reinke V et al (2009) A *C. elegans* LSD1 demethylase contributes to germline immortality by reprogramming epigenetic memory. Cell 137:308–320
6. Lee TW, David HS, Engstrom AK et al (2019) Repressive H3K9me2 protects lifespan against the transgenerational burden of COMPASS activity in *C. elegans*. eLife 8:e48498
7. Moore RS, Kaletsky R, Murphy CT (2019) Piwi/PRG-1 argonaute and TGF-beta mediate transgenerational learned pathogenic avoidance. Cell 177:1827–1841 e1812
8. Posner R, Toker IA, Antonova O et al (2019) Neuronal small RNAs control behavior transgenerationally. Cell 177:1814–1826 e1815
9. Sulston JE, Horvitz HR (1977) Post-embryonic cell lineages of the nematode, Caenorhabditis elegans. Dev Biol 56:110–156
10. Bao Z, Murray JI, Boyle T et al (2006) Automated cell lineage tracing in Caenorhabditis elegans. Proc Natl Acad Sci U S A 103:2707–2712
11. Murray JI, Bao Z, Boyle TJ et al (2006) The lineaging of fluorescently-labeled Caenorhabditis elegans embryos with StarryNite and AceTree. Nat Protoc 1:1468–1476
12. Boyle TJ, Bao Z, Murray JI et al (2006) AceTree: a tool for visual analysis of Caenorhabditis elegans embryogenesis. BMC Bioinform 7:275
13. Hashimshony T, Feder M, Levin M et al (2015) Spatiotemporal transcriptomics reveals the evolutionary history of the endoderm germ layer. Nature 519:219–222
14. Packer JS, Zhu Q, Huynh C et al (2019) A lineage-resolved molecular atlas of *C. elegans* embryogenesis at single-cell resolution. Science 365:eaax1971
15. Tintori SC, Osborne Nishimura E, Golden P et al (2016) A transcriptional lineage of the early *C. elegans* embryo. Dev Cell 38:430–444
16. Zacharias AL, Walton T, Preston E et al (2015) Quantitative differences in nuclear beta-catenin and TCF pattern embryonic cells in *C. elegans*. PLoS Genet 11:e1005585

CHAPTER 3

C. elegans Establishes Germline Versus Soma by Balancing Inherited Histone Methylation

Adapted from *C. elegans* establishes germline versus soma by balancing inherited histone methylation. Carpenter BS, Lee TW, Plott CF, **Rodriguez JD**, Brockett JS, Myrick DA, Katz DJ. Development. 2021 Feb 10;148(3):dev196600. doi: 10.1242/dev.196600. PMID: 33462111; PMCID: PMC7888751**.**

C. elegans establishes germline versus soma by balancing inherited histone methylation

Brandon S. Carpenter[1], Teresa W. Lee[1], Caroline F. Plott[2], **Juan D**. **Rodriguez[1]**, Jovan S. Brockett[3], Dexter A. Myrick[1], David J. Katz[1*]

[1]Department of Cell Biology, Emory University School of Medicine, Atlanta GA 30322, USA.

[2]Johns Hopkins University School of Medicine, Baltimore MD 21205, USA.

[3]Department of Biology, Oglethorpe University, Atlanta GA 30319, USA.

*corresponding author:
David J. Katz
Associate Professor
Department of Cell Biology
Room 443, Whitehead Biomedical Research Building
Emory University School of Medicine
Atlanta, GA 30322, USA
Phone: (404) 727-3403
djkatz@emory.edu

KEY WORDS

histone methylation, developmental delay, maternal reprogramming, transgenerational inheritance, epigenetics

SUMMARY STATEMENT

Maternally deposited histone modifying enzymes prevent the ectopic expression of germline genes in somatic tissues and developmental delay by coordinately regulating the inheritance of histone methylation.

ABSTRACT

Formation of a zygote is coupled with extensive epigenetic reprogramming to enable appropriate inheritance of histone methylation and prevent developmental delays. In *C. elegans,* this reprogramming is mediated by the H3K4me2 demethylase, SPR-5, and the H3K9 methyltransferase, MET-2. In contrast, the H3K36 methyltransferase, MES-4, maintains H3K36me2/3 at germline genes between generations to facilitate re-establishment of the germline. To determine whether the MES-4 germline inheritance pathway antagonizes *spr-5; met-2* reprogramming, we examined the interaction between these two pathways. We find that the developmental delay of *spr-5; met-2* mutant progeny is associated with ectopic H3K36me3 and the ectopic expression of MES-4 targeted germline genes in somatic tissues. Furthermore, the developmental delay is dependent upon MES-4 and the H3K4 methyltransferase, SET-2. We propose that MES-4 prevents critical germline genes from being repressed by antagonizing maternal *spr-5; met-2* reprogramming. Thus, the balance of inherited histone modifications is necessary to distinguish germline versus soma and prevent developmental delay.

INTRODUCTION

In multicellular organisms, developmental cell fate decisions are established by tightly controlled spatial and temporal gene expression (Frum and Ralston, 2015; Gregor et al., 2014; Maduro, 2010). One key control of gene expression is through the regulation of histone methylation, which controls gene expression by regulating the accessibility of DNA to transcription factors and RNA polymerase (Burton and Torres-Padilla, 2014; Hirabayashi and Gotoh, 2010; Jambhekar et al., 2019). For example, methylation of either lysine 4 or 36 on histone 3, (H3K4me and H3K36me) is associated with active transcription, whereas methylation of lysine 9 on the same histone (H3K9me) is commonly associated with transcriptional repression (Bannister et al., 2005; Barski et al., 2007; Bernstein et al., 2002; 2005). In addition, histone methylation on the N-terminal tails of histone proteins can be heritable through cell division, and across generations via both the sperm and oocyte. Inheritance of histone methylation across generations results in the maintenance of transcriptional states, which can affect the development and survivability of the offspring (Gaydos et al., 2014; Jambhekar et al., 2019; Kaneshiro et al., 2019; Öst et al., 2014; Siklenka et al., 2015; Tabuchi et al., 2018).

Histone methylation is dynamically regulated by the specific and tightly controlled activity of histone modifying enzymes (Morgan and Shilatifard, 2020), which regulate gene expression during development (Jambhekar et al., 2019). For example, mono- and di-methylation of lysine 4 on histone H3 (H3K4me1/2) are removed by the demethylase LSD1/KDM1A (Y. Shi et al., 2004; Y.-J. Shi et al., 2005). In the nematode *C. elegans*, populations of mutants lacking the LSD1 ortholog, SPR-5, become increasingly sterile

over ~30 generations (Katz et al., 2009). Failure to erase H3K4me2 at fertilization between generations in *spr-5* mutants correlates with an accumulation of H3K4me2 and spermatogenesis gene expression across 30 generations, which leads to increasing sterility (Katz et al., 2009). These data demonstrate that H3K4me2 can function as an epigenetic transcriptional memory through cell divisions and across generations. In addition to transgenerational sterility, the accumulation of H3K4me2 in *spr-5* mutants is associated with meiotic defects, increased longevity and a synergistic increase in sterility in an *rbr-2* mutant background (Alvares et al., 2014; Greer et al., 2016; Nottke et al., 2011). These transgenerational phenotypes provide further evidence that H3K4 methylation functions as a transcriptional memory across generations.

More recently, it was demonstrated that SPR-5 synergizes with the H3K9me2 methyltransferase, MET-2, to regulate maternal epigenetic reprogramming (Greer et al., 2014; Kerr et al., 2014). Progeny of mutants lacking both SPR-5 and MET-2 suffer from developmental delay and become completely sterile in a single generation. These phenotypes are associated with synergistic increases in both H3K4me2 and candidate germline gene expression in somatic tissues (Kerr et al., 2014). Together this work supports a model in which SPR-5 and MET-2 are maternally deposited into the oocyte, where they reprogram histone methylation to prevent inherited defects. Consistent with H3K9 methylation functioning together with the erasure of H3K4me2, loss of the histone demethylase JMJD-2, which can demethylate H3K9, partially suppresses the transgenerational sterility caused by loss of SPR-5 (Greer et al., 2014).

Following fertilization, the *C. elegans* embryo separates germline versus somatic lineages progressively through a series of asymmetric divisions (Strome, 2005). To

accomplish this, transcription factors coordinate with multiple histone modifications. For example, maternal deposition of PIE-1, a germline specific protein that asymmetrically segregates into germline blastomeres (P lineage cells), maintains the fate of germ cells by inhibiting POL-II elongation and preventing the ectopic expression of somatic genes (Batchelder et al., 1999; Mello et al., 1992; Seydoux et al., 1996). In the absence of transcription in the germline, the maternally provided H3K36me2/3 methyltransferase, MES-4, binds to a subset of germline genes that were previously expressed in the parental germline (Furuhashi et al., 2010; Rechtsteiner et al., 2010). These germline genes are recognized by MES-4 via H3K36me2/3 that was added in the parental germline by the transcription-coupled H3K36me2/3 methyltransferase, MET-1 (Kreher et al., 2018). MES-4 maintains H3K36me2/3 at these genes in the early embryo in a transcriptionally independent manner. Without maternally deposited MES-4, the germline cannot properly proliferate and animals are sterile (Capowski et al., 1991; Garvin et al., 1998). For the remainder of this study, we will refer to the genes that are bound by MES-4 and which maintain H3K36me3 throughout embryogenesis in a transcription independent fashion, as 'MES-4 germline genes'. In addition, the process through which the MES-4 germline inheritance system maintains these genes for re-activation in the offspring will be referred to as 'bookmarking'.

MES-4 bookmarking is antagonized in somatic tissues by transcriptional repressors and chromatin remodelers. For example, loss of the transcriptional repressors LIN-15B and LIN-35 at high temperatures leads to larval arrest (Petrella et al., 2011). This larval arrest can be suppressed by removing the MES-4 germline inheritance system (Petrella et al., 2011). Removing the MES-4 inheritance system also

suppresses the somatic expression of germline genes in *lin-35* mutants (Wang et al., 2005). Similar to LIN-15B and LIN-35, loss of the chromatin remodelers MEP-1 and LET-418 causes somatic expression of germline genes and larval arrest (Unhavaithaya et al., 2002). The somatic expression of germline genes and larval arrest in *mep-1* and *let-418* mutants is also dependent upon the MES-4 germline inheritance system (Unhavaithaya et al., 2002). Together, these findings demonstrate that transcriptional repressors antagonize H3K36 bookmarking by MES-4 in somatic tissues.

Recently, the repressive histone modification H3K9me2 has been implicated in the somatic repression of germline genes (Rechtsteiner et al., 2019). Some germline genes have H3K9me2 enrichment at their promoters in somatic tissues, suggesting that H3K9me2 mediates their repression somatically (Rechtsteiner et al., 2019). Loss of LIN-15B reduces this enrichment of H3K9me2 leading to the ectopic accumulation of H3K36me3 at gene bodies in somatic tissues (Rechtsteiner et al., 2019). This raises the possibility that LIN-15B may repress MES-4 germline inheritance in somatic tissues in part through the repressive histone modification H3K9me2. However, this model remains to be tested.

Despite the extensive knowledge of the transcriptional repression pathways that somatically antagonize the MES-4 germline inheritance system, it remains unclear why germline genes are bookmarked by H3K36 in the embryo. To address this gap, we examined somatic development in progeny deficient in SPR-5 and MET-2 maternal reprogramming. Our previous work suggests that maternal *spr-5; met-2* reprogramming prevents the transgenerational inheritance of H3K4me2 by erasing this mark and coupling it to the acquisition of H3K9me2 between generations (Kerr et al., 2014). Here

we show that H3K36me3 ectopically accumulates at MES-4 germline genes in the somatic tissues of *spr-5; met-2* double mutant progeny (hereafter referred to as *spr-5; met-2* progeny), and this accumulation correlates with the ectopic expression of these genes. In addition, we find that both the developmental delay and the ectopic expression of germline genes is rescued by RNAi-mediated depletion of MES-4 activity. These data provide evidence that the ectopic expression of MES-4 targeted germline genes in somatic tissues leads to developmental delay at the larval stage. In addition, we demonstrate that the severe developmental delay of *spr-5; met-2* progeny is rescued by the loss of the H3K4 methyltransferase SET-2. This finding suggests that the ectopic maintenance of the MES-4 germline inheritance system in *spr-5; met-2* progeny is driven by the inheritance of H3K4 methylation. Finally, by demonstrating that loss of maternal *spr-5; met-2* reprogramming leads to expression of MES-4 germline genes in somatic tissues, our data suggest that H3K36 methylation bookmarking functions to antagonize *spr-5; met-2* maternal reprogramming. Thus, we propose that *C. elegans* balances three different histone modifications to distinguish between the competing fates of soma and germline.

RESULTS

Loss of *spr-5* and *met-2* causes a severe developmental delay

Previous observations from our lab indicated that progeny from *spr-5; met-2* mutants may develop abnormally (Kerr et al., 2014). To further characterize this phenotype, we synchronized embryos laid by wild type (N2), *spr-5*, *met-2*, and *spr-5; met-2* mutant hermaphrodites and monitored their development from hatching to adults.

By 72 hours, all wild type progeny (469/469), most of the *spr-5* progeny (363/385), and many of *met-2* progeny (386/450) were fertile adults (Fig. 1A, B, C, and E, Fig. S1A-C). In contrast, *spr-5; met-2* progeny displayed a severe developmental delay, with none of the progeny (0/463) reaching adulthood by 72 hours (Fig. 1D, E; and Fig. S1D). The majority of *spr-5; met-2* progeny (371/463) resembled L2 larvae at 72 hours, while a smaller percentage of the population developed to later larval stages (42/463) (supplementary file 1). This larval delay occurs despite embryogenesis being accelerated in *spr-5; met-2* progeny versus wild type (Fig. S2). This indicates that the larval delay is not just due to a general delay in all cell divisions. By seven days post synchronized lay, a small number of *spr-5; met-2* progeny (35/876) developed into adults and the majority (31/35) of these adults displayed protruding vulva (Pvl) (Fig. S1E-G and (Kerr et al., 2014)). All 35 of the *spr-5; met-2* mutant progeny that developed to adulthood were sterile.

MES-4 germline genes are ectopically expressed in *spr-5; met-2* mutant soma

Previously we showed that H3K4me2 is synergistically increased in *spr-5; met-2* progeny compared to *spr-5* and *met-2* single mutant progeny, and that this increase in H3K4me2 correlates with a synergistic increase in candidate germline gene expression in somatic tissues (Kerr et al., 2014). To test the extent to which germline genes are ectopically expressed in somatic tissues, we examined somatic expression genome-wide. To do this, we performed RNA-seq on *spr-5; met-2* L1 progeny compared to wild type L1 progeny. We chose to perform this analysis on L1 larvae because this stage immediately precedes the L2 larval delay that we observe in *spr-5; met-2* progeny (see

Fig. 1D). In addition, L1 larvae are composed of 550 somatic cells and two germ cells. Therefore, L1 larvae are primarily composed of somatic tissue. As a control, we also performed RNA-seq on L1 progeny from *spr-5* and *met-2* single mutants that were isolated from early generation animals, within the first five generations. These generations are well before the onset of sterility that we previously reported (Katz et al., 2009; Kerr et al., 2014).

We identified 778 differentially expressed transcripts in *spr-5; met-2* progeny compared to wild type (Fig. S3A-B, Fig. S4C, F, and supplementary file 4), many of which also overlap with genes differentially expressed in *spr-5* (113/343, hypergeometric test, p-value <6.88e-75) and *met-2* single mutants (159/413, hypergeometric test, p-value < 7.15e-119) compared to wild type (Fig. S3A-B, Fig. S4A, B, D, E, and supplementary file 2-3). Gene Ontology (GO) analysis did not identify any categories of genes misexpressed in the *spr-5* or *met-2* single mutants. However, the GO analysis revealed that genes differentially expressed in *spr-5; met-2* progeny were significantly enriched (based on Combined Score, (Chen et al., 2013)) for biological processes and cellular components characteristic of the germline; including meiosis, P-granules and negative regulation of the cell cycle (Fig. S3C-D). Many of these germline functioning genes are expressed in the germline of the parental generation, bound by the H3K36 methyltransferase MES-4 in the early embryo, and marked by H3K36me2/3, independent of POL-II (referred to as MES-4 germline genes) (Rechtsteiner et al., 2010). As a result, we were interested in the potential overlap between genes that are misregulated in *spr-5; met-2* progeny and MES-4 germline genes.

Rechtsteiner and colleagues identified approximately 200 MES-4 germline genes (Rechtsteiner et al., 2010). We reasoned that the absence of SPR-5 and MET-2 reprogramming may cause these germline genes to be aberrantly targeted by MES-4 in the soma, leading to ectopic expression. To investigate this possibility, we examined the overlap between differentially expressed genes in *spr-5; met-2* L1 progeny and MES-4 germline genes. Out of 196 MES-4 germline genes, 34 overlapped with genes up-regulated in *spr-5; met-2* progeny compared to wild type (Fig. S5A, hypergeometric test, p-value < 6.44e-20), while zero overlapped with genes down-regulated in *spr-5; met-2* progeny compared to wild type (Fig. S5B). In addition, when we compared the log2 fold change (FC) in expression of all of the MES-4 germline genes in *spr-5*, *met-2*, and *spr-5; met-2* mutant progeny compared to wild type, we observed that 108 of the MES-4 germline genes were synergistically increased in *spr-5; met-2* progeny compared to single mutant progeny (Fig. S5C and supplementary file 6).

During this initial RNA-seq analysis we had to genotype every *spr-5; met-2* L1 because the balancer chromosome (a chromosome that blocks homologous recombination) that was available did not completely balance *spr-5*. As a result, the RNA-seq was performed using a low-input sequencing technique (see methods). However, during the course of the experiments, a new balancer became available that completely balances *spr-5*. This enabled us to repeat the *spr-5; met-2* RNA-seq experiments using standard amounts of RNA. In the repeat *spr-5; met-2* RNA-seq experiment (referred to as repeat experiment two), we identified significantly more differentially expressed genes compared to wild type (4223 vs. 778 in the initial low-input analysis, Fig. S6A-B). However, despite the larger number of differentially

expressed genes, MES-4 germline genes remained similarly enriched. Out of 196 MES-4 germline genes, 112 overlapped with genes up-regulated in *spr-5; met-2* progeny compared to wild type (Fig. 2A, hypergeometric test, P-value < 1.20e-54, Fig. S6C-D, and supplementary file 5), while only two overlapped with genes down-regulated in *spr-5; met-2* progeny compared to wild type (Fig. 2B). We also compared the log2FC in expression of all of the MES-4 germline genes in *spr-5; met-2* mutant progeny compared to wild type. This analysis revealed that the MES-4 germline genes in repeat experiment two were similarly overexpressed in *spr-5; met-2* progeny compared to wild type (Fig. 2C, Fig. S6E and supplementary file 6). Interestingly, while MES-4 germline genes were enriched in both *spr-5; met-2* RNA-seq experiments, there were some differences in the specific MES-4 germline genes that were overexpressed, and the extent to which they were overexpressed (Fig. S6E and supplementary file 6).

smFISH confirmation of MES-4 germline gene expression in *spr-5; met-2* mutant soma

To confirm that MES-4 germline genes are somatically expressed in *spr-5; met-2* L1 progeny, we performed single molecule fluorescent *in situ* hybridization (smFISH) on two MES-4 germline targets, *htp-1* and *cpb-1* (Fig. 3). Both of these genes were amongst the genes that were ectopically expressed in *spr-5; met-2* L1 progeny compared to wild type L1 progeny. In wild type L1 larvae, *htp-1* (Fig. 3A-C, insets) and *cpb-1* (Fig. 3G-I, insets) were restricted to the two primordial germ cells, Z2 and Z3, which go on to form the entire adult germline. This confirms that these transcripts are confined to the germline as expected. In contrast, in *spr-5; met-2* progeny *htp-1* was

ectopically expressed throughout the soma (Fig. 3D-F). This expression pattern is similar to what we observed with the ubiquitously expressed subunit of RNA polymerase II, *ama-1* (Fig. S7), which was unchanged in our RNA-seq analysis. *cpb-1* was also ectopically expressed in *spr-5; met-2* progeny, though the ectopic expression was not as ubiquitous as *htp-1* (Fig. 3J, L). To determine if *htp-1* is also ectopically expressed in earlier embryonic stages, we performed smFISH on the embryos of *spr-5; met-2* progeny. In wild type embryos, *htp-1* is restricted to Z2 and Z3 at the 200+ cell stage (Fig. 8SA-C). In contrast, in *spr-5; met-2* progeny at the 200+ cell stage we detect the ectopic expression of *htp-1* (Fig. S8D-F), indicating that *htp-1* is ectopically expressed prior to the L1 larval stage.

MES-4 germline genes maintain ectopic H3K36me3 in *spr-5; met-2* mutants

To test whether MES-4 germline genes that are ectopically expressed in the soma of *spr-5; met-2* progeny also ectopically maintain H3K36me3, we performed H3K36me3 ChIP-seq. MES-4 germline genes have low levels of H3K36me3 in wild type L1 progeny. However, compared to wild type L1 progeny, *spr-5; met-2* L1 progeny displayed increased enrichment for H3K36me3 across gene bodies at MES-4 germline genes (Fig. 4A-C; Fig. S9A-C, W, X). For example, the MES-4 germline genes *cpb-1*, *T05B9.1, Y18D10A.11*, *fbxa-101* and *htp-1* that are ectopically expressed in our RNA-seq analysis, showed increased levels of H3K36me3 in *spr-5; met-2* progeny (Fig. 4O-S; Fig. S9O-S) compared to wild type progeny (Fig. 4G-K; Fig. S9G-K). As a control, we examined H3K36me3 enrichment at genes that are not affected in *spr-5; met-2* progeny. These control genes include: *ceh-13*, a gene enriched in hypodermal and

ventral nerve chord in L1 progeny (Fig. 4L, T; Fig. S9L, T), *ama-1*, a subunit of RNA polymerase II that is expressed ubiquitously (Fig. 4M, U; Fig. S9M, U), and *act-1*, a ubiquitously expressed actin related protein (Fig. 4N, V; Fig. S9N, V). Each of these control genes displayed similar H3K36me3 enrichment in both *spr-5; met-2* and wild type L1 progeny (compare Fig. 4T-V and Fig. S9T-V to Fig. 4L-N and Fig. S9L-N, respectively). In addition, we found that the enrichment in H3K36me3 is substantially reduced when we examine H3K36me3 across all germline genes (Fig. 4D-F; Fig. S9D-F). This suggests that the enrichment in H3K36me3 is confined to the subset of germline genes that are MES-4 targets.

MES-4 germline genes display H3K9me2 at their promoter peaks

Recent work discovered that some germline specific genes contain H3K9me2 peaks at their promoters in wild type L1 progeny (Rechtsteiner et al., 2019). This finding implicates H3K9me2 enrichment at promoters of germline genes as being a critical component for repressing germline genes in somatic tissues. If SPR-5 and MET-2 are functioning to prevent MES-4 germline genes from being ectopically expressed in somatic tissues, we would expect MES-4 germline genes that are ectopically expressed in the somatic tissues of *spr-5; met-2* progeny to normally continue to be targeted by H3K9 methylation in these tissues. To examine this possibility, we re-analyzed L1 stage H3K9me2 Chip-seq data from Rechsteiner et al. 2019 (Rechtsteiner et al., 2019). This re-analysis showed that many of the MES-4 germline genes were enriched for H3K9me2 at their promoters (Fig. S10A), including the majority of MES-4 germline genes that were ectopically expressed in the soma of *spr-5; met-2* progeny (Fig. S10B).

For example, the MES-4 germline genes *cpb-1*, *T05B9.1*, *Y18D10A.11*, *fbxa-101* and *htp-1* that were misexpressed somatically and accumulated ectopic H3K36me3 in the somatic tissues of *spr-5; met-2* progeny, had H3K9me2 peaks at their promoters (Fig. S10C-G). In contrast, our control genes *ceh-13*, *ama-1*, and *act-1*, that were not misexpressed, were also not enriched for H3K9me2 at their promoters (Fig. S10H-J).

Knocking down MES-4 rescues ectopic expression of germline genes in *spr-5; met-2* mutant soma

To test whether the ectopic expression of MES-4 germline genes in *spr-5; met-2* progeny is dependent on the ectopic H3K36me3, we examined whether the expression of these genes was dependent upon MES-4. We performed quantitative real-time PCR (qRT-PCR) on L1 progeny from *spr-5; met-2* hermaphrodites fed control (L4440) RNAi versus *mes-4* RNAi (Fig. 5). For this analysis, we selected candidate MES-4 germline genes that were ectopically expressed and displayed an ectopic H3K36me3 peak in *spr-5; met-2* L1 progeny compared to wild type L1 progeny. Consistent with our RNA-seq analysis, all nine of the candidate MES-4 germline genes that we examined were ectopically expressed >2 fold in *spr-5; met-2* L1 progeny compared to wild type L1 progeny (Fig. 5). Strikingly, the ectopic expression of the nine MES-4 candidate germline genes was dependent upon MES-4. Nine out of nine of these genes were significantly decreased in L1 progeny from *spr-5; met-2* hermaphrodites treated with *mes-4* RNAi (Fig. 5; unpaired t-test, p-value < 0.001), and all but one (*T05B9.1*) were reduced to levels that were similar to wild type L1 progeny. During this analysis, expression levels were normalized to the ubiquitously expressed large subunit of RNA

polymerase (AMA-1), which was unaffected. This suggests that the effects of *mes-4* RNAi are confined to the ectopically expressed MES-4 germline genes. Additionally, to confirm that the reduced expression of MES-4 germline genes in *spr-5; met-2* progeny treated with *mes-4* RNAi was due to the elimination of the ectopic expression of MES-4 germline genes, we performed smFISH on the two MES-4 germline targets, *htp-1* and *cpb-1,* in L1 progeny from *spr-5; met-2* hermaphrodites fed control (L4440) RNAi versus *mes-4* RNAi (Fig. S11). *mes-4* RNAi eliminated the ectopic smFISH signal. This demonstrated that the expression of these two MES-4 germline targets in somatic tissues was dependent upon MES-4.

MES-4 is not ectopically expressed in *spr-5; met-2* progeny

It is possible that SPR-5 and MET-2 may target MES-4 germline genes directly. Alternatively, SPR-5 and MET-2 could target the *mes-4* locus, resulting in indirect effects on MES-4 germline genes. To distinguish between these possibilities, we determined whether MES-4 is ectopically expressed in *spr-5; met-2* progeny by examining the expression of a MES-4::GFP transgene in these animals. We do not detect any ectopic expression of MES-4 in *spr-5; met-2* progeny (Fig. S12). This suggests that SPR-5 and MET-2 do not function indirectly by repressing *mes-4.*

Knocking down MES-4 rescues developmental delay in *spr-5; met-2* progeny

To test whether the developmental delay phenotype that we observe in *spr-5; met-2* progeny is also dependent on the ectopic expression of MES-4 germline genes, we fed *spr-5; met-2* hermaphrodites *mes-4* RNAi and monitored their progeny for 72

hours after a synchronized lay. If the developmental delay is dependent upon the ectopic expression of MES-4 germline genes, it should be suppressed when this ectopic expression is eliminated via *mes-4* RNAi. By 72 hours, all of the wild type progeny from hermaphrodites fed either L4440 control (1089/1089) or *mes-4* (1102/1102) RNAi were adults (Fig. 6A, B, and G). Also, consistent with our previous observations, all but one of the *spr-5; met-2* mutant progeny (729/730) from hermaphrodites fed control RNAi remained in the L2-L3 larval stages (Fig. 6D, G). In contrast, most of *spr-5; met-2* progeny (569/618) from hermaphrodites fed *mes-4* RNAi developed to adults (Fig. 6E, G, unpaired t-test, $p<0.0001$). Though as expected, these animals remained sterile due to the *mes-4* RNAi preventing any germline formation.

Knocking down SET-2 rescues *spr-5; met-2* developmental delay

If the developmental delay of *spr-5; met-2* mutants is caused by ectopic inheritance of H3K4me2 driving the expression MES-4 germline genes in somatic tissues, we would expect the developmental delay of *spr-5; met-2* progeny to be dependent upon the H3K4 methyltransferase, SET-2. To test this, we monitored the development of progeny of *spr-5; met-2* hermaphrodites fed *set-2* RNAi for 72 hours after a synchronized lay. Identical to wild type progeny from hermaphrodites fed control RNAi, *set-2* RNAi had no effect on the development of wild-type animals, as all of the wild type progeny from hermaphrodites fed *set-2* RNAi developed to adults by 72 hours (1114/1114) (Fig. 6C, G). However, in contrast to *spr-5; met-2* progeny fed control RNAi that were developmentally delayed, most of the progeny from *spr-5; met-2*

hermaphrodites fed *set-2* RNAi developed to adults (347/384) (Fig. 6F, G, unpaired t-test, $p<0.0001$).

spr-5; met-2 progeny acquire transgene silencing in somatic tissues

The somatic expression of MES-4 germline genes involved in germline transgene silencing (Fig. S4C and Fig. S5C) raises the possibility that the somatic tissues in *spr-5; met-2* progeny may acquire the ability to silence transgenes, a function normally restricted to germline cells. To test this, we examined the somatic expression of an extrachromosomal multicopy *let-858* transgene that is normally silenced in the germline by both transcriptional and posttranscriptional germline silencing mechanisms (Kelly and Fire, 1998). This analysis was performed in *spr-5; met-2* mutant L2 larvae that were undergoing developmental delay. In wild type, most of the L2 progeny (117/132) expressed ubiquitous high levels of LET-858::GFP throughout the entire soma (Fig. 7A, B, and K), while the remaining progeny (15/132) expressed what we describe as a "faint" level of expression (Fig. 7C, D, and K). In contrast, almost none of the *spr-5; met-2* L2 progeny (2/87) displayed high level of transgene expression that is comparable to the high level seen in most wild type progeny (Fig. 7E, F, and K). Instead, the majority of *spr-5; met-2* progeny (64/87) had faint LET-858::GFP expression that is comparable to the faint expression observed in wild type progeny (Fig. 7G, H, and K). The remaining 21 *spr-5; met-2* progeny had no LET-858::GFP expression. Because less than 50% of progeny inherited the *let-858* transgene, we normalized the percentage of progeny scored as "off" for LET-858::GFP to the presence of the *let-858* transgene based on genotyping for *gfp* (see methods). For wild type, all of the 60 L2 progeny that were

scored as “off” failed to inherit the *let-858* transgene, indicating that the transgene is never silenced in wild type progeny (data not shown). However, for *spr-5; met-2* L2 progeny, eight out of 50 progeny that were scored as “off” inherited the *let-858* transgene indicating that the *let-858* transgene can be completely silenced in some *spr-5; met-2* progeny. After normalization for the transgene inheritance, we observed that 21/87 of *spr-5; met-2* progeny displayed no visible expression of the LET-858::GFP transgene (Fig. 7I, J, and K).

DISCUSSION

spr-5; met-2 maternal reprogramming prevents developmental delay by restricting ectopic MES-4 bookmarking

SPR-5 and MET-2 act maternally to reprogram histone methylation and prevent the transcriptional state of the parent from being inappropriately transmitted to the offspring (Kerr et al., 2014). In this study, we find that the loss of SPR-5 and MET-2 maternal reprogramming led to a severe developmental delay that was associated with the ectopic expression of MES-4 germline genes in somatic tissues. This finding raises the possibility that SPR-5 and MET-2 reprogramming blocks the ectopic expression of MES-4 germline genes by preventing the accumulation of MES-4 dependent H3K36me3 at a subset of germline genes in somatic tissues. Consistent with this possibility, most of the MES-4 germline genes were increased in *spr-5; met-2* mutants compared to wild type in L1 larvae. Using smFISH, we confirmed the somatic expression of two ectopically expressed MES-4 germline genes, *htp-1* and *cpb-1*. While *htp-1* mRNA was ectopically detected in many somatic tissues, the ectopic expression

of *cpb-1* mRNA was more restricted, suggesting that the extent of ectopic expression is dependent upon the locus. However, further experiments are required to determine why some MES-4 germline genes may be more ectopically expressed than others.

In the absence of SPR-5 and MET-2 reprogramming, MES-4 germline genes accumulate ectopic H3K36me3 in the soma. This suggests that without SPR-5 and MET-2 reprogramming, MES-4 ectopically maintains H3K36me3 at these genes in somatic tissues. Consistent with this finding, Greer et al. previously reported that there are elevated bulk levels of H3K36me3 in mixed populations of *spr-5* single mutants (Greer et al., 2014). Of note, we observe a low level of H3K36me3 at germline genes in the somatic tissues of wild type progeny. It is unclear why there is a low level of H3K36me3 normally in somatic tissues in wild type animals. Nevertheless, the absence of transcription associated with this low level of H3K36me3 indicates that an increased level of H3K36me3 is necessary to cause ectopic transcription.

If the ectopic maintenance of H3K36me3 in the soma of *spr-5; met-2* mutant progeny is causing the developmental delay, then removal of MES-4 should rescue the ectopic expression and developmental delay. Indeed, we find that the removal of MES-4 rescued both the ectopic transcription of MES-4 germline genes in the soma of *spr-5; met-2* progeny, and the developmental delay. Taken together, our data provide evidence that the developmental delay of *spr-5; met-2* progeny is caused by the ectopic expression of MES-4 germline genes.

How does an ectopic transcriptional program interfere with developmental timing?

How does the ectopic expression of germline genes interfere with somatic tissues to cause developmental delay? One possibility is that the ectopic expression of MES-4 germline genes causes the soma to take on germline character. To begin to address this, we asked whether *spr-5; met-2* double mutants can silence an extrachromosomal array in somatic tissues. The silencing of extrachromosomal arrays is normally restricted to the germline (Kelly and Fire, 1998). However, we find that *spr-5; met-2* progeny acquired some ability to silence an extrachromosomal multicopy array in somatic cells. Consistent with this finding, loss of the somatic repressor LIN-35 also results in the somatic silencing of a GFP transgene (Wang et al., 2005), suggesting that LIN-35 also contributes to the repression of germline genes in somatic tissues.

In the *spr-5; met-2* mutant RNA-seq we detected the ectopic expression of RNA-dependent RNA polymerase genes (e.g. *rrf-1* and *gld-2*) as well as genes involved in the RNAi effector complex (e.g. *hrde-1* and *ppw-1*) (supplementary file 13). These pathways have previously been implicated in gene silencing (Buckley et al., 2012; Sijen et al., 2001; Tijsterman et al., 2002). Thus, similar to what has been found in *lin-35* mutants (Wang et al., 2005), it is possible that the somatic silencing of the transgene in *spr-5; met-2* mutants is due to the induction of the germline small RNA pathway. In a reciprocal fashion, heritable silencing via small RNAs requires MET-2 (Lev et al., 2017). This interaction between MET-2 and small RNAs in the germline is consistent with the possibility that the chromatin and small RNA pathways may also be functioning together in the soma.

Normally in L1 larvae, the primordial germ cells, Z2 and Z3, are arrested at the G2/M checkpoint (Fukuyama et al., 2006). In the *spr-5; met-2* mutant RNA-seq, we

detected the ectopic expression of genes involved in the negative regulation of proliferation and the cell cycle, as well as G2/M checkpoint genes. Thus, it is possible that ectopic expression of germline genes normally expressed only in Z2 and Z3 contributes to the developmental delay through the ectopic activation of germline cell cycle control. Regardless, the silencing of the extrachromosomal multicopy array suggests that the somatic tissues in *spr-5; met-2* progeny make functional proteins that can perform some germline functions. We propose that either ectopic germline transcription, or an ectopic germline function resulting from this ectopic transcription, interferes with the ability of somatic cells to properly enact their transcriptional program. This background noise delays the proper adoption of cell fate, leading to an overall delay in the development of the tissue.

A model for how the inheritance of histone methylation is balanced to specify germline versus soma

By linking maternal *spr-5; met-2* reprogramming to the MES-4 germline inheritance system, our data provide a rationale for the existence of MES-4 bookmarking, through the following model. *spr-5; met-2* reprogramming prevents H3K4me2 transcriptional memory from being inappropriately propagated from one generation to the next. MES-4 antagonizes this reprogramming to help germline genes reactivate in the embryonic germline. When *spr-5; met-2* reprogramming is defective, MES-4 ectopically maintains H3K36me3 in the soma, causing developmental delay.

The model that we are proposing is based on the following evidence. In the germline, transcriptional elongation is blocked by PIE-1, which segregates to germline

blastomeres during embryogenesis (Batchelder et al., 1999; Mello et al., 1992; Seydoux et al., 1996) (Fig. 8A, B). In the soma of the early embryo, there is also very little transcription, because the bulk of zygotic transcription does not begin until approximately the 60-cell stage. This stage is just prior to when the primordial germ cells, Z2 and Z3, are specified (Sulston et al., 1983). Thus, in *C. elegans,* germline versus soma is largely specified without transcription.

During normal maternal reprogramming, SPR-5 and MET-2 are deposited into the oocyte. At fertilization they facilitate the reprogramming of previously expressed genes from an active chromatin state to a repressed chromatin state by removing H3K4me2 and adding H3K9me2 (Kerr et al., 2014) (Fig. 8A). This reprogramming is necessary to prevent the transcriptional memory of the previous generation from being inappropriately propagated to the progeny. Genes epigenetically reprogrammed by SPR-5 and MET-2 include ubiquitously expressed genes and germline expressed genes, a subset of which are MES-4 germline genes. The MES-4 germline genes are subsequently targeted by the transcription independent H3K36 methyltransferase, MES-4, to maintain H3K36me3 in the germ lineage during embryogenesis (Fig. 8A, B). We propose that H3K36 methylation bookmarking antagonizes the repression caused by the erasure of H3K4me2 and the addition of H3K9me2. Without the transcription independent maintenance of inherited H3K36 methylation from the mother to antagonize this repression, the germline fails to proliferate and animals are sterile (Capowski et al., 1991; Garvin et al., 1998). The failure to proliferate and sterility caused by loss of MES-4 may be in part because germline genes that are targeted by MES-4 fail to reactivate, though it has yet to be demonstrated. Thus, the MES-4 bookmarking

system may be necessary for critical germline genes to bypass the global epigenetic reprogramming that occurs at fertilization to prevent transgenerational inheritance. We refer to this initial phase of filtering inherited histone methylation at fertilization as the establishment phase. Importantly, since multiple studies have shown that small RNAs are required for transgenerational inheritance (Ashe et al., 2012; Buckley et al., 2012; Lev et al., 2017), it is possible that small RNAs facilitate the inheritance of MES-4 dependent H3K36 methylation. The ectopic expression of some RNA machinery in *spr-5; met-2* double mutants hints at this potential connection. However, no direct link has been found yet between small RNAs and the MES-4 inheritance system.

Following this establishment phase, a maintenance phase is required to propagate this initial pattern of histone methylation throughout embryogenesis. The MES-4 bookmarking system is localized primarily to the primordial germ cells in later embryonic development (Furuhashi et al., 2010; Rechtsteiner et al., 2010). This concentration of MES-4 to the germline helps to maintain MES-4 bookmarking for germline specification later in embryonic development. However, MES-4 is also present in somatic cells (Furuhashi et al., 2010; Rechtsteiner et al., 2010). This makes germline genes targeted by MES-4 vulnerable to the ectopic maintenance of H3K36me3 bookmarking by MES-4 in the soma. Consistent with MES-4 being present in somatic cells during embryogenesis, we first detect the ectopic expression of *htp-1* in the embryo, after zygotic genome activation. The presence of MES-4 in somatic cells during embryogenesis may explain why additional transcriptional repressors, such as LIN-15B and LIN-35, as well as MEP-1 and LET-418, function in somatic tissues to restrict H3K36 bookmarking by MES-4 to the germline. Thus, in the maintenance phase, the

balance of MES-4 and the pathways that somatically antagonize MES-4, maintain the histone methylation pattern that is initiated during the establishment phase. Interestingly, LET-418 may also help to maintain SPR-5 repression in the *C. elegans* germline, as SPR-5 and LET-418 have been shown to function synergistically to prevent somatic reprogramming of germline stem cells (Käser-Pébernard et al., 2014). Taken together, we propose that SPR-5, MET-2 and MES-4 carefully balance the inheritance of three different histone modifications, H3K4, H3K9, and H3K36 methylation, to ensure the proper specification of germline versus soma in the absence of transcription.

The model that we have proposed makes the following two predictions. First, MES-4 germline genes should normally be targeted for continued silencing by H3K9me2 in somatic tissues. It has recently been shown that a subset of germline specific genes contain H3K9me2 at their promoters in somatic tissues (Rechtsteiner et al., 2019). We re-examined the H3K9me2 ChIP-seq dataset from this work and found that the MES-4 germline genes that are ectopically expressed in the somatic tissues of *spr-5; met-2* progeny also displayed unique H3K9me2 promoter peaks. This confirms that MES-4 germline genes are normally repressed by H3K9me2 in somatic tissues.

The second prediction from our model is that the ectopic inheritance of H3K4 methylation at MES-4 germline genes overwhelms the somatic repression systems. Despite the presence of these transcriptional repressor complexes and chromatin remodelers to antagonize MES-4 bookmarking in the soma, loss of *spr-5; met-2* maternal reprogramming results in the somatic expression of MES-4 germline genes. This suggests that the failure to add H3K9me2, as well as the inappropriate retention of H3K4me2, results in a chromatin environment that is permissive for the ectopic

maintenance of H3K36me3 in the soma, even in the presence of the pathways that repress MES-4 bookmarking somatically (Fig. 8B). If this is the case, then the developmental delay in *spr-5; met-2* progeny should also be dependent upon the activity of the H3K4 methyltransferase. We find that RNAi-mediated depletion of SET-2, the H3K4me1/2 methyltransferase, rescued the developmental delay that we observe in *spr-5; met-2* progeny. These findings suggest that the inheritance of ectopic H3K4 methylation enables the ectopic accumulation of MES-4 dependent H3K36me3, and the subsequent ectopic expression of MES-4 germline genes in somatic tissues of *spr-5; met-2* progeny. Consistent with SPR-5 and MET-2 functioning directly at MES-4 targets, we find no evidence of ectopic MES-4 in *spr-5; met-2* progeny. It is not entirely clear how the subsequent ectopic maintenance of H3K36me3 facilitates ectopic expression. However, it should be noted that there were some differences in which MES-4 germline genes were ectopically expressed between our two *spr-5; met-2* RNA-seq experiments. This stochasticity is consistent with H3K36me3 being permissive, rather than instructive, for transcription. If this is the case, it is doubtful that the *spr-5; met-2* developmental delay is caused by the inappropriate expression of any single MES-4 germline gene. Rather, it is likely that the developmental delay is caused by either the inappropriate expression of multiple MES-4 germline genes, or the ectopic activation of the MES-4 germline program.

The model that we have presented here is composed of two phases, an initiation phase and a maintenance phase. The timing of these two phases is consistent with the known expression patterns of the enzymes in *C. elegans*. For example, maternal SPR-5 is present in the early embryo up to the 8-cell stage, but gone in later embryos (Katz et

al., 2009). In contrast, maternal MES-4 continues to be expressed in much later staged embryos (Rechtsteiner et al., 2010). The timing presented in our model is also partially based on the known requirement for maternal LSD1 (vertebrate SPR-5 ortholog) to function between fertilization and the two-cell stage in mice (Wasson et al., 2016). Nevertheless, no definitive evidence exists that the two phases are distinct timing wise. Thus, further investigation will be required to substantiate the proposed timing in our model.

Conservation of maternal epigenetic reprogramming between invertebrates and vertebrates

Epigenetic reprogramming at fertilization is a problem that all sexually reproducing organisms must solve (Lee and Katz, 2020). Thus, it is possible that the mechanisms of epigenetic reprogramming may be conserved. Along with the Heard lab, we previously demonstrated that progeny from mice that lack maternal KDM1A/LSD1 ectopically maintain the expression of germline genes in the embryo, leading to embryonic arrest at the two-cell stage (Ancelin et al., 2016; Wasson et al., 2016). Similarly, maternal loss of the MET-2 ortholog SETDB1 or the MES-4 ortholog NSD1 in mice results in early embryonic lethality (J. Kim et al., 2016; Rayasam et al., 2003). Together these results underscore the developmental importance of properly regulating histone methylation between generations and raise the possibility that the mechanism we have uncovered is conserved in mammals.

The model that we have proposed may also help explain the mechanism underlying patients harboring mutations in various histone-modifying enzymes. Recent

genome sequencing has revealed that several neurodevelopmental disorders are caused by mutations in histone modifying enzymes (extensively reviewed by (J.-H. Kim et al., 2017). These include mutations in: 1) the H3K36 methyltransferase *Setd2* and the H3K27 demethylase *Kdm6a,* which cause Kabuki Syndrome (Lederer et al., 2012), 2) the human ortholog of *spr-5, Lsd1,* which causes a Kabuki-like Syndrome (Chong et al., 2016; Tunovic et al., 2014), and 3) the H3K36 methyltransferase *Nsd1* which causes Sotos Syndrome (Kurotaki et al., 2002). Similar to what we observed in *spr-5; met-2* mutant progeny, many of the human patients with mutations in these histone modifying enzymes suffer from global developmental delay. Based on our model, it is possible that the developmental delay in these patients may be caused by the failure to properly regulate histone methylation during critical developmental transitions. The resulting inappropriate inheritance of histone methylation could result in the ectopic expression of a developmental program in an inappropriate tissue, leading to background noise and developmental delay.

MATERIALS AND METHODS

Strains. All *Caenorhabditis elegans strains* were grown and maintained at 20° C under standard conditions, as previously described (Brenner, 1974). The *C. elegans spr-5 (by101)(I)* strain was provided by R. Baumeister. The N2 Bristol wild-type (wild type) strain was provided by the *Caenorhabditis* Genetics Center. The *met-2 (n4256)(III) strain* was provided by R. Horvitz. The *mes-4(bn149(mes-4::gfp::ha::6xhis))(V)* strain was provided by Susan Strome. The *hT2 [bli-4(e937)let-?(q782)qIs48] (I;III)* balancer strain was used to maintain *spr-5 (by101)(I); met-2 (n4256)(III)* double-mutant animals

as heterozygotes. Because the *hT2 [bli-4(e937)let-?(q782)qls48](I;III)* balancer allele does not extend completely to the *spr-5* locus on chromosome I, the F0 animals used to generate F1 *spr-5; met-2* progeny were cloned out and genotyped to confirm the presence of the *spr-5 (by101)(I)* allele. For genotyping, single animals were picked into 5-10ul of lysis buffer (50mM KCl, 10mM Tris-HCl (pH 8.3), 2.5mM $MgCl_2$, 0.45% NP-40, 0.45% Tween-20, 0.01% gelatin) and incubated at 65°C for 1 hour followed by 95°C for 30 minutes. PCR reactions were performed with AmpliTaq Gold (Invitrogen) according to the manufacturer's protocol and reactions were resolved on agarose gels (see supplementary file 9 for genotyping primer sequences). Before completing this study we acquired the FX30208 *tmC27 [unc-75(tmls1239*)](I) from the *Caenorhabditis* Genetics Center that completely covers the *spr-5* locus on chromosome I. The *qC1 [qls26 (lag2::GFP + rol-6(su1006)](III)* strain was obtained from W. Kelly and crossed to *met-2 (n4256)(III)* to maintain *met-2(n4256)(III)* as heterozygotes. The *spr-5 (by101)(I)*/*tmC27[unc-75(tmls1239)](I); met-2 (n4256) (III*)/qC1 [qls26 (lag2::gfp+ rol-6(su1006))](III) strain was then re-created for this study to maintain *spr-5 (by101)(I); met-2 (n4256)(III)* double-mutant animals as balanced heterozygotes. The LET-858::GFP (*pha-1*(e2123ts)(III); *let-858::gfp* (ccEx7271)) (Kelly and Fire, 1998) transgenic strain used in somatic transgene silencing assays was acquired from W. Kelly.

Scoring developmental delay. *C. elegans* adult hermaphrodites were allowed to lay embryos for 2-4 hours and then removed in order to synchronize the development of progeny. Progeny were then imaged and scored for development to the adult stage at either 72 hours or seven days after synchronized lay, depending on the experiment. To

monitor embryogenesis, *C. elegans* adult hermaphrodites were dissected and the four-cell stage was established as the starting point, 0 min, for each strain. Subsequently, time-lapse images were obtained at 30 min, 60 min, and 120 min.

RNA sequencing and analysis. Total RNA was isolated using TRIzol reagent (Invitrogen) from 200-250 starved L1 larvae born at room temperature (21°C - 22°C) overnight in M9 Buffer. Due to difficulty in isolating large numbers of *spr-5; met-2* double-mutant progeny from the *hT2 [bli-4(e937)let-?(q782)qIs48](I;III)* balancer strain, we submitted total RNA to the Genomic Services Laboratory (GSL) (HudsonAlpha, Huntsville, Alabama) for low input RNA-seq services. This service utilizes the Ovation RNA-Seq System V2 kit (Nugen) for initial RNA amplification prior to library preparation and sequencing (Illumina HiSeq v4, 50bp paired-end reads). For each genotype, 2 biological replicates were obtained. During the course of these experiments, the FX30208 *tmC27 [unc-75(tmIs1239*)](I) balancer became available from the *Caenorhabditis* Genetics Center. This balancer completely covers the *spr-5* locus on chromosome I. Using this balanced strain, we performed a repeat *spr-5; met-2* RNA-seq experiment with three additional biological replicates of *spr-5; met-2* versus wild type L1 progeny. We submitted the total RNA from new replicates of the repeat RNA-seq to Georgia Genomics and Bioinformatics Core (University of Georgia, Athens, Georgia) for standard Poly-A RNA-seq services (Illumina Nextseq, 50bp paired-end reads). Downstream quality control and analysis were performed identically for both RNA-seq experiments. For both the low-input and repeat standard RNA-seq, sequencing reads were checked for quality using FastQC (Wingett and Andrews, 2018), filtered using Trimmomatic (Bolger et al., 2014), and remapped to the *C. elegans* transcriptome

(ce10, WS220) using HISAT2 (D. Kim et al., 2015). Read count by gene was obtained by FeatureCounts (Liao et al., 2014). Differentially expressed transcripts for the low-input RNA-seq experiment (significance threshold, Wald test, p-value < 0.05) and the repeat RNA-seq experiment (significance threshold, Wald test, p-adj < 0.05) were determined using DESEQ2 (v.2.11.40.2) (Love et al., 2014). Transcripts per million (TPM) values were calculated from raw data obtained from FeatureCounts output. Subsequent downstream analysis was performed using R with normalized counts and p-values from DESEQ2 (v.2.11.40.2). Heatmaps were produced using the ComplexHeatmap R Package (Gu et al., 2016). Data was scaled and hierarchical clustering was performed using the complete linkage algorithm. In the linkage algorithm, distance was measured by calculating pairwise distance. Volcano plots were produced using the EnhancedVolcano package (v.0.99.16). Additionally, Gene Ontology (GO) Pathway analysis was performed using the online platform WormEnrichr (Chen et al., 2013; Kuleshov et al., 2016). R scripts for heatmaps, volcano plots, and GO analysis have been deposited into Gene Expression Omnibus (www.ncbi.nlm.nih.gov/geo) under accession code GSE143839. Rechtsteiner and colleagues identified 214 MES-4 germline genes (Rechtsteiner et al., 2010). 17 of these genes are pseudogenes that we were unable to convert from Ensembl transcript IDs to RefSeq mRNA accession, and another gene was duplicated, so we removed those genes. This leaves 196 MES-4 germline genes that we used for our analysis. An additional heatmap comparison of differentially expressed genes between *spr-5*, *met-2*, and *spr-5; met-2* progeny compared to wild type progeny was generated in Microsoft Excel using log2 fold change

values from the DESEQ2 analysis. Because transcript isoforms were ignored, we discuss the data in terms of “genes expressed” rather than “transcripts expressed”.

Chromatin immunoprecipitation sequencing and analysis. Chromatin immunoprecipitation (ChIP) experiments were performed as described by Katz and colleagues (Katz et al., 2009). Briefly, 600 starved L1 larvae born at room temperature (21°C - 22°C) overnight in M9 Buffer were collected, frozen in liquid nitrogen, and stored at -80°C prior to homogenization. Frozen pellets were disrupted by a glass Dounce homogenizer, fixed with formaldehyde (1% final concentration), and quenched with glycine. ChIP samples were processed with a Chromatin Immunoprecipitation Assay Kit (Millipore), according to manufacturer’s instructions. Samples were sonicated using a Diagenode Bioruptor UCD-200 at 4°C on the “high” setting for a total of 30min with a cycle of 45sec on and 15sec off. A total of 12.5µL (5ug) H3K36me3 antibody (cat. 61021; Active motif) was used for immunoprecipitation. The Genomic Services Laboratory (GSL) (HudsonAlpha, Huntsville, Alabama) performed library preparation and sequencing (Illumina HiSeq v4, 50bp single-end reads). Reads were checked for quality using FastQC (Wingett and Andrews, 2018) and remapped to the *C. elegans* transcriptome (ce10, WS220) using Bowtie2 (Langmead and Salzberg, 2012; Langmead et al., 2009) under default parameters. bamCoverage in deepTools2 (Ramírez et al., 2016) was used to generate bigwig coverage tracks in 50bp bins, with blacklisted regions from McMurchy et al. 2017 excluded, using the following parameters: -bs 50, --normalizeUsing RPKM (McMurchy et al., 2017). MACS2 (Feng et al., 2012; Zhang et al., 2008) default parameters were used to call peaks and create bedgraph files for sequenced and mapped H3K36me3 ChIP samples and input DNA

samples with the following adjustments to account for H3K36me3 broader domains: Broad-cutoff =0.001. Blacklisted regions from McMurchy et al. 2017 were excluded for this analysis (McMurchy et al., 2017). Using published H3K36me3 modMine Chip-chip called broad peaks (modENCODE_3555) from wild type L1 larvae as a guide, we then merged called broad peaks within 1200bp using Bedtools: MergeBED (Quinlan and Hall, 2010). H3K9me2 bedgraph files used in our analysis were from a published dataset (Rechtsteiner et al., 2019). Integrative Genome Viewer (IGV) was used to visualize H3K36me3 reads normalized to reads per kilobase millions (RPKM) and H3K9me2 reads normalized to 15 million reads (genome wide coverage of H3K9me2; (Rechtsteiner et al., 2019).

RNAi methods. RNAi by feeding was carried out using clones from the Ahringer library (Kamath and Ahringer, 2003). Feeding experiments were performed on RNAi plates (NGM plates containing 100 ug/ml ampicillin, 0.4mM IPTG, and 12.5ug/ml tetracycline). F0 worms were placed on RNAi plates as L2 larvae and then moved to fresh RNAi plates 48hrs later where they were allowed to lay embryos for 2-4 hrs. F0 worms were then removed from plates and sacrificed or placed in M9 buffer overnight so that starved L1 progeny could be isolated for quantitative PCR (qPCR). F1 progeny were scored 72hrs after the synchronized lay for developmental progression. For each RNAi experiment, *pos-1* RNAi was used as a positive control. Each RNAi experiment reported here *pos-1* RNAi resulted in >95% embryonic lethality, indicating that RNAi plates were optimal.

Real-time expression analysis. Total RNA was isolated using TRIzol reagent (Invitrogen) from synchronized L1s born at room temperature (21°C – 22°C). cDNA

synthesis and qPCR were carried out as described (Kerr et al. 2014). A total of two biological replicates were performed and for both biological replicates experiments were performed in triplicate and normalized to *ama-1* mRNA expression (see supplementary file 10 for RT-PCR primer sequences).

Differential interference contrast microscopy. Worms were immobilized in 0.1% levamisole and placed on a 2% agarose pad for imaging at either 10x or 40x magnification. 40x DIC images were overlaid together using Adobe photoshop to generate high resolution images of whole worms. For the embryogenesis time course, dissected four-cell embryos were mounted on a 2% agarose pad, covered with a coverslip, and sealed with petroleum jelly. Embryos were imaged at 100x magnification.

Single Molecule Fluorescent *in situ* Hybridization (smFISH). Quasar 570 labeled smFISH probe sets for *htp-1* and *cpb-1* were designed using Stellaris Probe Designer (Biosearch) (see supplementary file 7-8 for probe sequences). The *htp-1* smFISH probes were designed using the complete 1,059nt *htp-1* protein-coding sequence. Likewise, The *cpb-1* smFISH probes were designed using the complete 1,683nt *cpb-1* protein-coding sequence. In addition, an smFISH fluorescent probe set for *ama-1* was purchased from the DesignReady catalog (cat#: VSMF-6002-5, Biosearch). Synchronized L1 larvae for smFISH were obtained by bleaching 300-500 gravid hermaphrodites and allowing embryos to hatch overnight on 6cm NGM plates lightly seeded OP50 bacteria. L1 larvae were then washed into 1.5ul Eppendorf tubes using nuclease-free M9 buffer. Fixation and hybridization steps followed the Stellaris RNA FISH protocol for *C. elegans* adapted from RAJ lab protocol (Raj and Tyagi, 2010). In brief, we resuspended L1 larvae in fixation buffer (3.7% formaldehyde in 1 x PBS) for 15

minutes at room temperature then transferred tubes to liquid nitrogen. Samples were thawed in water and placed on ice for 20 minutes. In our hands, we obtain better fluorescent signal by freeze cracking L1 larvae. Following fixation, L1 Larvae were resuspended in 70% EtOH and stored at 4°C for 24-48 hours. For all probe sets, we incubated L1 larvae in 100ul hybridization buffer (containing 10% formamide and 125nm probe) for 4 hours at 37°C. After hybridization, samples were washed in wash buffer at 37°C for 30 minutes, incubated in 50ng/mL DAPI in wash buffer at 30°C for 30 minutes, washed once in 2x SSC for 2 minutes at room temperature, and mounted in Vectashield mounting medium. Mounted slides were imaged immediately using a 100x objective on a spinning-disk confocal Nikon-TiE imaging system. Images were captured using NIS-Elements software (Nikon) and ImageJ (NIH, http://imagej.nih.gov/ij/) was used for viewing. ImageJ maximum projection was used to project z-stack images to a single plane. The fluorescent intensity of smFISH dots were > 2-fold above background as expected (Ji and van Oudenaarden, 2012).

Immunofluorescence staining. L1 larvae were permeabilized on slides using the freeze-crack method and immediately fixed with methanol/acetone as previously described (Duerr, 2013). Following fixation, slides were washed once with 1x PBST (phosphate buffer saline w/ 0.1% Tween-20) then blocked for 30 minutes in Antibody Buffer (1x PBST with 0.5% BSA and 0.01% sodium azide). Primary antibody staining to detect the *mes-4(bn149(mes-4::gfp::ha::6xhis))(V)* allele was performed overnight at room temperature using a rabbit polyclonal anti-GFP antibody (cat. ab6556, Abcam) at a 1:500 dilution. After three washes with 1x PBST, Secondary antibody staining was performed for 1 hour at room temperature using an Alexa Fluor 594-conjugated goat

anti-rabbit antibody (cat. A32740, Invitrogen) at a 1:500 dilution. Following incubation with secondary antibody, slides were washed twice with 1x PBST and once with 1x PBST containing 200 ng/ml DAPI. After three washes with 1x PBST, slides were mounted in Vectashield mounting medium and imaged immediately using a 100x objective on a spinning-disk confocal Nikon-TiE imaging system.

LET-858::GFP transgene silencing assay. First generation *spr-5; met-2* hermaphrodites were crossed to *let-858* transgenic males to generate *spr-5/*+; *met-2/*+; *let-858::gfp* animals. The let-858 transgene is an extrachromosomal multicopy *let-858* array (Kelly and Fire, 1998). From these animals we generated *spr-5; met-2; let-858::gfp* animals and scored them for somatic expression of LET-858::GFP using a standard stereoscope. L2 progeny from wild type and *spr-5; met-2* progeny expressing the LET-858::GFP transgene were scored as “bright” (High level ubiquitous expression) , faint (barely visible and ubiquitous expression), or off (no expression). Because less than 50% of progeny inherit the *let-858* transgene, we normalized the percentage of progeny scored as “off” for LET-858::GFP to presence of the *let-858* transgene based on genotyping for *gfp.* For wild type, 0 out of 60 progeny that were scored as “off” failed to inherit the *let-858* transgene indicating that the transgene is never silenced in wild type progeny (data not shown, see supplementary file 9 for *gfp* genotyping primer sequences). For *spr-5; met-2* progeny, 8 out of 50 progeny that were scored as “off” inherited the *let-858* transgene indicating that the *let-858* transgene is completely silenced in some *spr-5; met-2* progeny (data not shown).

ACKNOWLEDGEMENTS

We are grateful to members of the Katz lab, as well as T. Caspary and C. Bean, for their helpful discussion and critical reading of the manuscript; M. J. Rowley for advice on bioinformatics; S. Strome and L. Petrella for helpful discussion and experimental advice; C. Cockrum in the Strome lab for sharing the transgenic MES-4 strain in advance of publication, D. Lerit, R. Deal, V. Corces, and W. Kelly for the generous sharing of reagents and equipment. We thank R. Horvitz, W. Kelly, and the *Caenorhabditis* Genetics Center (funded by NIH P40 OD010440) for strains. **Funding:** This work was funded by a grant to D.J.K. (NSF IOS1931697); T.W.L. and B.S.C. were supported by the Fellowships in Research and Science Teaching IRACDA postdoctoral program (NIH K12GM00680-15); and B.S.C. was also supported by NIH F32 GM126734-01. J.D.R was supported by NIH F31 HD100145. **Author Contributions:** B.S.C. and D.J.K. conceived and designed the study and wrote the manuscript. B.S.C. performed experiments under the direction of D.J.K. B.S.C and D.J.K. analyzed data and interpreted results, with help from T.W.L. J.S.B. initially performed *set-2* RNAi rescue experiment and C.F.P. initially performed the *let-858* transgene silencing experiment. J.D.R. performed the embryonic timing experiment. D.A.M. helped with RNA-seq analysis. All authors discussed the results. **Data availability**: Raw and processed genomic data has been deposited with the Gene Expression Omnibus (www.ncbi.nlm.nih.gov/geo) under accession code GSE143839.

REFERENCES

Alvares, S.M., Mayberry, G.A., Joyner, E.Y., Lakowski, B., Ahmed, S., 2014. H3K4 demethylase activities repress proliferative and postmitotic aging. Aging Cell 13, 245–253. doi:10.1111/acel.12166

Ancelin, K., Syx, L., Borensztein, M., Ranisavljevic, N., Vassilev, I., Briseño-Roa, L., Liu, T., Metzger, E., Servant, N., Barillot, E., Chen, C.-J., Schüle, R., Heard, E., 2016. Maternal LSD1/KDM1A is an essential regulator of chromatin and transcription landscapes during zygotic genome activation. Elife 5, 4615. doi:10.7554/eLife.08851

Ashe, A., Sapetschnig, A., Weick, E.-M., Mitchell, J., Bagijn, M.P., Cording, A.C., Doebley, A.-L., Goldstein, L.D., Lehrbach, N.J., Le Pen, J., Pintacuda, G., Sakaguchi, A., Sarkies, P., Ahmed, S., Miska, E.A., 2012. piRNAs can trigger a multigenerational epigenetic memory in the germline of *C. elegans*. Cell 150, 88–99. doi:10.1016/j.cell.2012.06.018

Bannister, A.J., Schneider, R., Myers, F.A., Thorne, A.W., Crane-Robinson, C., Kouzarides, T., 2005. Spatial distribution of di- and tri-methyl lysine 36 of histone H3 at active genes. J Biol Chem 280, 17732–17736. doi:10.1074/jbc.M500796200

Barski, A., Cuddapah, S., Cui, K., Roh, T.-Y., Schones, D.E., Wang, Z., Wei, G., Chepelev, I., Zhao, K., 2007. High-resolution profiling of histone methylations in the human genome. Cell 129, 823–837. doi:10.1016/j.cell.2007.05.009

Batchelder, C., Dunn, M.A., Choy, B., Suh, Y., Cassie, C., Shim, E.Y., Shin, T.H., Mello, C., Seydoux, G., Blackwell, T.K., 1999. Transcriptional repression by the Caenorhabditis elegans germ-line protein PIE-1. Genes Dev. 13, 202–212. doi:10.1101/gad.13.2.202

Bernstein, B.E., Humphrey, E.L., Erlich, R.L., Schneider, R., Bouman, P., Liu, J.S., Kouzarides, T., Schreiber, S.L., 2002. Methylation of histone H3 Lys 4 in coding regions of active genes. PNAS 99, 8695–8700. doi:10.1073/pnas.082249499

Bernstein, B.E., Kamal, M., Lindblad-Toh, K., Bekiranov, S., Bailey, D.K., Huebert, D.J., McMahon, S., Karlsson, E.K., Kulbokas, E.J., Gingeras, T.R., Schreiber, S.L., Lander, E.S., 2005. Genomic maps and comparative analysis of histone modifications in human and mouse. Cell 120, 169–181. doi:10.1016/j.cell.2005.01.001

Bolger, A.M., Lohse, M., Usadel, B., 2014. Trimmomatic: a flexible trimmer for Illumina sequence data. Bioinformatics 30, 2114–2120. doi:10.1093/bioinformatics/btu170

Brenner, S., 1974. The genetics of Caenorhabditis elegans. Genetics 77, 71–94.

Buckley, B.A., Burkhart, K.B., Gu, S.G., Spracklin, G., Kershner, A., Fritz, H., Kimble, J., Fire, A., Kennedy, S., 2012. A nuclear Argonaute promotes multigenerational epigenetic inheritance and germline immortality. Nature 489, 447–451. doi:10.1038/nature11352

Burton, A., Torres-Padilla, M.-E., 2014. Chromatin dynamics in the regulation of cell fate allocation during early embryogenesis. Nat. Rev. Mol. Cell Biol. 15, 723–734. doi:10.1038/nrm3885

Capowski, E.E., Martin, P., Garvin, C., Strome, S., 1991. Identification of grandchildless loci whose products are required for normal germ-line development in the nematode Caenorhabditis elegans. Genetics 129, 1061–1072.

Chen, E.Y., Tan, C.M., Kou, Y., Duan, Q., Wang, Z., Meirelles, G.V., Clark, N.R., Ma'ayan, A., 2013. Enrichr: interactive and collaborative HTML5 gene list enrichment analysis tool. BMC Bioinformatics 14, 128. doi:10.1186/1471-2105-14-128

Chong, J.X., Yu, J.-H., Lorentzen, P., Park, K.M., Jamal, S.M., Tabor, H.K., Rauch, A., Saenz, M.S., Boltshauser, E., Patterson, K.E., Nickerson, D.A., Bamshad, M.J., 2016. Gene discovery for Mendelian conditions via social networking: de novo variants in KDM1A cause developmental delay and distinctive facial features. Genet. Med. 18, 788–795. doi:10.1038/gim.2015.161

Duerr, J.S., 2013. Antibody staining in *C. elegans* using "freeze-cracking". J Vis Exp. doi:10.3791/50664

Feng, J., Liu, T., Qin, B., Zhang, Y., Liu, X.S., 2012. Identifying ChIP-seq enrichment using MACS. Nat Protoc 7, 1728–1740. doi:10.1038/nprot.2012.101

Frum, T., Ralston, A., 2015. Cell signaling and transcription factors regulating cell fate during formation of the mouse blastocyst. Trends Genet. 31, 402–410. doi:10.1016/j.tig.2015.04.002

Fukuyama, M., Rougvie, A.E., Rothman, J.H., 2006. *C. elegans* DAF-18/PTEN mediates nutrient-dependent arrest of cell cycle and growth in the germline. Curr. Biol. 16, 773–779. doi:10.1016/j.cub.2006.02.073

Furuhashi, H., Takasaki, T., Rechtsteiner, A., Li, T., Kimura, H., Checchi, P.M., Strome, S., Kelly, W.G., 2010. Trans-generational epigenetic regulation of *C. elegans* primordial germ cells. Epigenetics Chromatin 3, 15. doi:10.1186/1756-8935-3-15

Garvin, C., Holdeman, R., Strome, S., 1998. The phenotype of mes-2, mes-3, mes-4 and mes-6, maternal-effect genes required for survival of the germline in Caenorhabditis elegans, is sensitive to chromosome dosage. Genetics 148, 167–185.

Gaydos, L.J., Wang, W., Strome, S., 2014. Gene repression. H3K27me and PRC2 transmit a memory of repression across generations and during development. Science 345, 1515–1518. doi:10.1126/science.1255023

Greer, E.L., Becker, B., Latza, C., Antebi, A., Shi, Y., 2016. Mutation of *C. elegans* demethylase spr-5 extends transgenerational longevity. Cell Res 26, 229–238. doi:10.1038/cr.2015.148

Greer, E.L., Beese-Sims, S.E., Brookes, E., Spadafora, R., Zhu, Y., Rothbart, S.B., Aristizábal-Corrales, D., Chen, S., Badeaux, A.I., Jin, Q., Wang, W., Strahl, B.D., Colaiácovo, M.P., Shi, Y., 2014. A histone methylation network regulates transgenerational epigenetic memory in *C. elegans*. Cell Rep 7, 113–126. doi:10.1016/j.celrep.2014.02.044

Gregor, T., Garcia, H.G., Little, S.C., 2014. The embryo as a laboratory: quantifying transcription in Drosophila. Trends Genet. 30, 364–375. doi:10.1016/j.tig.2014.06.002

Gu, Z., Eils, R., Schlesner, M., 2016. Complex heatmaps reveal patterns and correlations in multidimensional genomic data. Bioinformatics 32, 2847–2849. doi:10.1093/bioinformatics/btw313

Hirabayashi, Y., Gotoh, Y., 2010. Epigenetic control of neural precursor cell fate during development. Nat Rev Neurosci 11, 377–388. doi:10.1038/nrn2810

Jambhekar, A., Dhall, A., Shi, Y., 2019. Roles and regulation of histone methylation in animal development. Nat. Rev. Mol. Cell Biol. 20, 625–641. doi:10.1038/s41580-019-0151-1
Ji, N., van Oudenaarden, A., 2012. Single molecule fluorescent in situ hybridization (smFISH) of *C. elegans* worms and embryos. WormBook 1–16. doi:10.1895/wormbook.1.153.1
Kamath, R.S., Ahringer, J., 2003. Genome-wide RNAi screening in Caenorhabditis elegans. Methods 30, 313–321. doi:10.1016/s1046-2023(03)00050-1
Kaneshiro, K.R., Rechtsteiner, A., Strome, S., 2019. Sperm-inherited H3K27me3 impacts offspring transcription and development in *C. elegans*. Nat Commun 10, 1271. doi:10.1038/s41467-019-09141-w
Katz, D.J., Edwards, T.M., Reinke, V., Kelly, W.G., 2009. A *C. elegans* LSD1 demethylase contributes to germline immortality by reprogramming epigenetic memory. Cell 137, 308–320. doi:10.1016/j.cell.2009.02.015
Käser-Pébernard, S., Müller, F., Wicky, C., 2014. LET-418/Mi2 and SPR-5/LSD1 cooperatively prevent somatic reprogramming of *C. elegans* germline stem cells. Stem Cell Reports 2, 547–559. doi:10.1016/j.stemcr.2014.02.007
Kelly, W.G., Fire, A., 1998. Chromatin silencing and the maintenance of a functional germline in Caenorhabditis elegans. Development 125, 2451–2456.
Kerr, S.C., Ruppersburg, C.C., Francis, J.W., Katz, D.J., 2014. SPR-5 and MET-2 function cooperatively to reestablish an epigenetic ground state during passage through the germ line. Proc. Natl. Acad. Sci. U.S.A. 111, 9509–9514. doi:10.1073/pnas.1321843111
Kim, D., Langmead, B., Salzberg, S.L., 2015. HISAT: a fast spliced aligner with low memory requirements. Nat. Methods 12, 357–360. doi:10.1038/nmeth.3317
Kim, J., Zhao, H., Dan, J., Kim, S., Hardikar, S., Hollowell, D., Lin, K., Lu, Y., Takata, Y., Shen, J., Chen, T., 2016. Maternal Setdb1 Is Required for Meiotic Progression and Preimplantation Development in Mouse. PLoS Genet. 12, e1005970. doi:10.1371/journal.pgen.1005970
Kim, J.-H., Lee, J.H., Lee, I.-S., Lee, S.B., Cho, K.S., 2017. Histone Lysine Methylation and Neurodevelopmental Disorders. Int J Mol Sci 18, 1404. doi:10.3390/ijms18071404
Kreher, J., Takasaki, T., Cockrum, C., Sidoli, S., Garcia, B.A., Jensen, O.N., Strome, S., 2018. Distinct Roles of Two Histone Methyltransferases in Transmitting H3K36me3-Based Epigenetic Memory Across Generations in Caenorhabditis elegans. Genetics 210, 969–982. doi:10.1534/genetics.118.301353
Kuleshov, M.V., Jones, M.R., Rouillard, A.D., Fernandez, N.F., Duan, Q., Wang, Z., Koplev, S., Jenkins, S.L., Jagodnik, K.M., Lachmann, A., McDermott, M.G., Monteiro, C.D., Gundersen, G.W., Ma'ayan, A., 2016. Enrichr: a comprehensive gene set enrichment analysis web server 2016 update. Nucleic Acids Res. 44, W90–7. doi:10.1093/nar/gkw377
Kurotaki, N., Imaizumi, K., Harada, N., Masuno, M., Kondoh, T., Nagai, T., Ohashi, H., Naritomi, K., Tsukahara, M., Makita, Y., Sugimoto, T., Sonoda, T., Hasegawa, T., Chinen, Y., Tomita Ha, H.-A., Kinoshita, A., Mizuguchi, T., Yoshiura Ki, K.-I., Ohta, T., Kishino, T., Fukushima, Y., Niikawa, N., Matsumoto, N., 2002. Haploinsufficiency of NSD1 causes Sotos syndrome. Nat. Genet. 30, 365–366. doi:10.1038/ng863

Langmead, B., Salzberg, S.L., 2012. Fast gapped-read alignment with Bowtie 2. Nat. Methods 9, 357–359. doi:10.1038/nmeth.1923
Langmead, B., Trapnell, C., Pop, M., Salzberg, S.L., 2009. Ultrafast and memory-efficient alignment of short DNA sequences to the human genome. Genome Biol. 10, R25. doi:10.1186/gb-2009-10-3-r25
Lederer, D., Grisart, B., Digilio, M.C., Benoit, V., Crespin, M., Ghariani, S.C., Maystadt, I., Dallapiccola, B., Verellen-Dumoulin, C., 2012. Deletion of KDM6A, a histone demethylase interacting with MLL2, in three patients with Kabuki syndrome. Am. J. Hum. Genet. 90, 119–124. doi:10.1016/j.ajhg.2011.11.021
Lee, T.W., Katz, D.J., 2020. Hansel, Gretel, and the Consequences of Failing to Remove Histone Methylation Breadcrumbs. Trends Genet. 36, 160–176. doi:10.1016/j.tig.2019.12.004
Lev, I., Seroussi, U., Gingold, H., Bril, R., Anava, S., Rechavi, O., 2017. MET-2-Dependent H3K9 Methylation Suppresses Transgenerational Small RNA Inheritance. Curr. Biol. 27, 1138–1147. doi:10.1016/j.cub.2017.03.008
Liao, Y., Smyth, G.K., Shi, W., 2014. featureCounts: an efficient general purpose program for assigning sequence reads to genomic features. Bioinformatics 30, 923–930. doi:10.1093/bioinformatics/btt656
Love, M.I., Huber, W., Anders, S., 2014. Moderated estimation of fold change and dispersion for RNA-seq data with DESeq2. Genome Biol. 15, 550. doi:10.1186/s13059-014-0550-8
Maduro, M.F., 2010. Cell fate specification in the *C. elegans* embryo. Developmental Dynamics 239, 1315–1329. doi:10.1002/dvdy.22233
McMurchy, A.N., Stempor, P., Gaarenstroom, T., Wysolmerski, B., Dong, Y., Aussianikava, D., Appert, A., Huang, N., Kolasinska-Zwierz, P., Sapetschnig, A., Miska, E.A., Ahringer, J., 2017. A team of heterochromatin factors collaborates with small RNA pathways to combat repetitive elements and germline stress. Elife 6, 7931. doi:10.7554/eLife.21666
Mello, C.C., Draper, B.W., Krause, M., Weintraub, H., Priess, J.R., 1992. The pie-1 and mex-1 genes and maternal control of blastomere identity in early *C. elegans* embryos. Cell 70, 163–176. doi:10.1016/0092-8674(92)90542-k
Morgan, M.A.J., Shilatifard, A., 2020. Reevaluating the roles of histone-modifying enzymes and their associated chromatin modifications in transcriptional regulation. Nat. Genet. 52, 1271–1281. doi:10.1038/s41588-020-00736-4
Nottke, A.C., Beese-Sims, S.E., Pantalena, L.F., Reinke, V., Shi, Y., Colaiácovo, M.P., 2011. SPR-5 is a histone H3K4 demethylase with a role in meiotic double-strand break repair. Proc. Natl. Acad. Sci. U.S.A. 108, 12805–12810. doi:10.1073/pnas.1102298108
Öst, A., Lempradl, A., Casas, E., Weigert, M., Tiko, T., Deniz, M., Pantano, L., Boenisch, U., Itskov, P.M., Stoeckius, M., Ruf, M., Rajewsky, N., Reuter, G., Iovino, N., Ribeiro, C., Alenius, M., Heyne, S., Vavouri, T., Pospisilik, J.A., 2014. Paternal diet defines offspring chromatin state and intergenerational obesity. Cell 159, 1352–1364. doi:10.1016/j.cell.2014.11.005
Petrella, L.N., Wang, W., Spike, C.A., Rechtsteiner, A., Reinke, V., Strome, S., 2011. synMuv B proteins antagonize germline fate in the intestine and ensure *C. elegans* survival. Development 138, 1069–1079. doi:10.1242/dev.059501

Quinlan, A.R., Hall, I.M., 2010. BEDTools: a flexible suite of utilities for comparing genomic features. Bioinformatics 26, 841–842. doi:10.1093/bioinformatics/btq033
Raj, A., Tyagi, S., 2010. Detection of individual endogenous RNA transcripts in situ using multiple singly labeled probes. Meth. Enzymol. 472, 365–386. doi:10.1016/S0076-6879(10)72004-8
Ramírez, F., Ryan, D.P., Grüning, B., Bhardwaj, V., Kilpert, F., Richter, A.S., Heyne, S., Dündar, F., Manke, T., 2016. deepTools2: a next generation web server for deep-sequencing data analysis. Nucleic Acids Res. 44, W160–5. doi:10.1093/nar/gkw257
Rayasam, G.V., Wendling, O., Angrand, P.-O., Mark, M., Niederreither, K., Song, L., Lerouge, T., Hager, G.L., Chambon, P., Losson, R., 2003. NSD1 is essential for early post-implantation development and has a catalytically active SET domain. EMBO J. 22, 3153–3163. doi:10.1093/emboj/cdg288
Rechtsteiner, A., Costello, M.E., Egelhofer, T.A., Garrigues, J.M., Strome, S., Petrella, L.N., 2019. Repression of Germline Genes in Caenorhabditis elegans Somatic Tissues by H3K9 Dimethylation of Their Promoters. Genetics 212, 125–140. doi:10.1534/genetics.118.301878
Rechtsteiner, A., Ercan, S., Takasaki, T., Phippen, T.M., Egelhofer, T.A., Wang, W., Kimura, H., Lieb, J.D., Strome, S., 2010. The histone H3K36 methyltransferase MES-4 acts epigenetically to transmit the memory of germline gene expression to progeny. PLoS Genet. 6, e1001091. doi:10.1371/journal.pgen.1001091
Seydoux, G., Mello, C.C., Pettitt, J., Wood, W.B., Priess, J.R., Fire, A., 1996. Repression of gene expression in the embryonic germ lineage of *C. elegans*. Nature 382, 713–716. doi:10.1038/382713a0
Shi, Y., Lan, F., Matson, C., Mulligan, P., Whetstine, J.R., Cole, P.A., Casero, R.A., Shi, Y., 2004. Histone demethylation mediated by the nuclear amine oxidase homolog LSD1. Cell 119, 941–953. doi:10.1016/j.cell.2004.12.012
Shi, Y.-J., Matson, C., Lan, F., Iwase, S., Baba, T., Shi, Y., 2005. Regulation of LSD1 histone demethylase activity by its associated factors. Mol. Cell 19, 857–864. doi:10.1016/j.molcel.2005.08.027
Sijen, T., Fleenor, J., Simmer, F., Thijssen, K.L., Parrish, S., Timmons, L., Plasterk, R.H., Fire, A., 2001. On the role of RNA amplification in dsRNA-triggered gene silencing. Cell 107, 465–476. doi:10.1016/s0092-8674(01)00576-1
Siklenka, K., Erkek, S., Godmann, M., Lambrot, R., McGraw, S., Lafleur, C., Cohen, T., Xia, J., Suderman, M., Hallett, M., Trasler, J., Peters, A.H.F.M., Kimmins, S., 2015. Disruption of histone methylation in developing sperm impairs offspring health transgenerationally. Science 350, aab2006–aab2006. doi:10.1126/science.aab2006
Strome, S., 2005. Specification of the germ line. WormBook 1–10. doi:10.1895/wormbook.1.9.1
Sulston, J.E., Schierenberg, E., White, J.G., Thomson, J.N., 1983. The embryonic cell lineage of the nematode Caenorhabditis elegans. Dev. Biol. 100, 64–119. doi:10.1016/0012-1606(83)90201-4
Tabuchi, T.M., Rechtsteiner, A., Jeffers, T.E., Egelhofer, T.A., Murphy, C.T., Strome, S., 2018. Caenorhabditis elegans sperm carry a histone-based epigenetic memory of both spermatogenesis and oogenesis. Nat Commun 9, 4310. doi:10.1038/s41467-018-06236-8

Tijsterman, M., Okihara, K.L., Thijssen, K., Plasterk, R.H.A., 2002. PPW-1, a PAZ/PIWI protein required for efficient germline RNAi, is defective in a natural isolate of *C. elegans*. Curr. Biol. 12, 1535–1540. doi:10.1016/s0960-9822(02)01110-7

Tunovic, S., Barkovich, J., Sherr, E.H., Slavotinek, A.M., 2014. De novo ANKRD11 and KDM1A gene mutations in a male with features of KBG syndrome and Kabuki syndrome. Am. J. Med. Genet. A 164A, 1744–1749. doi:10.1002/ajmg.a.36450

Unhavaithaya, Y., Shin, T.H., Miliaras, N., Lee, J., Oyama, T., Mello, C.C., 2002. MEP-1 and a homolog of the NURD complex component Mi-2 act together to maintain germline-soma distinctions in *C. elegans*. Cell 111, 991–1002.

Wang, D., Kennedy, S., Conte, D., Kim, J.K., Gabel, H.W., Kamath, R.S., Mello, C.C., Ruvkun, G., 2005. Somatic misexpression of germline P granules and enhanced RNA interference in retinoblastoma pathway mutants. Nature 436, 593–597. doi:10.1038/nature04010

Wasson, J.A., Simon, A.K., Myrick, D.A., Wolf, G., Driscoll, S., Pfaff, S.L., Macfarlan, T.S., Katz, D.J., 2016. Maternally provided LSD1/KDM1A enables the maternal-to-zygotic transition and prevents defects that manifest postnatally. Elife 5, 296. doi:10.7554/eLife.08848

Wingett, S.W., Andrews, S., 2018. FastQ Screen: A tool for multi-genome mapping and quality control. F1000Res 7, 1338. doi:10.12688/f1000research.15931.2

Zhang, Y., Liu, T., Meyer, C.A., Eeckhoute, J., Johnson, D.S., Bernstein, B.E., Nusbaum, C., Myers, R.M., Brown, M., Li, W., Liu, X.S., 2008. Model-based analysis of ChIP-Seq (MACS). Genome Biol. 9, R137. doi:10.1186/gb-2008-9-9-r137

FIGURES and FIGURES LEGENDS

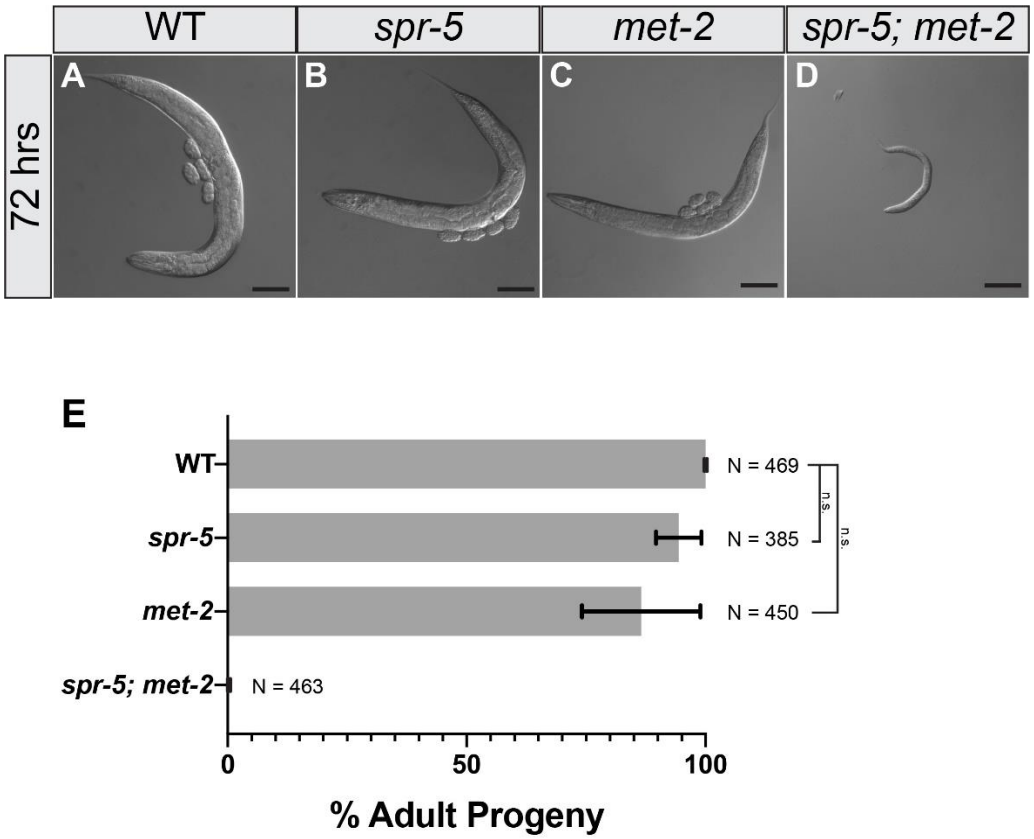

Fig. 1. *spr-5; met-2* mutants display severe developmental delay. 10x Differential Interference Contrast (DIC) images of wild type (A), *spr-5* (B*)*, *met-2* (C), and *spr-5; met-2* progeny (D) 72 hours post synchronized lay. Scale bar: 100µm. (E) Percentage of wild type, *spr-5*, *met-2*, and *spr-5; met-2* progeny that reached the adult stage (% Adult Progeny) by 72 hours post synchronized lay. Error bars represent the standard deviation of the mean from three experiments. N= the total number of progeny 20-25 hermaphrodites scored over three experiments. (unpaired t-test, n.s. represents a p-value >0.05).

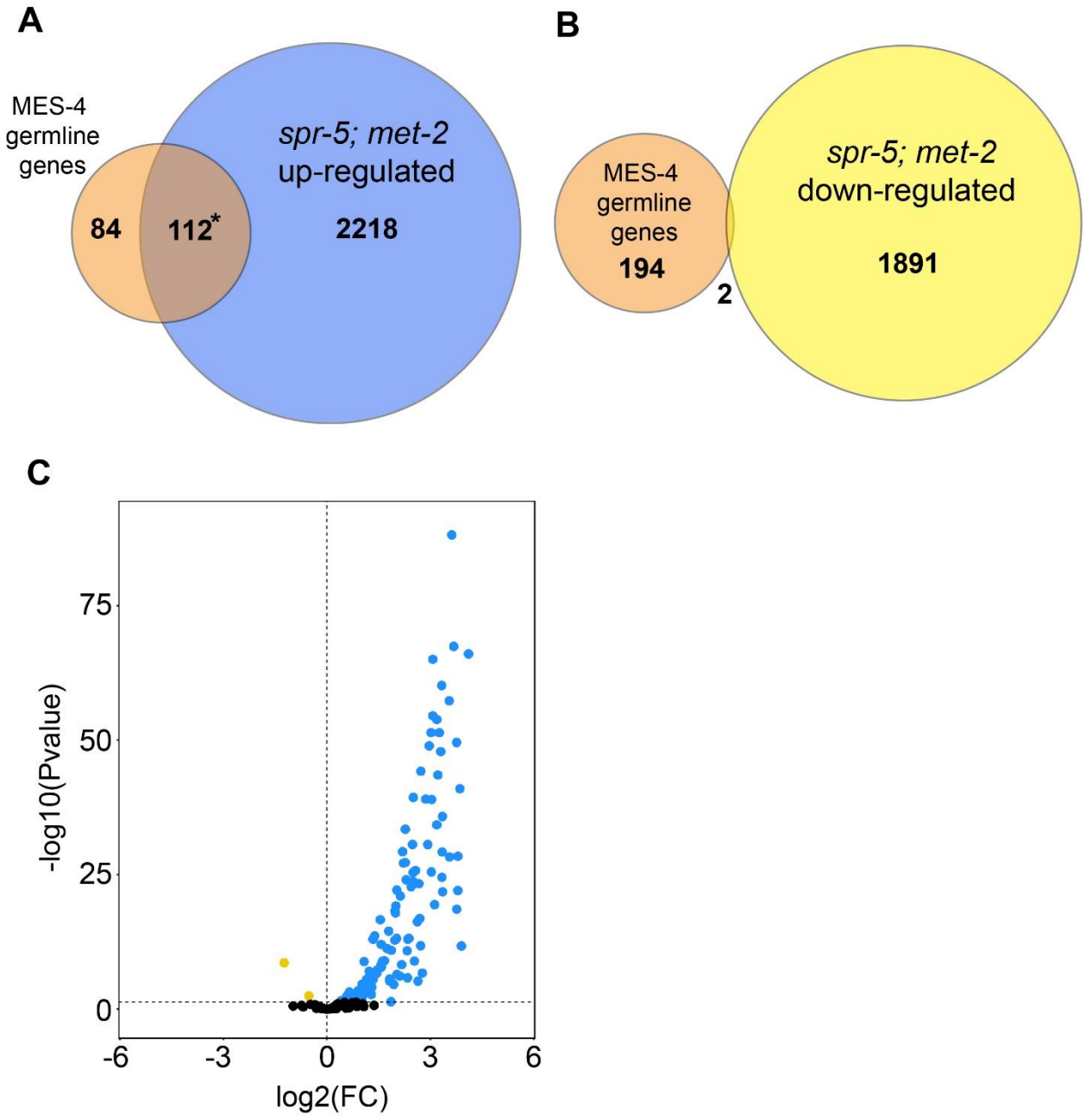

Fig. 2. MES-4 germline genes are ectopically expressed in *spr-5; met-2* mutant soma in RNAseq repeat experiment two. Overlap between MES-4 germline genes and genes up-regulated (A) and down-regulated (B) in *spr-5; met-2* L1 progeny (first repeat experiment shown in Fig. S3-S6). Significant over-enrichment in A was determined by the hypergeometric test (*P-value < 1.20E-54). (C) Volcano plot of log2 fold changes (FC) of 196 MES-4 germline gene expression (x-axis) in *spr-5; met-2* L1 Progeny compared to wild type L1 progeny by statistical significance ($-Log_{10}$ P-value; y-axis). Yellow represents significantly down-regulated genes and blue represents significantly up-regulated genes determined by DESEQ2 analysis (see methods, Wald test, p-adj < 0.05).

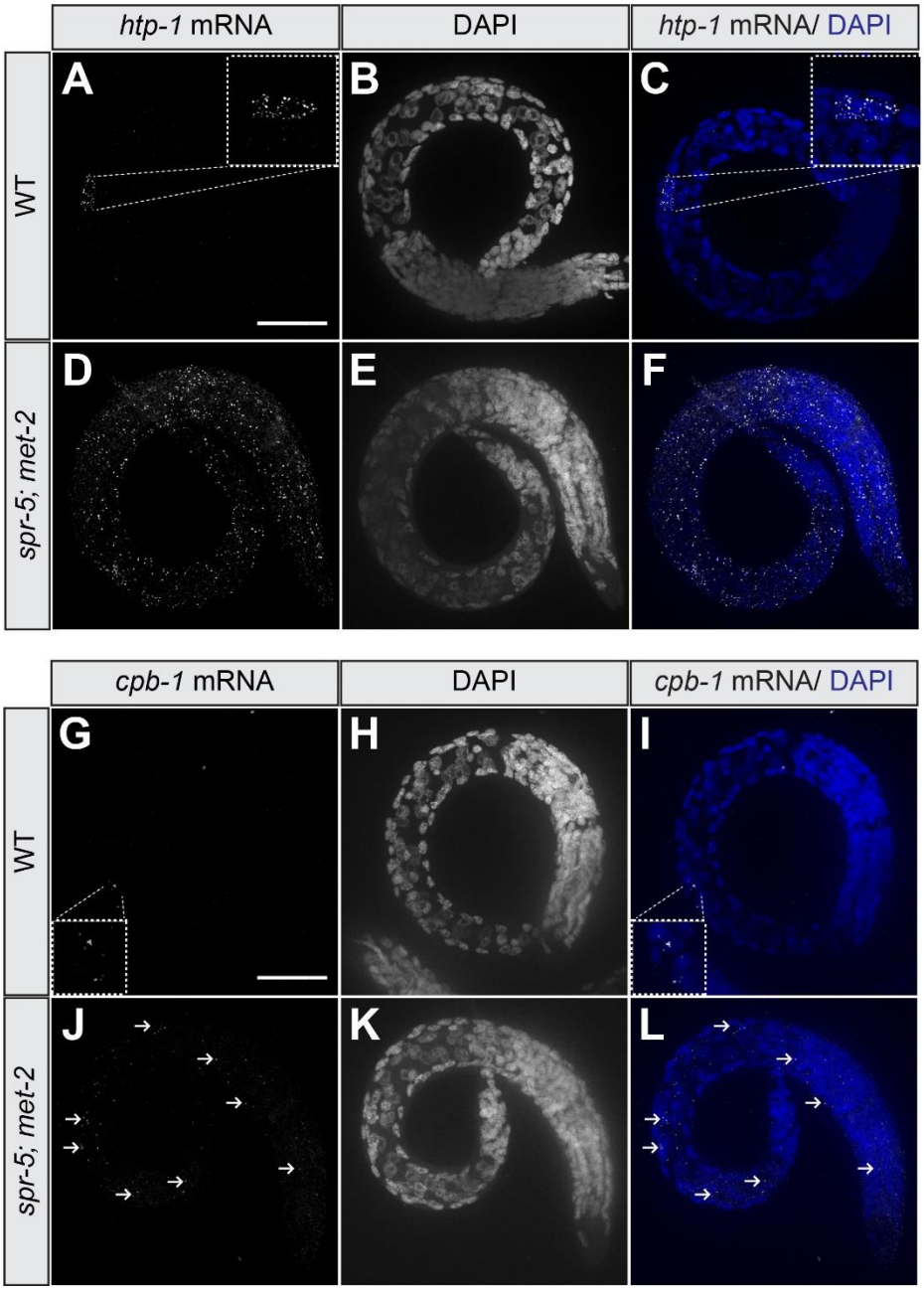

Fig. 3. *spr-5; met-2* L1 progeny ectopically express MES-4 germline genes in multiple somatic tissues. 40x smFISH images of *htp-1* (A, C, D, F) and *cpb-1* (G, I, J, L) endogenous mRNAs in wild type (A-C, G-I) and *spr-5; met-2* (D-F, J-L) L1 progeny. DAPI was used as a nuclear marker (B, C, E, F, H, I, K, L). Insets are high magnification images of the germ cells, Z2 and Z3, in wild type L1 progeny. Arrows (J, L) denote ectopic *cpb-1* mRNA foci in somatic cells. Scale bar 40μm.

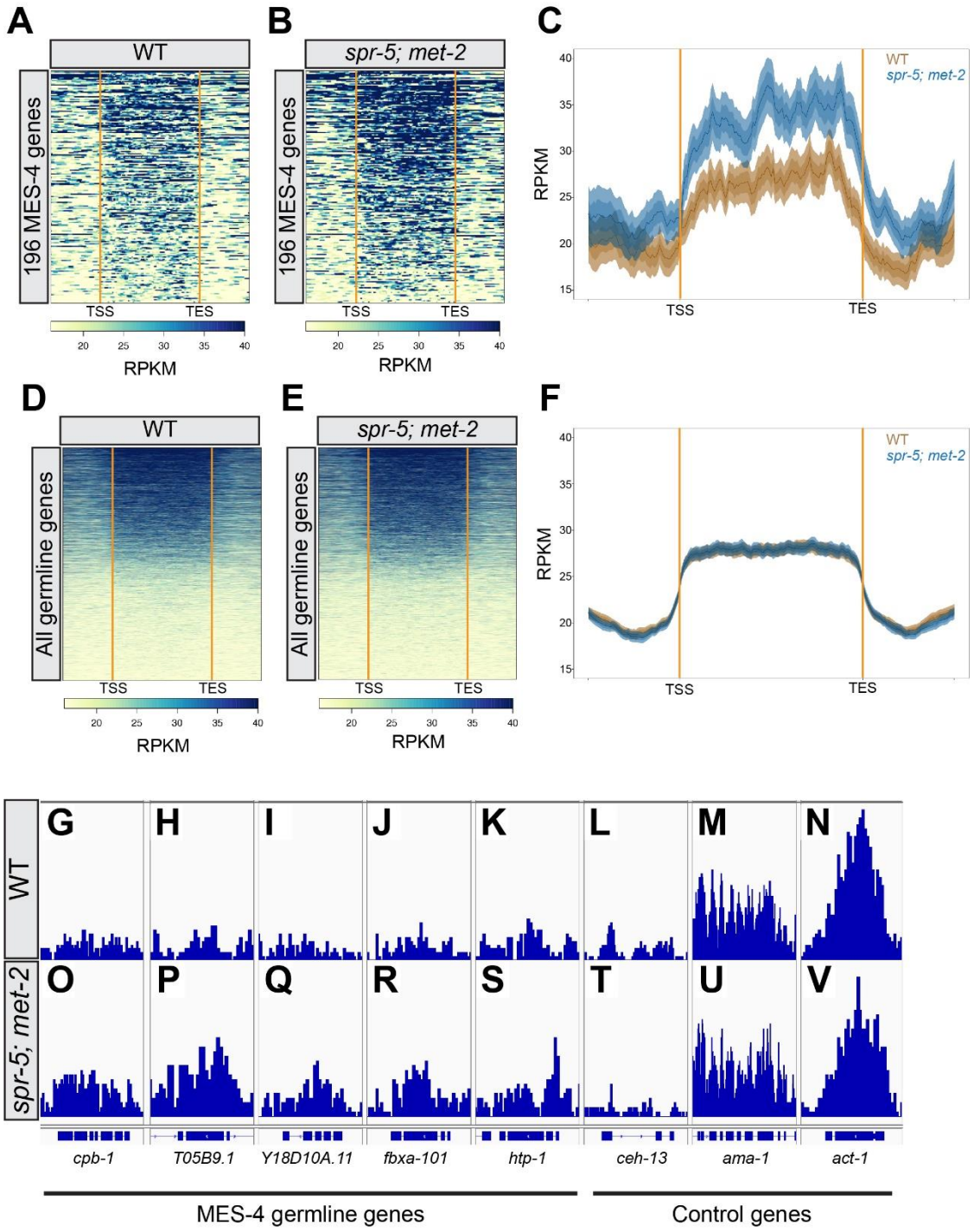

Fig. 4. MES-4 germline genes display ectopic H3K36me3 in *spr-5; met-2* L1 progeny. Heatmap of H3K36me3 ChIP-seq reads normalized to reads per kilobase million (RPKM) over the gene bodies of 196 MES-4 germline genes in wild type (A) versus *spr-5; met-2* (B) L1 progeny (second replicate in Figure S9). (C) Plot profile corresponding to heatmaps in (A) (wild type, brown) and (C) (*spr-5; met-2*, blue). Heatmap of H3K36me3 ChIP-seq reads normalized to reads per kilobase million (RPKM) over the gene bodies of all germline genes in wild type (D) versus *spr-5;*

met-2 (E) L1 progeny. (F) Plot profile corresponding to heatmaps in (D) (wild type, brown) and (E) (*spr-5; met-2*, blue). Gene bodies were pseudoscaled to 1kb with 500bp borders separated by orange bars that represent the transcriptional start site (TSS) and transcriptional end site (TES). Integrative Genome Viewer (IGV) image of H3K36me3 ChIP-seq reads normalized to RPKM at MES-4 germline genes (G-K) and control genes (O-S) in wild type (G-N) versus *spr-5; met-2* (O-V) L1 progeny. RPKM IGV windows were scaled between 0 and 202 RPKM for all genes.

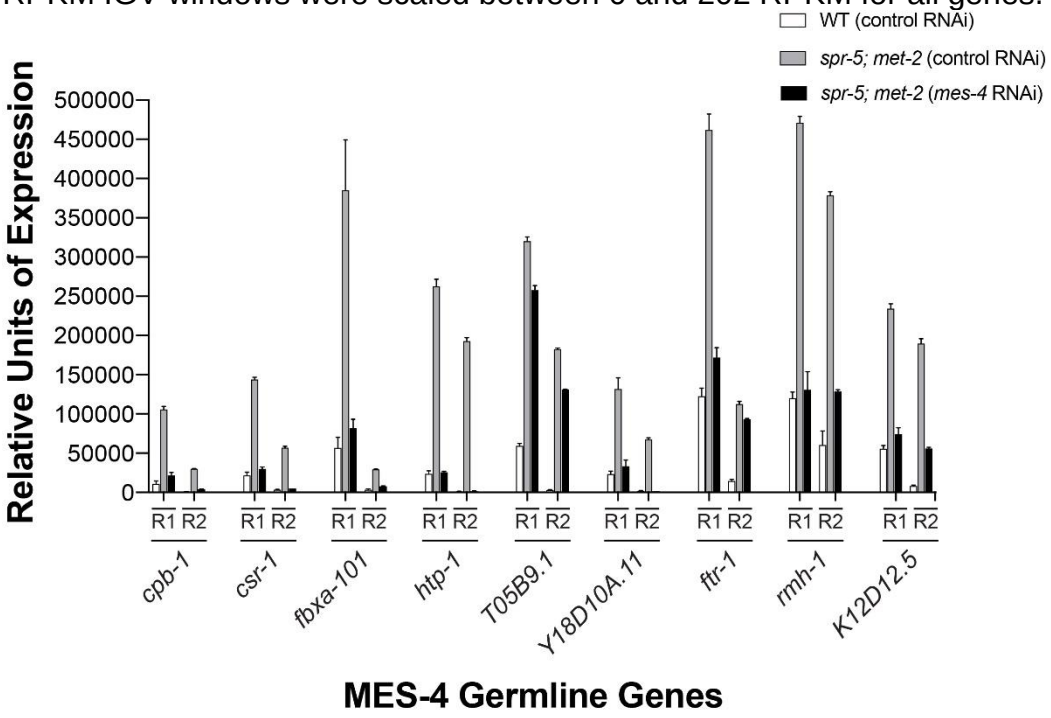

Fig. 5. Knocking down MES-4 rescues ectopic expression of MES-4 germline genes in *spr-5; met-2* L1 progeny. Quantitative RT-PCR showing the relative units of expression for nine MES-4 germline genes (*cpb-1, csr-1*, *fbxa-101*, *htp*-1, *T05B9.1*, *Y18D10A.11*, *ftr-1*, *rmh-1*, *K12D12.5*) in L1 progeny of *spr-5; met-2* hermaphrodites fed either control L4440 RNAi (grey bars) or *mes-4* RNAi (black bars) versus wild type fed control L4440 RNAi (white bars). Relative units of expression from two biological replicates (R1 and R2) were calculated for each gene by averaging triplicate RT_PCR reactions and normalizing to a control gene, *ama-1 (see supplementary file 11 for raw values from RT-PCR analysis)*. Error bars represent the standard error of the mean (SEM) for triplicate RT_PCR reactions. For all nine genes, *mes-4* RNAi significantly reduced the relative expression of *spr-5; met-2* compared to *spr-5; met-2* fed L4440 control RNAi (unpaired t-test, p-value <0.001).

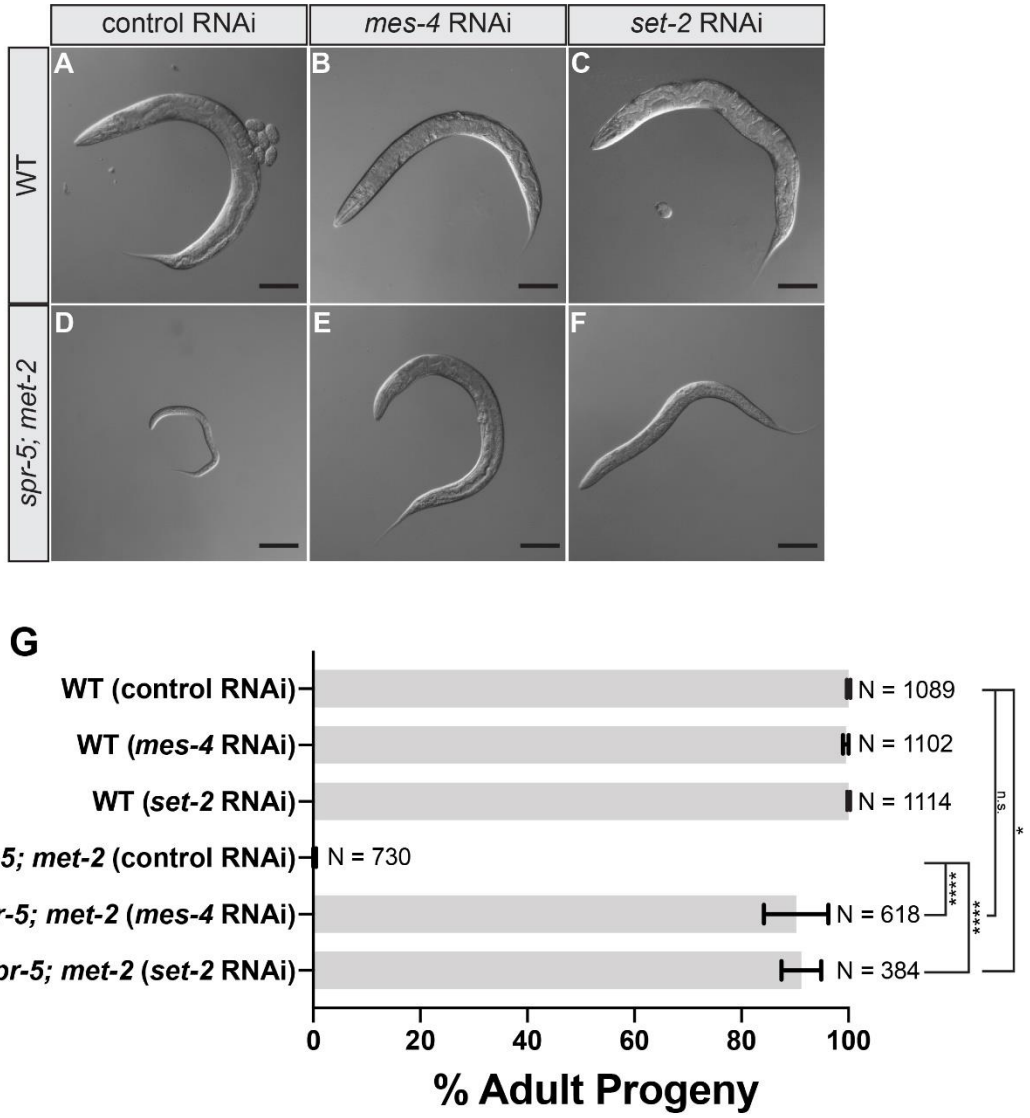

Fig. 6. Knocking down MES-4 rescues developmental delay in *spr-5; met-2* progeny. DIC images of wild type (A-C) or *spr-5; met-2* (E-F) progeny from hermaphrodite parents treated with control (L4440 vector only) RNAi (A, D), *mes-4* RNAi (B, E), or *set-2* RNAi (C, F) 72 hours post synchronized lay. Scale bar: 100μm. (G) Quantification of the number of progeny (represented as % Adult Progeny) from A-H that made it to adults by 72 hours. Error bars represent the standard deviation of the mean from two or three experiments. N represents the total number of progeny from 30-40 hermaphrodites scored across independent experiments. (unpaired t-test, **** represent a p-value <0.0001, * represent a p-value <0.05, and n.s. represents p-value >0.05).

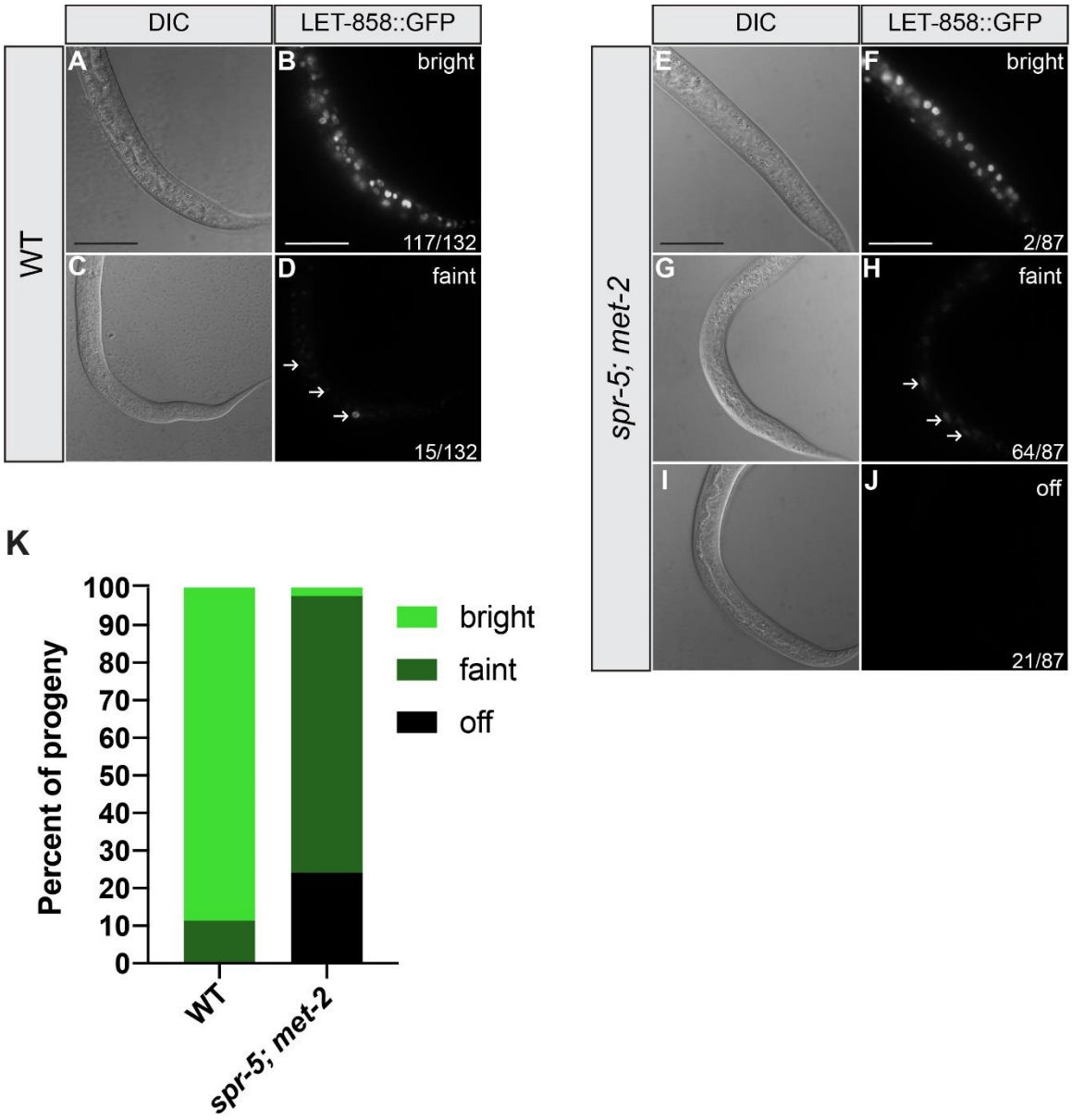

Fig. 7. *let-858* transgene silencing in the soma of *spr-5; met-2* mutants. 40x differential contrasting interference (DIC) (A, C, E, G, and I) and immunofluorescent (B, D, F, H, and J) images of wild type (A-D) and *spr-5; met-2* (E-J) L2 progeny. Arrows denote faint expression of LET-858::GFP. Scale bar: 50 μm. Scale bar is the same for all panels. Percentage of animals where the expression level of LET-858::GFP was scored as either bright expressing (bright green, representative shown in panel B and F), faint expressing (dark green, representative shown in panel D and H), or not expressing (black, representative shown in panel J) in wild type (N=132) versus *spr-5; met-2* (N=87) progeny (K). The quantification represents the percentages of LET-858::GFP expressing progeny from two independent experiments. To control for the segregation of the *let-858* transgene, progeny scored as "off" were normalized for the presence of the *let-858* transgene in animals as detected by PCR (see methods).

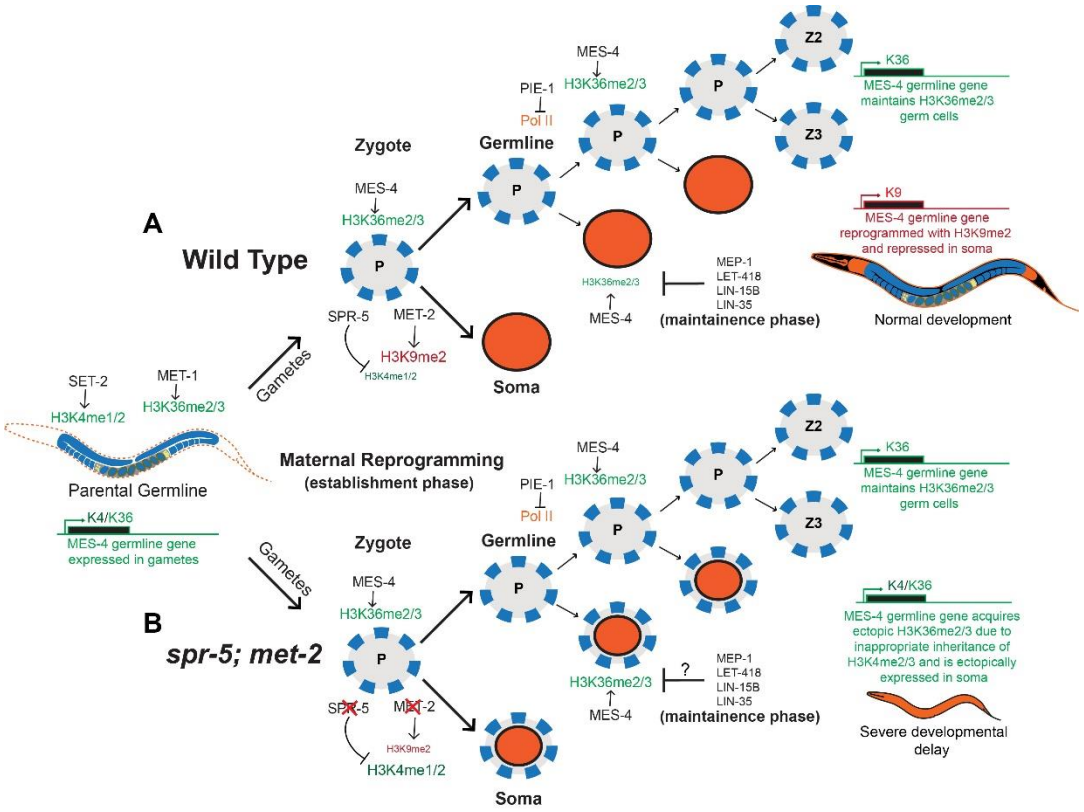

Fig. 8. A model for how maternal reprogramming of inherited histone methylation helps to specify germline versus soma. During development, SET-2 and MET-1 add transcriptionally coupled H3K4me1/2 and H3K36me2/3 to germline expressed genes in the parental germline, respectively. (A) At fertilization, these germline expressed genes undergo maternal epigenetic reprogramming (establishment phase) by SPR-5 and MET-2 to remove H3K4me1/2 and add H3K9me1/2. In the germline blastomeres of the embryo, PIE-1 prevents global transcription by inhibiting POL-II. In the absence of transcription, MES-4 maintains H3K36me2/3 at MES-4 germline genes that have acquired transcriptionally coupled H3K36me2/3 in the previous germline. This enables these genes to avoid being repressed by maternal *spr-5; met-2* reprogramming and ensures that these genes remain bookmarked for re-expression once the germline begins to proliferate later in development. In addition, multiple systems, such as LIN-15B and LIN-35, as well as MEP-1 and LET-418, function in somatic tissues to further antagonize H3K36 bookmarking by MES-4 (maintenance phase). (B) Without SPR-5 and MET-2 maternal reprogramming, H3K4me1/2 is inappropriately inherited in somatic tissues, allowing MES-4 to ectopically add H3K36me2/3 at these germline genes. This leads to ectopic expression of MES-4 germline genes in somatic tissues and a severe developmental delay. Orange circles represent somatic cells, Grey circles outlined in blue dashed-lines represent germ cells, and orange circles outlined in dashed-blue lines depict somatic cells that ectopically express MES-4 germline genes. P-lineage, germline blastomeres, are indicated by the letter P, and the primordial germline cells are indicated by Z2 and Z3.

CHAPTER 4

Ectopic transcription due to inappropriately inherited histone methylation may interfere with the ongoing function of terminally differentiated cells

Juan D. **Rodriguez[1]**, Hsiao-Lin Wang[2], Monica Reeves[1], Jaely Chavez[3], Rhea Rastogi[1], Sindy Chavez[1], Madhav Chadha[1], Emily J. Hill[2], Victor G. Corces[2], Karen Schmeichel[3] ,David J. Katz[1*]

[1]Department of Cell Biology, Emory University School of Medicine, Atlanta GA 30322, USA.
[2]Department of Human Genetics, Emory University School of Medicine, Atlanta GA 30322, USA.
[3]Department of Biology, Oglethorpe University, Brookhaven GA 30319, USA.

ABSTRACT

Many human neurodevelopmental disorders are caused by *de novo* mutations in histone modifying enzymes. These patients have craniofacial defects, developmental delay, intellectual disability and behavioral abnormalities, but it remains unclear how the mutations lead to such developmental defects. Here we take advantage of the invariant *C. elegans* lineage, along with a unique double mutant in the H3K4me1/2 demethylase SPR-5/LSD1/KDM1A, and the H3K9 methyltransferase MET-2/SETDB1 to address this question. We demonstrate that *spr-5; met-2* double mutant worms have a severe chemotaxis defect that is dependent upon the ectopic expression of germline genes in somatic tissues. In addition, by performing single-cell RNAseq, we find that germline genes begin to be ectopically expression widely in *spr-5; met-2* embryos. However, surprisingly we found that *spr-5; met-2* mutants have no somatic lineage defects p to the 200-cell stage of embryogenesis. This suggests that the altered chemotaxis behavior may be due to ongoing defect in terminally differentiated cells rather than a defect in development. To test this directly, we used RNAi to shut off the ectopic expression of germline genes in L2 *spr-5; met-2* larvae, which have a fully formed nervous system. Remarkably, we find that shutting off the ectopic germline expression rescues normal chemotaxis behavior in the same adult worms that previously had a chemotaxis defect at the L2 stage. This suggests that ongoing ectopic transcription can block normal behavior in a fully intact nervous system. These data raise the possibility that intellectual disability and altered behavior in neurodevelopmental syndromes, caused by mutations in histone modifying enzymes, could be due to ongoing ectopic transcription and may be reversible.

INTRODUCTION

Many human neurodevelopmental disorders are caused by de novo mutations in chromatin regulators. For example, Kabuki syndrome is caused by mutations in the H3K4 methyltransferase KMT2D and the H3K27 demethylase KDM6A (Schwenty-Lara et al., 2020). Kabuki syndrome patients have developmental delay, craniofacial defects and intellectual disability. Additionally, three patients have been identified with mutations in the H3K4me1/2 demethylase LSD1/KDM1A (referred to as SPR-5 in *C. elegans*). These LSD1 patients have been referred to as Kabuki-like because their characteristics are nearly identical to Kabuki Syndrome patients (Sobreira et al., 2017). However, it remains unclear how defects in the regulation of histone modifications give rise to neurodevelopmental disorders, such as Kabuki Syndrome.

H3K4 methylation is acquired co-transcriptionally via the COMPASS complex interacting with RNA polymerase and is associated with actively transcribed genes (Wood et al., 2007). H3K4 methylation may function as an epigenetic memory, maintaining transcription over time or through mitotic cell divisions. As a result, H3K4 methylation that is acquired during the production of gametes may have to be erased to prevent this epigenetic memory from being propagated across generations. In *C. elegans*, SPR-5 is required maternally to erase H3K4me2 and prevent it from being inherited transgenerationally (Katz et al, 2009). Without SPR-5 worms become increasingly sterile across generations (termed germline mortality) due to the transgenerational accumulation of H3K4me2 and the increasing expression of germline genes. Similarly, when LSD1 is mutated maternally in mice, it results in embryonic lethality at the 2-cells stage (Wasson et al., 2016). This demonstrates that SPR-5/LSD1

has a conserved role in maternal epigenetic reprogramming. H3K9 methylation is associated with repressed transcription. In *C. elegans*, loss of the H3K9 methyltransferase MET-2 (referred to as SETDB1 in mammals) also results in a germline mortality phenotype and a double mutant of *spr-5* and *met-2* has an exacerbated maternal effect sterility phenotype (Greer et al., 2014) (Kerr et al., 2014). This suggests that SPR-5 and MET-2 cooperate in maternal epigenetic reprogramming. The function of MET-2 in maternal reprogramming may be conserved, as maternal loss of SETDB1 in mice also results in early embryonic lethality.

In *C. elegans*, another transcription-associated histone modification, H3K36me3, is acquired via the H3K36 methyltransferase MET-1 during production of the gametes. In the embryo, this H3K36 methylation is maintained by a transcription-independent H3K36 methyltransferase MES-4 at 176 critical germline genes (Furuhashi et al., 2010). For the remainder of the manuscript, we will refer to these genes as MES-4 targeted germline genes. *mes-4* mutants have a maternal effect sterility phenotype, suggesting that MES-4-dependent H3K36me3 may function as a type of bookmark to help re-specify the germline in the subsequent generation. At around the 60-cell stage, the germline blastomere P4 divides to give rise to the primordial germ cells, termed Z2 and Z3. Once the embryo hatches, the MES-4 targeted germline genes are expressed as Z2 and Z3 begin to proliferate and play a critical role in specifying the germline. The transcription factor LSL-1 also play a critical role in germline function. LSL-1 is first transcribed in P4, continues to be expressed during germline development in all four stages of larval development (L1 to L4), and remains on into the adult. Without, LSL-1

the germline has many defects including defects in meiosis, germline apoptosis and the production of almost no functional gametes (Rodriguez-Crespo et al., 2022).

spr-5; met-2 double mutants have a severe developmental delay at the L2 larval stage that is associated with the ectopic expression of MES-4 targeted germline genes in somatic tissues. In addition, *spr-5; met-2* mutants have ectopic H3K36me3 at MES-4 targeted genes in somatic tissues. When mes-4 is knocked down by RNA interference in *spr-5; met-2* mutants, this ectopic expression is eliminated and the L2 larval delay is rescued, suggesting that severe developmental delay in *spr-5; met-2* mutants is caused by the ectopic expression of MES-4 targeted genes. The ectopic maintenance of H3K3me3 is likely propagated by H3K4 methylation, because the developmental delay of *spr-5; met-2* mutants is also dependent on the H3K4 methyltransferase SET-2 (Carpenter et al 2021). Similar to *spr-5; met-2* mutants, loss of a NuRD complex component MEP-1 or DREAM complex component LIN-35 also exhibits the ectopic expression of germline genes that is dependent on MES-4 (Erdelyi et al 2017). This suggests that these complexes may be functioning to reinforce SPR-5/MET-2 maternal reprogramming in somatic tissues. In the germline, the function of NuRD is antagonized by the germline transcription factor LSL-1.

In *C. elegans*, the embryonic lineage is completely invariant. This means that every wild-type embryo undergoes the same pattern of cell division and cell migration (Sulston et al 1983). The invariant cell lineage of *C. elegans* enabled the discovery of programmed cell death (apoptosis). In order to facilitate study of the invariant lineage, the Waterston lab developed automated lineage tracing. The system utilizes a ubiquitously expressed histone-mCherry fusion protein to track cells via their nuclei with

3D time-lapse confocal imaging (Boyle et al., 2006). In *spr-5; met-2* double mutants, there is a massive accumulation of H3K4me2 and the ectopic expression of MES-4 targeted germline genes (Carpenter et al 2021). The automated lineage tracing system, along with the invariant *C. elegans* lineage, provide the unique opportunity to understand how the inappropriate inheritance of chromatin and the ectopic expression of genes affects cells at the single cell level and gives rise to phenotypes in *spr-5; met-2* mutants.

To determine what embryonic cell types the MES-4 targeted germline genes are ectopically expressed in and how this may alter the embryonic lineage, we performed single-cell RNAseq and automated lineage tracing on *spr-5; met-2* mutants. We find that MES-4 targeted germline genes begin to be ectopically expressed broadly in many embryonic lineages, except in the germline itself where MES-4 targeted germline genes may not be fully activated possiblu due to absence of transcription. Surprisingly, the ectopic expression of MES-4 targeted germline genes in somatic lineages does not result in any somatic lineage defects through the 200-cell stage of embryogenesis. This raises the possibility that the ectopic expression of MES-4 germline genes does not alter development, but instead causes an ongoing defect in differentiated cells. While performing these experiments, we noticed that *spr-5; met-2* mutants fail to move toward OP50 bacteria. Using chemotaxis assays, we found that *spr-5; met-2* mutants have a chemotaxis defect that begins at the L2 stage and is dependent upon MES-4, suggesting that it is dependent on the ectopic expression of MES-4 targeted germline genes. This observation provided the opportunity to test whether the ectopic expression of MES-4 targeted germline genes may be actively interfering with the function of

differentiated cells by determining whether blocking the ectopic expression of these genes restores normal chemotaxis. Remarkably, we find that shutting off the ectopic expression of the MES-4 after the L2 stage rescues normal chemotaxis behavior. From these data, we conclude that the ectopic expression of MES-4 targeted germline genes can alter normal behavior in a fully intact nervous system. More importantly, these findings indicate altered somatic behaviors derived from transgenerational inheritance may be modified/rescued in mature organisms.

RESULTS

Germline genes are ectopically expressed in the somatic lineages of *spr-5; met-2* mutant embryos

Previously we found in *spr-5; met-2* mutants that MES-4 targeted germline genes are ectopically expressed in the soma at the L1 stage (Carpenter et al 2021). To determine how these genes are misexpressed in the embryo at the single-cell level, we performed single-cell RNA sequencing at the 100-160 cell stage, at this stage gastrulation is completed and zygotic transition is at its higher peak (Robertson et al., 2021). We obtained sequences from 686 *spr-5; met-2* mutant cells and 219 Wild Type (N2) cells and identified significantly changed genes using a 0.25-fold change cutoff. *Seurat* clustering analysis of the cells from both Wild Type and *spr-5; met-2* mutants identified 8 clusters (Figure 1A). The individual cells from both Wild Type and *spr-5; met-2* mutants fall within the same clusters, suggesting that gene expression is not dramatically changed overall in *spr-5; met-2* mutants compared to Wild Type (Figure 1B). Consistent with SPR-5 and MET-2 acting as transcriptional repressors, there are

3,660 genes significantly upregulated and only 1,679 genes significantly downregulated in our single-cell dataset.

To determine whether MES-4 targeted germline genes are ectopically expressed in each cluster, we examined the gene expression (normalized count matrices) of all MES-4 targeted germline genes in each cluster. In all 8 clusters, the average gene expression across all MES-4 targeted germline genes is higher in *spr-5; met-2* mutants compared to Wild Type. We also determined the percentage of cells within each cluster that express each of the MES-4 targeted germline genes (Figure 1C-J). In 5 of the 7 somatic clusters (0,1,4,5,6) there is a large increase the percentage of cells within the cluster that express MES-4 targeted germline genes (Figure 1C-G). Consistent with this, 25 of the 149 examined MES-4 targeted germline genes are significantly ectopically expressed in one of the 7 somatic clusters (Figure 1K). Together these results suggests that MES-4 targeted germline genes begin to be widely expressed in many somatic lineages in the embryo.

Despite the ectopic expression of MES-4 targeted germline genes in *spr-5; met-2* mutants overall, in the germline cluster (7) as well as the hypodermis and body wall muscle cluster (2) the percentage of cells within the cluster that express MES-4 targeted germline genes decreases in *spr-5; met-2* compared to Wild Type (Figure 1H,I). The decrease in the expression of MES-4 targeted genes in clusters 7 and 2 occurs despite there still being an increase in the average gene expression of the MES-4 targeted germline genes in these clusters. Consistent with this decrease in the expression of MES-4 targeted genes in the germline, there are only 20 MES-4 targeted germline genes significantly decreased in any cluster and 16 of them are in cells within the

germline cluster (7). Overall, the decrease in the expression of some MES-4 targeted germline genes in the germline cluster (7) is consistent with the possibility that MES-4 germline genes fail to activate in the germline of *spr-5; met-2* mutants. It is not entirely clear why MES-4 targeted germline genes are also expressed within fewer cells within cluster 2, but this effect appears to be driven by a higher percentage of these cells expressing MES-4 germline genes in Wild Type. Thus, it is possible that the higher level of expression of MES-4 germline genes that occurs normally in cluster 2 has to do with many of the cells within cluster 2 being immediately adjacent to the germline cluster (7). In the excretory, glia and seam somatic cell cluster (3), the percentage of cells within the cluster that express MES-4 targeted germline genes is unchanged between N2 and *spr-5; met-2* mutants (Figure 1J). This raises the possibility that cells of this lineage may be resistant to the ectopic expression of MES-4 targeted germline genes. Each cellular lineages show differential patterns of altered MES-4 targeted germline genes, consistent with the unique specificity cell regulation of each cell lineage.

To confirm that MES-4 targeted genes are ectopically expressed in *spr-5; met-2* mutants, we performed quantitative RT-PCR on 5 of the MES-4 targeted genes that were not significantly misexpressed in our single-cell dataset but where significantly misexpressed in the L1 stage (Carpenter et al 2021). We found that 4 out of the 5 genes tested were significantly upregulated with an average fold change of 3.5 (Supplemental Figure 1). Consistently, we previously found by single molecule RNA fluorescence *in situ* hybridization that one of the genes, *htp-1,* is widely ectopically expressed in the somatic cells of the embryo (*Carpenter et al 2021*). Finally, we also compared the ectopic expression of MES-4 targeted germline genes in our single-cell RNAseq dataset

to our previously published *spr-5; met-2* RNAseq performed at the L1 larval stage. In contrast to our single cell dataset, where only 25 MES-4 targeted germline genes are significantly upregulated, each only in a single cluster, in our previous L1 RNAseq dataset, there were 34 MES-4 targeted genes that were significantly upregulated across the entire L1 larvae. This suggests that MES-4 targeted germline genes are increasingly ectopically expressed at later stages. Overall, our scRNAseq data suggest that inappropriate chromatin inherited from the previous generation in *spr-5; met-2* mutants is permissive for facilitating ectopic expression beginning widely during embryonic stages, but this ectopic expression is less than at later stages.

spr-5; met-2 **mutants have a delay in the specification of the germline, but no defects in somatic embryonic development**

To determine if cell lineages specification is altered in *spr-5; met-2* mutants, we took advantage of the invariant embryonic lineage in *C. elegans*. By performing automated lineage tracing (*Boyle et al., 2006*), we tracked the number of cell divisions, timing of cell divisions and cell migration of all embryonic cells from the 2-cell stage through the 200-cell stage in *spr-5; met-2* mutants. Surprisingly, we found no defects in any somatic lineages deriving from either the AB or P1 blastomeres (Figure 2A-D). These data suggest that the embryonic somatic lineages is normal in *spr-5; met-2* mutants. In contrast, we noted significant variances within the germline lineages (Figure 2B,C). Normally, the germline blastomere divides to give rise to the two primordial germ cells, Z2 and Z3, around the 60-cell stage, ~80 minutes after the 2-cell embryo first divides. In Wild Type, it takes an average of 45 minutes from the time that P_4 first appears to when

P_4 divides to yield Z2 and Z3. In contrast, in *spr-5; met-2* mutants requite an average of 56 minutes (Figure 2C). The delay in the cell division of the germline blastomere P_4 occurs despite their being no delay in the cell D, directly adjacent to P_4 (Figure 2D). The P_4 delay correlates with the failure to fully express MES-4 targeted germline genes in the germline cluster (7)(Figure 1I), raising the possibility that the delayed division of P4 could be due to the failure to fully activate germline transcription.

***spr-5; met-2* mutants have a severe defect in chemotaxis towards OP50 bacteria**

While maintaining *spr-5; met-2* mutants and performing these experiments, we noticed that *spr-5; met-2* mutants fail to go towards the OP50 *E. coli* food source. To quantify this defect, we performed a chemotaxis assay and calculated the chemotaxis index (CI) (Figure 3). Compared to Wild Type worms which have a chemotaxis index of 0.9, *spr-5* and *met-2* single mutants have a small but significant defect in chemotaxis with chemotaxis indices of 0.7. In contrast, *spr-5; met-2* mutants have a chemotaxis index of 0.2, indicative of a more severe defect in chemotaxis (Figure 3A). Taken together, these findings demonstrate that *spr-5; met-2* chemotaxis mutants fail to go towards the OP50 *E. coli* food source, despite not having any developmental defects in the embryonic lineage. These chemotaxis defects persist in both L2 larvae and adult animals (Figure 4). Importantly, in the chemotaxis assay, any animals that fail to move from the origin are not included in the analysis, so this defect is not due to a failure in mobility. These findings suggests that the defect is not due to muscle deficiency instead to a neuronal function.

The *spr-5; met-2* chemotaxis defect is dependent upon the ectopic expression of MES-4 targeted germline genes

Previously we demonstrated that a severe developmental delay also observed in *spr-5; met-2* mutants can be rescued by knockdown of the H3K36 methyltransferase MES-4 (Carpenter et al 2021). This suggested that the developmental delay is dependent upon the ectopic expression of MES-4 targeted germline genes. To determine whether the chemotaxis defect of *spr-5; met-2* mutants is also dependent upon the ectopic expression of MES-4 germline genes, we measured chemotaxis in *spr-5; met-2* mutants in which *mes-4* is knocked down by RNA interference (RNAi), in both the F0, beginning at the L4 stage, and in the F1 progeny. RNAi of *mes-4* in *spr-5; met-2* mutants significantly rescued the chemotaxis defect, suggesting that the chemotaxis defects is also dependent upon the ectopic transcription of MES-4 targeted germline genes (Figure 3B).

Zygotically knockdown of the ectopic transcription of MES-4 targeted germline genes in L2 *spr-5; met-2* mutants, restores normal chemotaxis

The lack of embryonic developmental defects in *spr-5; met-2* mutants raised the possibility that the severe chemotaxis defect in these mutants could be due to the ongoing ectopic expression of MES-4 targeted germline genes. If this is the case, it might be possible to shut off the ectopic expression of the MES-4 targeted germline genes and restore normal chemotaxis. To test this possibility, we took L2 *spr-5; met-2* larvae which already have a severe chemotaxis defect and attempted to shut off the ectopic expression of MES-4 targeted germline genes by performing *mes-4* RNAi.

Importantly, because *spr-5; met-2* double mutants have a severe developmental delay, it takes ~5 days for them to develop from L2 larvae to adults. This gives the RNAi plenty of time to knockdown the ectopic transcription of the MES-4 targeted germline genes. Remarkably, we find that shutting off the ectopic germline expression of the MES-4 targeted germline genes after the L2 stage significantly rescues normal chemotaxis behavior (Figure 4). In these experiments, the RNAi is performed with HT115 bacteria rather than OP50, which reduced the chemotaxis index of Wild Type animals to 0.55, rather than the 0.9 chemotaxs index observed when OP50 bacteria is used. Nevertheless, compared to *spr-5; met-2* mutants with a chemotaxis index of 0.0, RNAi of *mes-4* after the L2 stage results in a significant rescue of chemotaxis to a CI of 0.28 (Figure 4).

MES-4 is required to propagate the ectopic transcription of MES-4 targeted germline genes to somatic tissues, but may not be completely required to continually maintain the ectopic transcription of MES-4 targeted germline genes in somatic cells. Therefore, we also tried to shut off the ectopic expression of MES-4 targeted germline genes by performing RNAi against *lsl-1.* LSL-1 is a germline transcription factor that actively required for the transcription of many germline expressed genes (*Rodriguez-Crespo et al., 2022*). We found that knockdown of LSL-1 results in an even stronger rescue of chemotaxis in *spr-5; met-2* mutants (CI of 0.35); (Figure 4). The percentage of worms that exhibit positive chemotaxis towards OP50 bacteria when *lsl-1* is knocked down after the L2 stage in *spr-5; met-2* mutants (67%) is similar to the 77.5% observed in Wild Type under these experimental conditions. Taken together these results suggest

that the ongoing ectopic transcription of MES-4 targeted germline genes can block normal chemotaxis behavior in a fully intact nervous system.

DISCUSSION

spr-5; met-2 double mutants inappropriately inherit chromatin from the previous generation and ectopically express germline genes in somatic tissues. This provided the unique opportunity to determine how the ectopic expression of genes when histone methylation is inappropriately inherited leads to phenotypes. Previously, we found that *spr-5; met-2* mutants have a severe L2 developmental delay that is associated with the ectopic expression of MES-4 targeted germline genes. Knock down of *mes-4* by RNA interference eliminates the ectopic expression of MES-4 targeted germline genes and rescues the L2 developmental delay, suggesting that the developmental delay is dependent upon the ectopic expression of MES-4 targeted germline genes (*Carpenter et al 2021*). Here we found that *spr-5; met-2* mutants also have a severe defect in chemotaxis towards OP50 bacteria at both the L2 larval stage and in adults. There is also a significant chemotaxis defect in both *spr-5* and *met-2* single mutants, but the chemotaxis defect is much more severe in *spr-5; met-2* double mutants, confirming their synergistic interaction. In addition, we find that the severe chemotaxis defect in *spr-5; met-2* mutants is dependent upon MES-4, suggesting that this phenotype is also dependent upon the ectopic expression of MES-4 targeted germline genes.

Single-cell RNAseq analysis of *spr-5; met-2* mutants at the ~200 cell stage demonstrated the MES-4 targeted germline genes begin to be ectopically expressed in the embryo. Although, the ectopic expression was less severe than what we previously observed at the L1 stage. One potential explanation for the increased ectopic expression at the L1 stage is that the permissive chromatin must be acted upon by transcription factors that are not expressed until the individual lineages are further

differentiated. This could potentially explain why some phenotypes are not observed until later in development. The ectopic expression of MES-4 targeted germline genes is observed equally in most somatic clusters. This is consistent with a model in which the ectopic chromatin is inherited fairly uniformly. However, we do not observe the ectopic expression of the MES-4 targeted germline genes in the excretory, glia and seam somatic cell cluster (3), so some lineages may not inherit the ectopic expression or may be resistant to the ectopic expression of these germline genes. Despite the ectopic expression of MES-4 germline genes, unsupervised clustering analysis of our *spr-5; met-2* single-cell RNAseq data demonstrated that these mutants have the same 8 clusters as Wild Type. This suggests that the ectopic transcription does not broadly interfere with cell specification in the embryo. Consistent with this possibility, our automated lineage tracing of *spr-5; met-2* mutants demonstrated that there are no obvious somatic defects in the embryonic lineage through the ~200 cell stage. The succession of normal lineages occurs despite there being a severe developmental delay and chemotaxis defect beginning at the L2 stage. These data are consistent with two possible models. One possibility is that embryonic development is resistant to the MES-4 targeted germline genes that are significantly ectopically expressed at the ~200 cell stage. In this scenario, the strong maternal programming and the invariant embryonic lineage may overcome the ectopic expression. Alternatively, it is possible that there are no somatic lineage defects because the critical MES-4 targeted germline genes that cause the L2 developmental delay and chemotaxis defect are not yet sufficiently misexpressed to cause these defects in the embryo. It is also possible that the critical MES-4 targeted germline genes that are causing the defects are expressed, but not at a

sufficient level to cause a defect. Regardless, the lack of somatic embryonic lineage defects raised the possibility that the L2 developmental delay and chemotaxis defects in *spr-5; met-2* mutants are not due to a failure to properly specify a specific lineage during embryogenesis.

Although we do not observe any somatic defects in the embryonic lineage of *spr-5; met-2* mutants, we detect a significant delay in duration of the germline blastomere P_4 before dividing to give rise to the primordial germ cells Z2 and Z3 in *spr-5; met-2* mutants compared to Wild Type. This delay occurs despite there being no corresponding delay in the P_4 sister cell D, arguing that the P_4 delay is highly specific to the germline lineage. While it remains unclear why there is a delay in the P_4 cell division in our single-cell data reveal MES-4 targeted genes fail to be fully expressed in the germline cluster (7). Therefore, it is possible that the failure to activate the transcription of the MES-4 germline genes causes a delay in the P_4 cell division. Previously, it has been shown that the target of SPR-5, H3K4me2, is specifically lost during the P_4 cell division to generate Z2 and Z3. Thus, it is possible that an increase in H3K4me2 in *spr-5; met-2* results in a failure to lose H3K4me2 in Z2 and Z3. This in turn could lead to the delay in the P_4 cell division, but this has yet to be examined.

The lack of somatic embryonic lineage defects in *spr-5; met-2* mutants raised the possibility that the chemotaxis defect is due to the ongoing ectopic expression of MES-4 targeted germline genes. If this were the case, we would expect that eliminating the ectopic expression in worms that already have a chemotaxis defect would eliminate the chemotaxis defect. To test this possibility, we performed *mes-4* RNAi beginning at the L2 stage in *spr-5; met-2* mutants to block the ectopic expression of MES-4 targeted

germline genes, when these mutants already have a chemotaxis defect. Importantly, at the L2 larval stage *C. elegans* already have a completely intact nervous system. Remarkably, we find that knock down of *mes-4* beginning at the L2 stage significantly rescues normal chemotaxis behavior in the same animals that were previously defective at the L2 stage. MES-4 is thought to function in propagating the inappropriate expression of MES-4 targeted germline genes in somatic tissues and may not be completely required to maintain the ectopic expression of these genes. Therefore, we also tried to block the ectopic expression of germline genes by performing RNA interference against the germline transcription factor LSL-1. LSL-1 is required for the transcription of many germline genes, including many MES-4 targeted germline genes. Knock down of *lsl-1* beginning at the L2 stage in *spr-5; met-2* mutants resulted in an even stronger rescue of normal chemotaxis behavior than knock down of *mes-4.* Taken together these results suggest that the ectopic expression of MES-4 targeted germline genes actively interferes with normal chemotaxis behavior in a completely intact nervous system.

It is unclear how the ectopic expression of germline genes actively interferes with normal chemotaxis behavior. One possibility is that some normal component of neuronal function is blocked at the transcription level; for example the expression of synaptic proteins or a chemoreceptor. An alternative not mutually exclusive possibility is that some aspect of germline function actively interferes with neuronal function. For example, meiosis genes could cause inappropriate chromosomal condensation. Regardless, our finding that ectopic transcription actively interferes with an intact nervous system has implications for neurodevelopmental diseases, such as Kabuki

Syndrome and LSD1 patients. Based on our results, it is possible that the intellectual disability or altered behavior in these patients could be due to an ongoing defect in a properly formed nervous system. Even though these patients have *de novo* mutations that were inherited from one of their parents or mutated in the very early embryo, it is possible that the inappropriately inherited chromatin results in a defect that only manifests itself later in development because the transcription factors that are required to interact with the permissive chromatin are only activated in certain differentiated cell types, such as neurons. Regardless of the etiology, if the nervous system defects in these patients are due to the ongoing ectopic expression of genes, it may be possible to rescue these defects by turning off the ectopic transcription. Consistent with the possibility, it has been recently shown that behavioral defects in the MeCP2 Rhett Syndrome mouse model can be rescued by re-expressing MeCP2 in adult mice (*Ure et al., 2016*). Our data provide a possible explanation for this result.

MATERIALS AND METHODS

Strains

All *C. elegans* strains were cultured at 20˚C on 60 mm nematode growth media (NGM) agar plates with OP50 bacteria grown in Luria Broth (LB). Strains used were: N2: wild-type (Bristol isolate); The *C. elegans spr-5 (by101)(I)* strain was provided by R. Baumeister (Albert Ludwig University of Freiburg, Germany); The MT13293: *met-2 (n4256)(III) strain* was provided by R. Horvitz (Massachusetts Institute of Technology, MA, USA); the JIM113: ujIs113 [Ppie-1::H2B::mCherry, unc-119(+); Pnhr-2::HIS-24::mCherry, unc-119(+) II, the strain was provided by J. Murray University of Pennsylvania, PA, USA). *spr-5(b101)/tmC27[unc-75(tmls1239)]* I*; met-2(n4256)]/qC1 qIs26 [lag-2::GFP + pRF4 rol-6(su1006)]* III strain was created to maintained as heterozygous. Automated cell lineage strain *spr-5(b101)/tmC27[unc-75(tmls1239)]* I; JIM113: ujIs113 [Ppie-1::H2B::mCherry, unc-119(+); Pnhr-2::HIS-24::mCherry, unc-119(+) II; *met-2(n4256)]/qC1 qIs26 [lag-2::GFP + pRF4 rol-6(su1006)]* III. The *spr-5;met-2* with the neurons markers;NeuroPAL strain: *spr-5(b101)/tmC27[unc-75(tmls1239)]* I*; met-2(n4256)]/qC1 qIs26 [lag-2::GFP + pRF4 rol-6(su1006)]* III; OH15262: otIs669 V

Single-worm genotyping

Single animals were picked into 5–10 ml of lysis buffer (50 mM KCl, 10 mM Tris-HCl (pH 8.3), 2.5 mM MgCl2, 0.45% NP-40, 0.45% Tween-20, 0.01% gelatin) and incubated at 65˚C for 1 hr followed by 95˚C for 30 min. PCR reactions were performed with AmpliTaq Gold (Invitrogen) according to the manufacturer's protocol and reactions were resolved on agarose gels. The following genotyping primers were used: spr-5 (*by101*)I:

fwd: AAACACGTGGCTCCATGAAT, rev(wt):GAGGTTTTGAGGGGTTCCAT, rev(mut):CTTGAAACAGACTTGAACATCAAAGATCGG; met-2 (n4256): fwd(wt):GTCACATCACCTGCATCAGC, rev(wt):ATTTCATTACGGC TGCCAAC, fwd(mut):ATTCGAAAAATGGACCGTTG, rev(mut):TCTATTCCCAGGAGCCAATG;

Quantitative PCR

Total RNA was isolated using TRIzol reagent (Invitrogen) from synchronized embryos at room temperature (21°C-22°C). cDNA synthesis and qPCR were carried out as previously described (Kerr et al., 2014). mRNA was quantified by real-time PCR, using iO SYBR Green Supermix (BioRad). The following primers were used: *htp-1* (ATTCGGAGGACAGTGACACAA and GTGCTTTCTCGAGAGACTCAGTTATATC) *cpb-1* (GTGCTGATTGATTGGCCTCG and CCGTTACAGCGCGTGAACCG); *rmh-1* (TGTAGTCATTATGCCAAGTATCTGC and ATCTGTTACTCGTATCTGTAGTAGCC); *ftr-1* (TCCGCTCACTTCGAATACGG and TACCATCGCGATTGTGAGC); *fbxa-101* (TATCGAAGACAAGCTCGCCG and TGCGAACGGAAATCCAATCG); *ama*-1 (TACCTACACTCCAAGTCCATCG and CGATGTTGGAGAGTACTGAG). Each mRNA expression were normalized to *ama-1* control. Fold enrichment was calculated mutant/N2.

RNA interference

Escherichia coli HT115 transformed with a vector expressing dsRNA of *mes-4*, *lsl-1*, L4440 and *ama-1* was obtained from the Ahringer library (Source BioScience). RNAi bacteria and empty vector control were grown at 37C and seeded on RNAi plates (standard NGM plates containing ampicillin (100 mg/ml) and isopropylthiogalactoside (IPTG; 0.4 mM)) left at room temperature to induce for at least 24 hr.

Chemotaxis assay

The experimental 60mm NGM plate was divided into four quadrants. A 5µL of two control LB/vehicle was pipetted into two quadrants. In the other two quadrants an experimental sample, 5µL of *Escherichia coli* OP50 was pipetted. The plate was placed into the fume hood for drying purposes. Worms were collected and rinsed 3 times with M9 buffer (22 mM KH_2PO_4, 42 mM Na_2HPO_4, 86 mM NaCl, and 1 mM $MgSO_4$). A total of 50 worms per plate were placed into the center of the experimental plate. Then the plates were incubated at 20°C for 1-3 hours. Worms that moved to any of the quadrants after the incubation time was recorded. A Chemotaxis Index was calculated as follows; (E1 + E2) – (C1 + C2)/ Total worms moved.

Lineage tracing

The experiment was carried out as previously described with some minor changes (***Boyle et al., 2006***). While using the 20µm beads we noticed that the embryo was moving away from the focus. We decided to use an NGM plate as a platform to place the embryo. The alternative approach is described in detail, (***Rodriguez et al., 2023***).

Single-cell sequencing and data analysis

Single-cell isolation was performed according to *Packer et al., 2019* with minor modifications. For a 100-200 cell stage, only one enzyme(Chitinase) was used for embryo eggshell disruption and single cells dissociation, (***Rodriguez et al.,* 2023**). Single-cell RNA sequencing was performed using the 10 x Genomics single-cell capturing system. Single cells were isolated from approximately 1,000 worms per strain. Ranging from 1,000 to 3,000 cells, were loaded on the 10 X Genomics Chromium

Controller. Single-cell cDNA libraries were prepared using the Chromium Next GEM Single Cell 3' LT Reagent Kits v3.1 (Dual Index). Libraries were sequenced by FSU College of Medicine Translational Science Laboratory (Florida State University, FL, USA). After the 10x QC, the N2 has 219 estimated number of Cells, 62,491 mean Reads per Cell and 1,067 Median Genes per cell. The *spr-5; met-2* has 686 estimated Number of Cells, 20,763 mean Reads per Cell and526 median genes per cell. Sequencing, 150 bp paired-end reads (Illumina NextSeq 600), samples received 28 million paired-end reads Cell Ranger Software Suite 3.0.2 (10x Genomics) was used for the alignment of the single-cell RNA-seq output reads and generation of feature, barcode and matrices. The Seurat analysis was used for the clusters formation.

ACKNOWLEDGEMENTS

We are grateful to the member of the Katz lab for their helpful discussion and critical reading of the chapter; J. Murray, C. Huynh, and A. Santella for advice on lineage tracing and single cell RNAseq; We thank J. Murray for the JIM113 strain. Juan D. Rodriguez was supported by NIH National Institute of Child Health and Human Development 3F31HD100145-03S1 grant and this work was supported by NSF IOS1354998.

REFERENCES

Adam Wood, Abhijit Shukla, Jessica Schneider, Jung Shin Lee, Julie D. Stanton, Tiffany Dzuiba, Selene K. Swanson, Laurence Florens, Michael P. Washburn, John Wyrick, Sukesh R. Bhaumik & Ali Shilatifard (2007) Ctk Complex-Mediated Regulation of Histone Methylation by COMPASS, Molecular and Cellular Biology, 27:2, 709-720, DOI: 10.1128/MCB.01627-06

Boyle, T. J., Bao, Z., Murray, J. I., Araya, C. L., & Waterston, R. H. (2006). AceTree: A tool for visual analysis of Caenorhabditis elegans embryogenesis. BMC Bioinformatics, 7. https://doi.org/10.1186/1471-2105-7-275

Carpenter, B. S., Lee, T. W., Plott, C. F., Rodriguez, J. D., Brockett, J. S., Myrick, D. A., & Katz, D. J. (2021). Caenorhabditis elegans establishes germline versus soma by balancing inherited histone methylation. *Development (Cambridge)*, *148*(3). https://doi.org/10.1242/dev.196600

Erdelyi, P., Wang, X., Suleski, M., & Wicky, C. (2017). A network of chromatin factors is regulating the transition to postembryonic development in Caenorhabditis elegans. G3: Genes, Genomes, Genetics, 7(2), 343–353. https://doi.org/10.1534/g3.116.037747

Furuhashi, H., Takasaki, T., Rechtsteiner, A., Li, T., Kimura, H., Strome, S., & Kelly, W. G. (2010). Trans-generational epigenetic regulation in *C. elegans* primordial germ cells. Developmental Biology. https://doi.org/10.1016/j.ydbio.2010.05.363

Greer, E. L., Beese-Sims, S. E., Brookes, E., Spadafora, R., Zhu, Y., Rothbart, S. B., … Shi, Y. (2014). A histone methylation network regulates transgenerational epigenetic memory in C.elegans. Cell Reports, 7(1), 113–126. https://doi.org/10.1016/j.celrep.2014.02.044

Katz, D. J., Edwards, T. M., Reinke, V., & Kelly, W. G. (2009). A *C. elegans* LSD1 Demethylase Contributes to Germline Immortality by Reprogramming Epigenetic Memory. Cell, 137(2), 308–320. https://doi.org/10.1016/j.cell.2009.02.015 evelopmental Cell, 5(5), 747–757. https://doi.org/10.1016/S1534-5807(03)00327-7

Kerr, S. C., Ruppersburg, C. C., Francis, J. W., & Katz, D. J. (2014). SPR-5 and MET-2 function cooperatively to reestablish an epigenetic ground state during passage through the germ line. Proceedings of the National Academy of Sciences, 111(26), 9509–9514. https://doi.org/10.1073/pnas.1321843111

Rodriguez-Crespo, D., Nanchen, M., Rajopadhye, S., & Wicky, C. (2022). The zinc-finger transcription factor LSL-1 is a major regulator of the germline transcriptional program in Caenorhabditis elegans. Genetics, 221(1), 1–15. https://doi.org/10.1093/genetics/iyac039

Schwenty-Lara, J., Nehl, D., & Borchers, A. (2020). The histone methyltransferase KMT2D, mutated in Kabuki syndrome patients, is required for neural crest cell formation and migration. Human Molecular Genetics, 29(2), 305–319. https://doi.org/10.1093/hmg/ddz284

Sobreira, N., Brucato, M., Zhang, L., Ladd-Acosta, C., Ongaco, C., Romm, J., … Bjornsson, H. T. (2017). Patients with a Kabuki syndrome phenotype demonstrate DNA methylation abnormalities. European Journal of Human Genetics, 25(12), 1335–1344. https://doi.org/10.1038/s41431-017-0023-0

Sulston, J. E., Schierenberg, E., White, J. G., & Thomson, J. N. (1983). The embryonic cell lineage of the nematode Caenorhabditis elegans. Developmental Biology, Vol. 100, pp. 64–119. https://doi.org/10.1016/0012-1606(83)90201-4

Ure, K., Lu, H., Wang, W., Ito-Ishida, A., Wu, Z., He, L. J., … Zoghbi, H. Y. (2016). Restoration of Mecp2 expression in GABAergic neurons is sufficient to rescue multiple disease features in a mouse model of Rett syndrome. ELife, 5(JUN2016), 1–21. https://doi.org/10.7554/eLife.14198

Wasson, J. A., Simon, A. K., Myrick, D. A., Wolf, G., Driscoll, S., Pfaff, S. L., … Katz, D. J. (2016). Maternally provided LSD1/KDM1A enables the maternal-to-zygotic transition and prevents defects that manifest postnatally. ELife, 5(JANUARY2016). https://doi.org/10.7554/eLife.08848

FIGURES and FIGURES LEGENDS

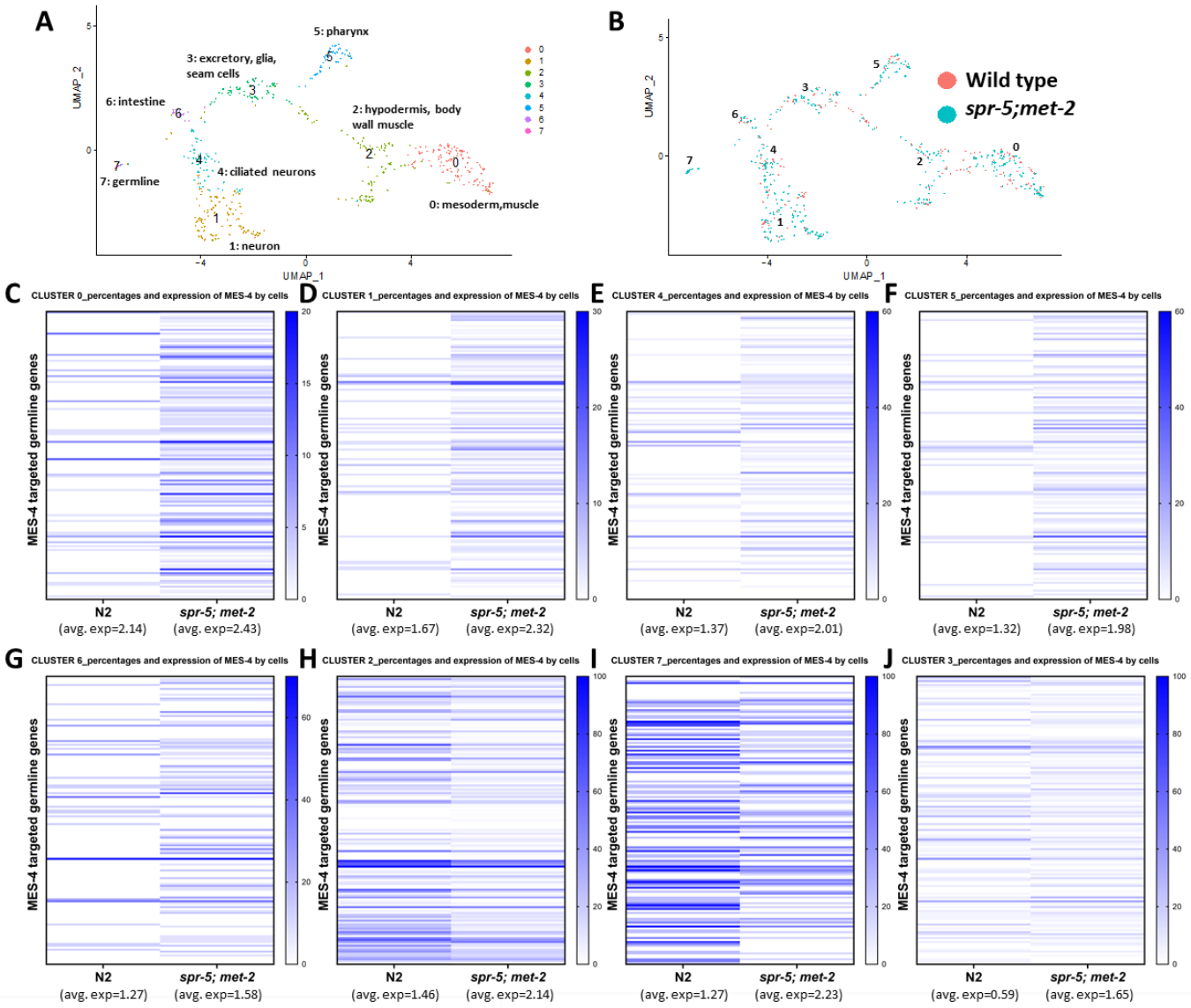

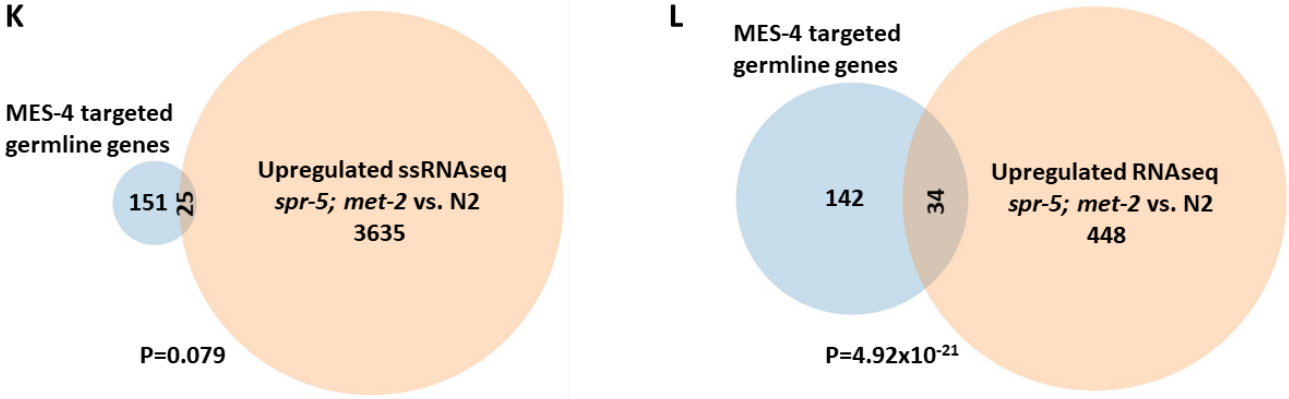

Figure 1. MES-4 targeted germline genes begin to be ectopically expressed during embryogenesis in *spr-5; met-2* mutants. (A) UMAP projection of all 219 Wild Type cells and 686 *spr-5; met-2* mutant cells from single-cell RNAseq formed 8 clusters. (B) All Wild Type (red) and *spr-5; met-2* double mutant (green) cells fall within these 8 clusters. (C-J) Heat maps from all 8 clusters (from A) showing the percentage of cells that express each of the 197 MES-4 targeted germline genes in Wild Type (N2) compared to *spr-5; met-2* mutants. The average gene expression across all 176 MES-4 targeted germline genes for each cluster is shown below the cluster. (K,L) Overlap between MES-4 targeted germline genes and total genes significantly upregulated in *spr-5; met-2* mutants in any of the 8 individual single-cell RNAseq clusters (K), or significantly upregulated in *spr-5; met-2* mutants at the L1 larval stage (L) from Carpenter et al. 2021. Significance in K and L was determined by a hypergeometric test.

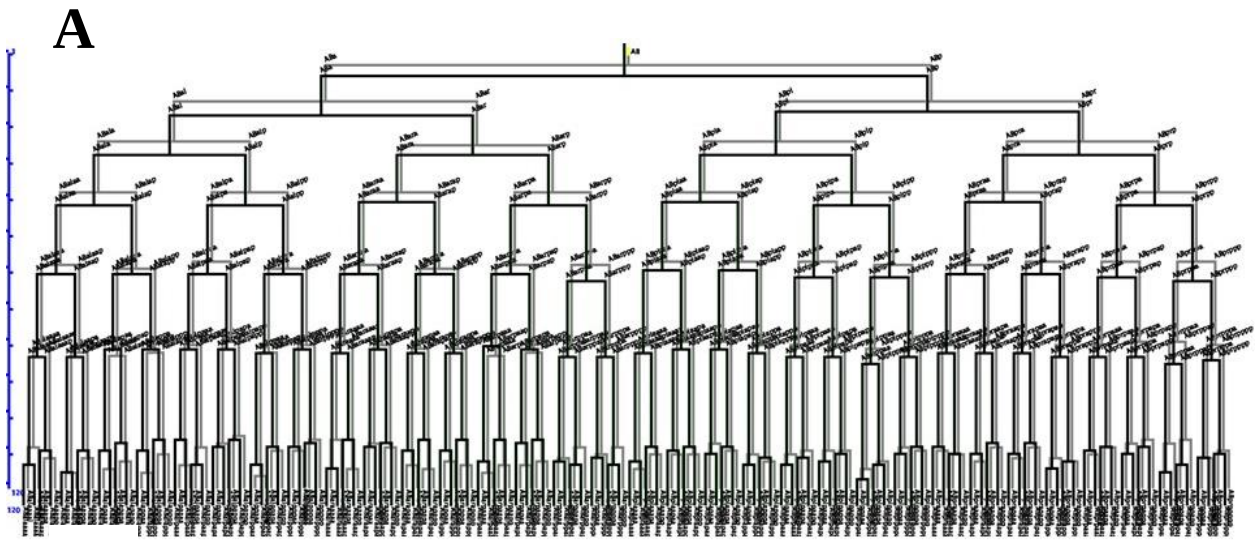
A

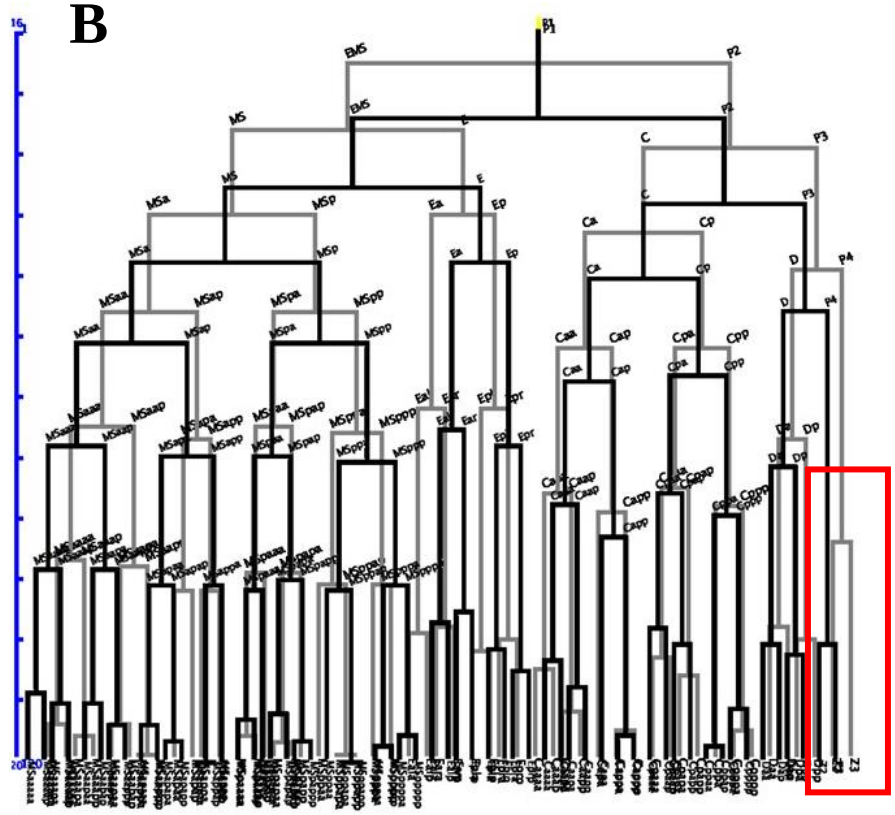
B

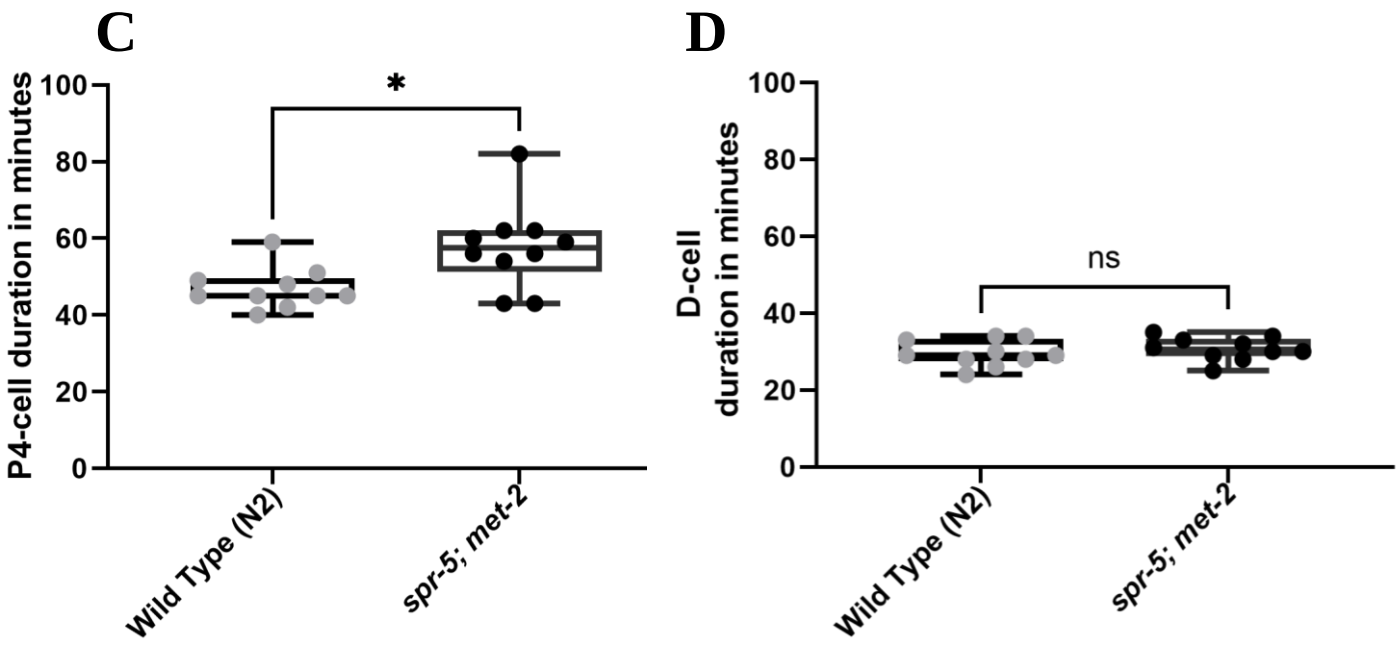

Figure 2. Comparison of the embryonic cell lineage in *spr-5; met-2* versus Wild Type (N2). Overlap between *spr-5; met-2* (black) and Wild Type (grey) in the AB (A) and P lineage (B) from the 2-cell stage through the ~200-cell stage. A total of 5 lineages of each were analyzed. The Y-axis indicates the end of cell division in minutes. The red box highlights the only observed defect, a delay in the division of the germline blastomere P_4 to the primordial germ cells, Z2 and Z3, quantified by duration in minutes in (C). (D) The corresponding duration in minutes of the cell D, immediately adjacent to P_4 in the embryo. (C,D) N= 10 for Wild Type and N=9 for *spr-5; met-2.* The error bars in C and D are S.E.M. Significance in C and D was determined by an unpaired t-test. *≤0.05

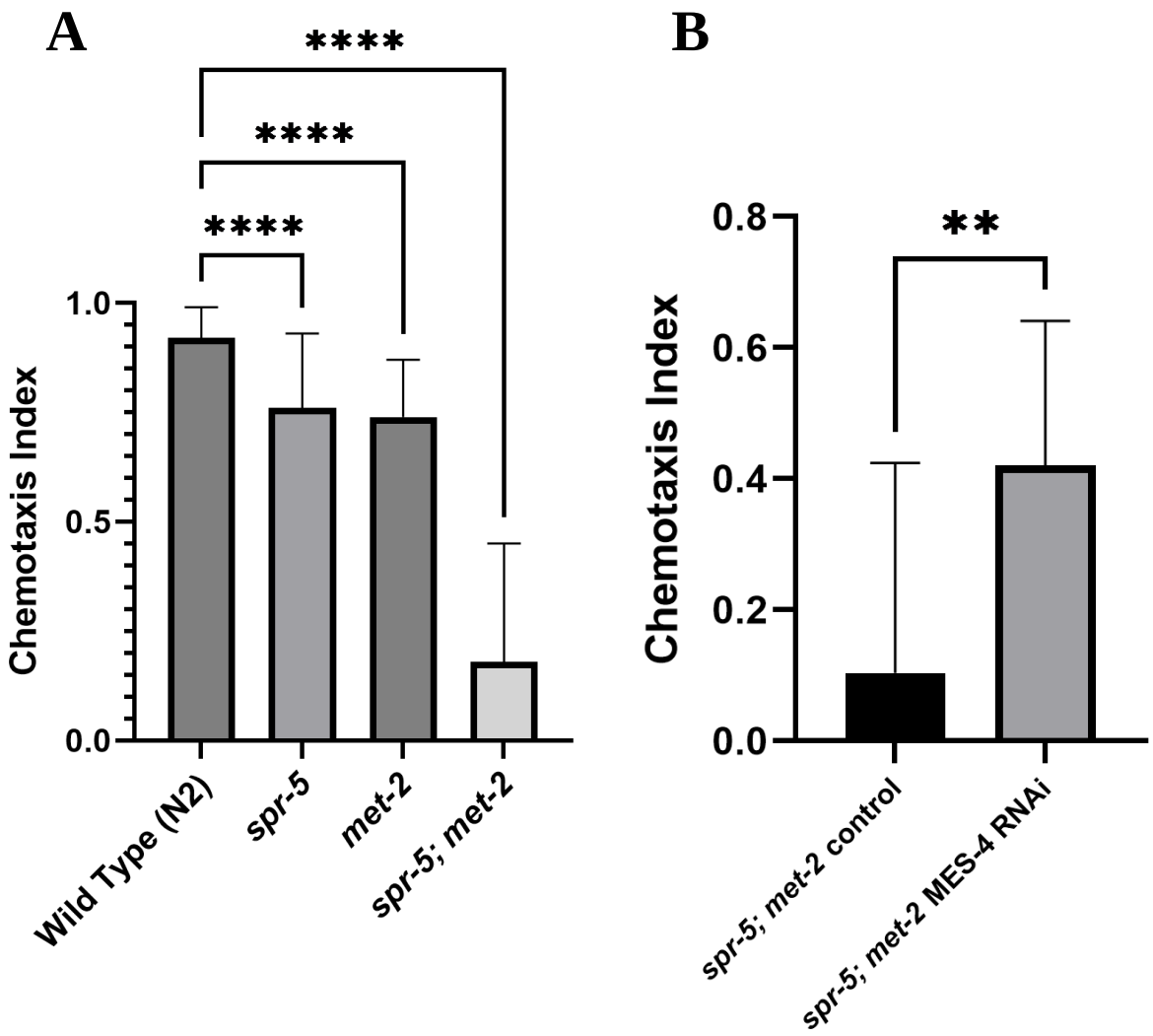

Figure 3. Chemotaxis defect in *spr-5; met-2* progeny. (A) The chemotaxis index of Wild Type (N2) N=1008, *spr-5* N=1661, *met-2* N=1117 and *spr-5; met-2* N=263. (B) The chemotaxis index of *spr-5; met-2* mutants is rescued by *mes-4* RNAi (N= 948) compared to control RNAi (N=690). The error bars represent the S.E.D.. Significance was calculated in (A) by one-way ANOVA and (B) by unpaired t-test. ****≤0.0001, **≤0.01.

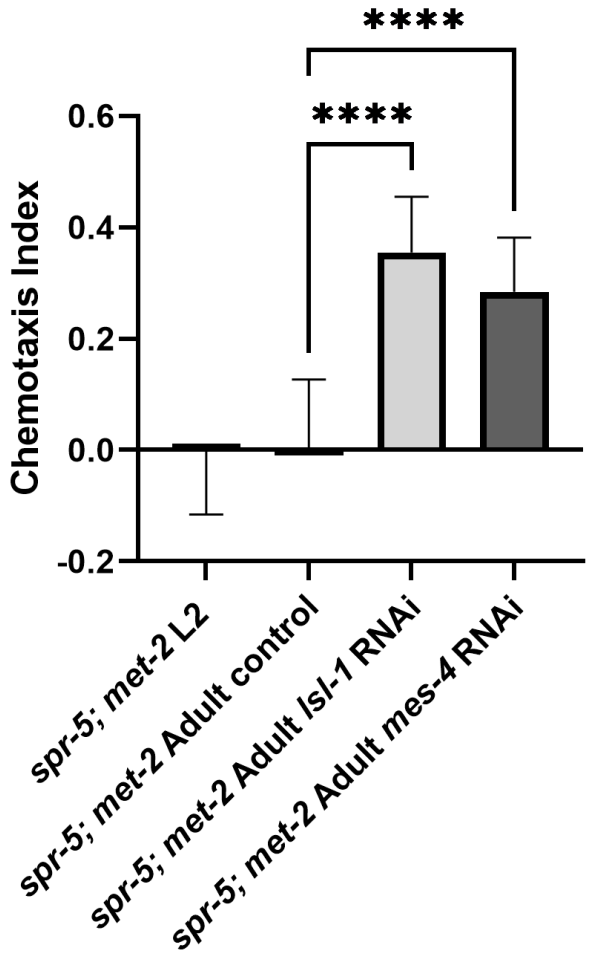

Figure 4. Blocking the ectopic transcription of MES-4 targeted germline genes in L2 *spr-5; met-2* mutants that already have a chemotaxis defect, restores normal chemotaxis. The chemotaxis index of L2 *spr-5; met-2* double mutants (N=2950) is significantly rescued *mes-4* (N=763) and *lsl-1* (761) RNAi but not control RNAi (N=603) in the same worms that were previously had a chemotaxis defect at the L2 stage. The error bars represent the S.E.M.. Significance was calculated by an unpaired t-test. ****= <0.0001

SUPPLEMENTAL MATERIALS

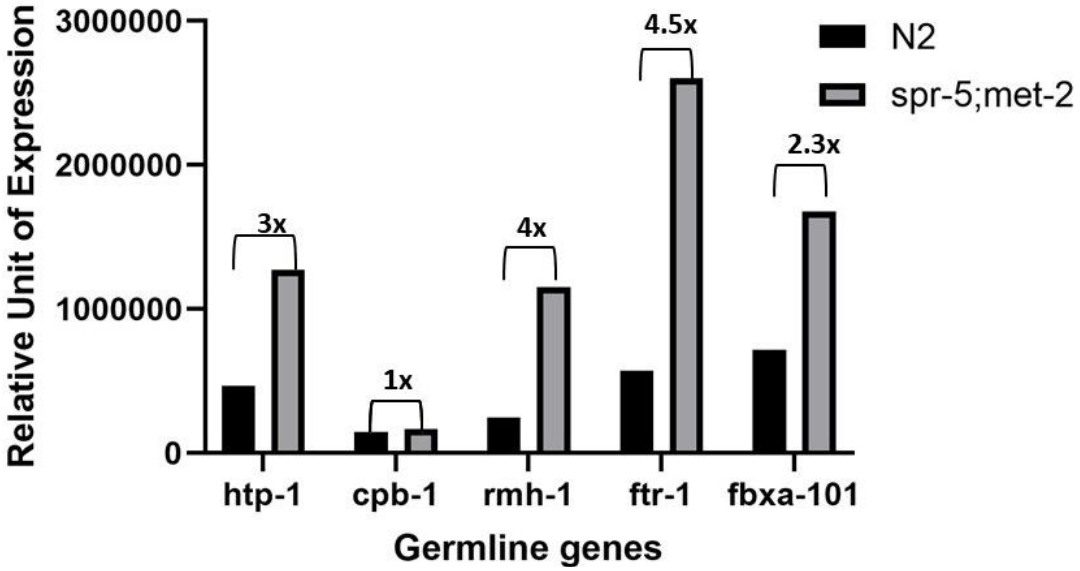

Supplemental Figure 1. Real-time RT-PCR data show levels of MES-4 germline gene expression. Each gene expression level was normalized against the ama-1 control. The fold change was calculated for each N2 and *spr-5; met-2*. Fold change represent the differences in level expression between N2 and *spr-5; met-2*. The embryos were synchronized at the 100-160 cell stage.

CHAPTER 5:

Discussion

5.1 Epigenetic reprograming at fertilization by SPR-5 and MET-2 is required to prevent embryonic and larvae phenotypes

At the beginning of this dissertation, I proposed that the inappropriate inheritance of histone methylation would cause a defect in cell specification. We have shown that the *spr-5; met-2* mutants have multiples phenotypes. These worms have a small percentage of embryonic lethality, ~15% (***Figure 1***). I haven't investigated what causes this embryonic lethality phenotype, but I have observed that the embryos died at different stages. For example, while setting up some movies for lineage tracing I observed embryos that died at the 40-60 cell stage, and others failed to hatch. This inconsistency could be due to the mutations slightly affecting the parental generation and failure to complete a key developmental process such as gastrulation. Interestingly, I noticed that embryos that were more round initially at the 2-cell stage tend to die more frequently in the eggshell. As a result, for the automated lineage tracing experiments, I started with only the embryos that were not round and included only embryos that hatched in the analysis. To investigate if the small percentage of embryonic lethality is due to failure to complete gastrulation or failure to hatch, I propose to start by performing DIC live imaging to monitor these stages. In addition, I could investigate these potential defects by using markers for gastrulation or muscle markers that are involved in the process of breaking the eggshell and hatching. This would

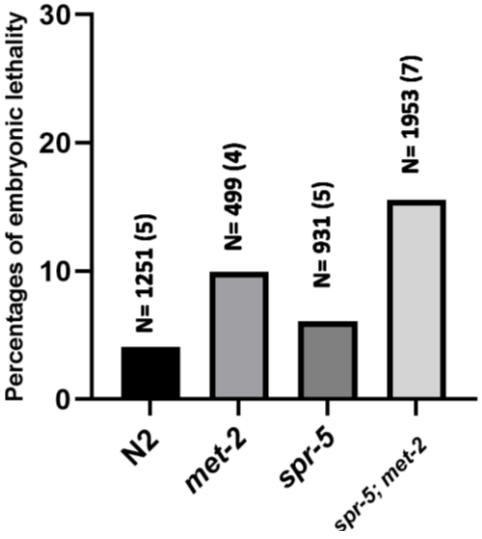

Figure 1. Embryonic lethalithy quantification. Four different worm strain N2(Wild-type), *met-2, spr*-5 and *spr-5; met-2* double mutant. N= total of worm, parenthesis number, parental used for each worm strains.

provide valuable information as to whether the protein involved in these processes is affected in the double mutant.

spr-5; met-2 double mutant larvae have a severe developmental delay. From previous data from the lab, we knew that the developmental delay depends on the ectopic expression of the MES-4 targeted germline genes. When *mes-4* is knocked down maternally by RNA interference and the ectopic expression is eliminated, the developmental delay is rescued in the double mutant. However, one question that remains is when the ectopic germline gene expression is triggered during development? We observed the expression of one of these germline genes by *in-situ* experiments at ~200 cell stage. In addition, I performed RT-PCR on synchronized embryos at ~100-cell stage to investigate if the MES-4 targeted germline genes are already misexpressed. These data suggest that some of the germline genes are already misexpressed at the embryonic level, although in most cases the expression is lower compared to what we previously observed by bulk RNAseq at L1 stage in the *spr-5; met-2* double mutant (*Carpenter et al., 2021*) (***Figure 2***). For example, the *cpb-1* gene is expression at a lower level at the ~100-cell stage and is dramatically increased at the L1-larvae stage. Consistent with this, in my ssingle-cellRNAseq I observe the ectopic expression of MES-4 targeted germline genes, but fewer of these genes are misexpressed than what we observe at the L1 stage (*Carpenter et al., 2021*). In addition, the MES-4 targeted genes are expressed more widely at the L1 stage than in the embryo. A possible explanation is that the ectopic expression of germline genes is building up during development because the accessible chromatin requires transcription factors to turn on the genes ectopically. These transcription factors may only be expressed with the

progress of developmental stages. To investigate this idea, I propose to perform the **A**ssay for **T**ransposase **A**ccessible **C**hromatin (ATAC-seq) at the 100-cell stage, L1 larval stage and in adult *spr-5; met-2* double mutants. ATAC-seq peaks correspond to transcription factor binding sites. Therefore, from the ATAC-seq I expect to see transcription factors binding increasingly to the ectopically expressed germline genes in more advanced developmental stages.

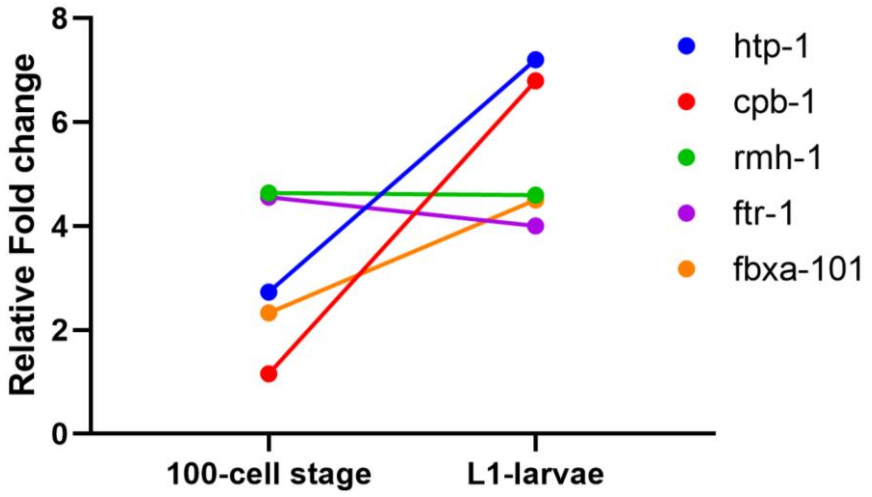

Figure 2. RT-PCR from two different developmental stages of the *spr-5; met-2* double mutant. The fold change expression of each gene were normalized against *ama-1* control

spr-5; met-2 double mutants eventually (>96hrs after hatching) reach the adult stage and are sterile. Moreover, we found that *spr-5; met-2* mutants have a defect in chemotaxis toward food defect beginning at the L2 stage. This phenotype could suggest that there is a lineage defect in the neuronal cell lineage, which could affect the ciliated neurons (AWA and AWC) that sense the food. However, we tracked the entire embryonic lineage of the double mutant and we didn't see any defect in cell division, migration, timing, or programmed cell death in this cell lineage. This suggests that the system is robust enough that the cell can make the correct decision even in the presence of the inappropriate inheritance of histone methylation and the ectopic

expression of MES-4 targeted germline genes. Thus, it would be interesting to investigate if the neurons that sense the food are present and functional in the double mutant. The *C. elegans* olfactory network system has been established (*Troemel and Bargmann et al* 1997) and the neuronal pathway that senses food is well known. In addition, the entire neuronal atlas of *C.elegans* has been mapped out and a *C. elegans* transgenic strain called NeuroPAL (neuronal polychromatic atlas of landmarks) was constructed that labels each of the 302 neurons fluorescently (*Yemini et al.,* 2021). To investigate if the chemotaxis defect is due to the absence of the olfactory neurons, I crossed the *spr-5; met-2* double mutant with the NeuroPAL strain (***Figure 3***). I took confocal pictures of the entire nervous system of the worms (head, midbody and tail). The goal is to analyze each image using the NeuroPAL-ID software and see if the *spr-5; met-2* contains the 302 neurons. Preliminarily, I do not detect any gross defects in the presence of neurons. If *spr-5; met-2* mutants contain the 302-neurons, then the chemotaxis phenotype could be due to ongoing defects in a fully established nervous system. A future experiment would be to test the function/activity of these neurons by performing calcium imaging with a GCaMP calcium sensor. GCaMP calcium sensors light up due to neuronal activity and calcium release (*Yemini et al.,* 2021). Strains that only express these sensors in either AWA or AWC can be used to specifically determine whether these neurons are active in the presence of OP50 bacteria. An alternate possible explanation is that neurons involved in sensing the food are transmitting the wrong message. For example, AWA and AWC also sense pathogens and avoid them. It could be that in *spr-5; met-2* mutants, these neurons are now sensing the OP50 (food source) as a pathogen and the worm is avoiding it in the chemotaxis assay. To test this

idea I could place the double mutants on a plate with two sources, OP50 and the pathogen. If the double mutant moves toward the pathogen and avoids the food, this would be consistent with a “switch” in the function of AWA and AWC.

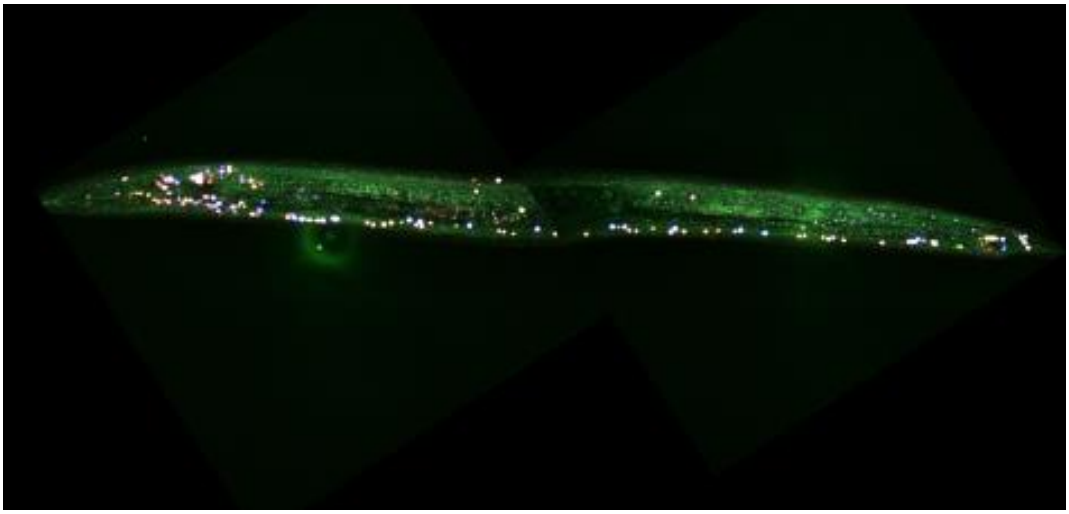

Figure 3. A Multicolor Atlas for Whole Neuronal system. The adult *spr-5; met-2* showing the color code neurons

Recently, the Katz lab obtained RNA-seq and chemotaxis data from the single mutants *spr-5* and *met*-2 across generations. The single mutants also show a slight chemotaxis defect at each generation, but the defect is not nearly as severe as double mutants and does not get more severe over generations. Since the single mutants misexpress many of the same germline genes over generations that are misexpressed in double mutants, the lack of severe chemotaxis defect in single mutants provided the opportunity to determine which ectopic germline genes might be causing the severe chemotaxis defect by subtracting germline genes that are misexpressed in single mutants from ones that are misexpressed in double mutants. To do this, the RNA-seq data from single mutants over generations were compared with the RNA-seq data from the *spr-5; met-2* double mutant. We found that genes involved in meiosis and chromatin condensation are misregulated in the *spr-5; met-2* double mutants but not in the single

mutants. Therefore, a possible explanation for the chemotaxis defect is that the chromatin is innaproppriately condensed in the neuronal cells involved in food sensing. To investigate this possibility, I could perform chromosome organization experiments such as a Hi-C or chromosomal paint, in the double mutant.

5.2 *spr-5; met-2* have a germline lineage defect

During the automated cell lineage analysis, we didn't expect to see any defect in the germline lineage because the P-lineage (germline) is normally transcriptionally quiescent. PIE-1 maintains the transcriptionally quiescent of the germline by preventing RNApolII from elongating (*Seydoux et al 1996*). This protects the germline lineage from adopting a somatic identity. In addition, epigenetic mechanisms also regulate the cell specification of the germline lineage. For example, the maternally deposited MES-4 maintains H3K36me at some germline genes during embryogenesis. Without maternal MES-4, progeny are sterile, indicating that MES-4 is required for germline specification (*Furuhashi et al., 2010*). Finally, H3K4me2 levels are maintained throughout the P-lineage, but are erased in the two primordial germ cells, Z2 and Z3 (*Schaner et al 2003*). To our surprise, we observed one constant defect in the embryonic lineage of *spr-5; met-2* mutants. All the double mutant lineages show a delay in cell division, from the germline blastomere P4 to the primordial germ cells, Z2 and Z3. This delay results in P4 persisting on average for 15-20 additional minutes. The coincidence of this delay with the erasure of H3K4me2 raised the possibility that the delay could be due to to the failure to erase H3K4me2 in Z2 and Z3. To investigate this idea, I performed immunofluorescence analysis and the preliminary data suggests that H3K4me2 is not

erased in the Z2 and Z3 cells in *spr-5; met-2* mutants. The failure to erase H3K4me2 in Z2 and Z3 could be due to an increase in H3K4me2, caused by the failure of SPR-5 to erase H3K4me2 and the failure of MET-2 to replace this H3K4me2 with H3K9me2 at fertilization. Consistent with this, H3K4me2 retention was observed in Z2 and Z3 at late generations in *spr-5* single mutants (*Katz et al., 2009*). Regardless of the mechanism, it is possible that the failure to erase H3K4me2 causes the delay in the P4 cell division. The failure to erase H3K4me2 in *spr-5;met-2* mutants is also consistent with the possibility that *spr-5; met-2* mutants are sterile because of the failure to erase H3K4me2 in Z2 and Z3. However, the analysis of H3K4me2 in Z2 and Z3 was complicated by the fact that P-granules are found ectopically in *spr-5; met-2* mutants. This made it impossible to definitively identify Z2 and Z3 in the analysis of H3K4me2.

Along with the delay in the P4 cell division, our single-cell RNAse data also indicates a potential defect in germline specification. We found that MES-4 targeted germline genes are upregulated in all somatic lineages of the embryo, but downregulated in the germline lineage. This suggests that MES-4 targeted germline genes fail to fully activate in the embryonic germline of *spr-5; met-2* mutants. Taken together, these data point to a possible model. The increased H3K4me2 in *spr-5; met-2* mutants overwhelms the erasure of H3K4me2 that normally occurs in Z2 and Z3. This results in a delay in the division from P4 to Z2 and Z3 and failure to properly activate MES-4 targeted germline genes, which contributes to the sterility observed in *spr-5; met-2* mutants.

5.3 Proposed mechanism

During embryogenesis, cells have to migrate to the correct place and the timing of cell division is crucial. The transcriptome and the epigenetic profile of the cells regulate these processes. It's well known that the expression of specific genes can drive the cell lineage specification. For example, in *C. elegans* the expression of PHA4 in the pharyngeal lineage is necessary for the development of the pharynx. Thus, altering the expression of fundamental genes or the chromatin in that cell can lead to different cell specification defects. In the *spr-5; met-2* mutant, H3K4me2 is inappropriately inherited and accumulates (*Kerr et al., 2014*). This suggests that the chromatin profile of some or all cells is altered, which could result in cell specification defects. Interestingly we didn't observe any defect in the somatic cells in the *spr-5; met-2* mutant, but we still observe somatic phenotypes later in development. A possible explanation for this is that even through the chromatin is permissive for transcription, cells of the early embryo lack the proper cell specification transcription factors to activate the permissive chromatin. As a result, the cells could all be properly specified. However, later in development when the cell specification transcription factors are activated, these transcription factors could activate the permissive chromatin, resulting in the ectopic expression of MES-4 targeted germline genes. This could actively inhibit the function of these more differentiated cells. For example, in the chemotaxis defect, the neurons that sense the food could be present but not working properly. To test this idea we knocked down MES-4 by RNAi zygotically to see if the chemotaxis defect can be rescued. Knock down of *mes-4* in *spr-5; met-2* mutants that previously failed the chemotaxis assay rescued the chemotaxis defect by shutting down the ectopic expression of MES-4 targeted germline genes. This suggests that the ectopic expression of the germline genes is interfering with the

function of the cells. This remarkable finding has major implications for human neurodevelopment patients.

5.4 Conclusions

The are a number of neurodevelopmental disorders caused by mutations in histone modifying enzymes. For example, Kabuki syndrome is caused by a mutation KMT2D gene (also known as MLL2) or the KDM6A gene. Kabuki patients have developmental delay, craniofacial defects, intellectual disability and behavioral abnormalities. In addition, three patients have been identified with mutations in LSD1/SPR-5/KDM1A. The LSD1 patients have phenotypes that are highly similar to Kabuki Syndrome. The function of histone modifications is highly conserved. Therefore, it is possible that the mechanism we uncovered in the *spr-5; met-2* double mutants could be relevant to these patients. For example, the intellectual disability and/or behavior abnormalities could be due to the ongoing misexpression of genes in a fully intact brain. If this were to be the case, it might be possible to rescue the abnormalities in these patients by restoring the chromatin and turning off the ectopic transcription. It is even possible that meiosis and chromosomal condensation germline genes, which we believe may be the problem in *spr-5; met-2* double mutants, may also be the problem in these patients. Our lab has developed a new mouse LSD1 model that recapitulates all of the defects observed in LSD1 patients and Kabuki syndrome. This will provide the opportunity to begin to test whether the mechanism that I uncovered in my thesis work can potentially lead to a treatment for these patients.

Appendix: A model for Epigenetic Inhibition via Transvection in the Mouse

Publication: A model for Epigenetic Inhibition via Transvection in the Mouse
Rodriguez JD, Myrick DA, Falciatori I, Christopher MA, Lee TW, Hannon GJ, et al. A Model for Epigenetic Inhibition via Transvection in. Genetics. 2017; 207(September):129–38. (Highlighted Article)

A Model for Epigenetic Silencing via Transvection in the Mouse

Juan D. Rodriguez[1], Dexter A. Myrick[1], Ilaria Falciatori[2], Michael A. Christopher[1], Teresa W. Lee[1], Gregory J. Hannon[2] and David J. Katz[1,4]

[1]Cell Biology Department, Emory University, Atlanta, GA 30322, USA
[2]Cancer Research UK Cambridge Institute, University of Cambridge, Cambridge, England

[3]Corresponding author
Telephone: (404) 727-3403
Fax: (404) 727-6256
E-mail: djkatz@emory.edu

Abstract

Recombination between *LoxP* recognition sequences has been widely utilized in the mouse for conditional gene targeting. During our attempt to engineer a mouse mutation with the germline expressed *Vasa-Cre* transgene, we observe a *Cre*-induced transvection event, where the efficiency of *LoxP* recombination is dramatically reduced. A similar phenomenon has previously been observed with another meiotic *Cre* transgene, *Sycp-1*. This second example of *LoxP* silencing by transvection reinforces the conclusion that certain meiotically expressed *Cre* alleles can initiate transvection in mammals. However, unlike what was previously observed with *Sycp-1*, we find that the inhibition of *LoxP* recombination cannot be accounted for by DNA methylation. In addition, we show that the inhibition of *LoxP* recombination can be alleviated by adding an extra generation between the initial recombination event and the *LoxP* silencing that occurs during passage through the subsequent germline. This finding confirms that the *LoxP* sites are silenced via an epigenetic mechanism, and provides a potential method for the use of other meiotically expressed *Cre* transgenes associated with a similar *LoxP* silencing event. Furthermore, the abrogation of *LoxP* silencing by the simple addition of an extra generation in our crosses establishes a unique mouse system for future studies to uncover the mechanism of transvection in mammals.

Introduction

Transvection refers to the ability of one locus to affect a homologous locus *in trans.* This phenomenon was first discovered in *Drosophila* at the *Bithorax* complex(Lewis, 1954). Subsequent examples have been found in both plants and fungi(Aramayo and Metzenberg, 1996; Coe, 1966; Woodhouse et al., 2006). However, although the few known examples of transvection occur in a wide range of taxa, to our knowledge only two cases have ever been observed in mammals(Rassoulzadegan et al., 2002; Sandhu et al., 2009).

One example of mammalian transvection was identified during an attempt to use the *Cre*/*LoxP* system to engineer a gene deletion in the mouse germline(Rassoulzadegan et al., 2002). *LoxP* sequences, originally identified in the P1 bacteriophage, recombine with nearly perfect efficiency in the presence of the CRE recombinase protein. As a result, the *Cre*/*LoxP* system has been successfully utilized for conditional gene targeting in virtually all mouse tissues (Sauer, 1998). However, using a transgene with *Cre* driven by the *Sycp-1* male meiosis-specific promoter, the Cuzin group identified a notable exception. During the initial exposure to CRE in the germline of male mice, they found that *LoxP* recombination occurs with very high efficiency (Rassoulzadegan et al., 2002). However, the recombination efficiency declined sharply during the second passage through the germline(Rassoulzadegan et al., 2002). These results suggest that the initial meiotic recombination event can lead to the silencing of the floxed (flanked by *LoxP* recombination sites) allele on the other homologous chromosome, a classic example of transvection. In addition, they observed that the methylation status of the *LoxP* sequences correlated with a failure to

recombine, and methylating the *LoxP* sequences in a plasmid prior to transfection into mammalian cells inhibited recombination (Rassoulzadegan et al., 2002). Based on this evidence, they concluded that the *LoxP* sites are silenced by DNA methylation, which they hypothesized blocks the CRE recombinase protein from recognizing its target sequence(Rassoulzadegan et al., 2002).

Recently, another example of transvection was identified in mammals. Imprinted loci are controlled by *cis*-acting sequences known as imprinting control regions (ICRs). Sandu *et al.* found that ICRs from several imprinted loci physically interact. This allows the CTCF binding sites at the *H19* ICR to influence the replication timing of other ICRs *in trans*(Sandhu et al., 2009). However, despite this second example, the mechanism of transvection remains unknown, and the small number of mammalian examples makes further investigation into this phenomenon prohibitive.

Although the mechanism of mammalian transvection remains unknown, two prevailing models have emerged. One possibility is that transvection occurs when homologous chromosomes are paired during meiosis. The example of CRE-driven transvection in mice is consistent with this first model, since *Cre* is expressed during male meiosis, when chromosomes are maintained in close proximity(Rassoulzadegan et al., 2002). This model is also supported by the second example of mammalian transvection, where ICRs physically interact, though this interaction occurs in germ cells that are not undergoing meiosis(Sandhu et al., 2009).

Alternatively, it is possible that transvection does not require any physical interaction between homologous chromosomes. In this case, transvection could be mediated by a molecule that diffuses between the two chromosomes(Arteaga-Vazquez

and Chandler, 2010). This model is supported by evidence from maize. At the b1 locus, the weakly expressed B' allele can epigenetically repress the B-I allele, causing it to become as weakly expressed as B'. This effect, known as paramutation, can be stably propagated throughout generations even in the absence of the initiating B' allele(Chandler, 2007). The mechanism of paramutation at the b1-locus is thought to be mediated by a small interfering RNA (siRNA) that diffuses between the two homologous chromosomes.

In this study, we attempted to use a germline *Cre*, *Vasa-Cre*, to conditionally delete the histone demethylase *Kdm1a/Lsd1* (hereafter referred to as *Kdm1a*) (Gallardo et al., 2007; Wang et al., 2007). Similar to what was previously reported with *Sycp1-Cre*, we find that recombination of the *Kdm1a* floxed allele becomes inhibited through a transvection event. This second example of *LoxP* silencing by transvection reinforces the conclusion that meiotically expressed *Cre* can initiate transvection in mammals. However, unlike the prior report, our data show that DNA methylation does not inhibit *LoxP* recombination. Furthermore, we demonstrate that the addition of an extra generation between the initial recombination event and the transvection event alleviates the inhibition of *LoxP* recombination. This result provides three critical insights. First, it suggests a useful strategy to overcome instances where other *Cre* transgenes lead to similar *LoxP* silencing events. Second, our observation that two genotypically identical mice with differing parental history can exhibit dramatically different outcomes provides strong evidence that transvection in these mice is an epigenetic phenomenon. Finally, the juxtaposition of our original crosses, where we observe *LoxP* silencing via

transvection, with our extra cross, where transvection is eliminated, establishes an ideal system for future studies to elucidate the mechanism of transvection in mammals.

Results

LoxP recombination is inhibited during germline conditional deletion

In order to conditionally delete a floxed allele of *Kdm1a* (Figure 1A,B), we crossed floxed *Kdm1a* mice (Wang et al., 2007) to a transgenic *Cre* recombinase line in which *Cre* is driven by the germline specific *Vasa/Ddx4* promoter (hereafter referred to as *Vasa-Cre*) (Figure 1B). The *Vasa-Cre* transgene is expressed exclusively in the germline of male and female mice beginning just prior to birth(Gallardo et al., 2007). Additionally, in mothers carrying the transgene, VASA-CRE protein is maintained in the mature oocyte and can induce *LoxP* recombination in the early embryo. Therefore to avoid the maternal contribution, *Vasa-Cre* males were used during F2 crosses (Figure 1B).

Upon crossing floxed F0 *Kdm1a* males to *Vasa-Cre* females, we observed 100% recombination between *LoxP* sites (Figure 1B). The high recombination efficiency in the initial F1 cross led us to expect the remaining floxed *Kdm1a* allele to recombine with similar high efficiency. However, during subsequent F2 crosses to generate homozygous conditional mutants, we find that the efficiency of *LoxP* recombination is dramatically reduced, with a failure to recombine observed in 67% of progeny (N=43). Importantly, this reduction in *LoxP* recombination efficiency is specific to the *Vasa-Cre* transgene, as 100% recombination is achieved in both F1 and F2 crosses when *Kdm1a*

is conditionally deleted with either of the oocyte-expressed *Cre* transgenes, *Zp3-Cre* and *Gdf9-Cre* (Ancelin et al., 2016; Wasson et al., 2016).

The *Vasa-Cre* transgene is still expressed during *LoxP* inhibition

It is possible that the dramatic reduction in the efficiency of *LoxP* recombination in F2 crosses is caused by silencing of the *Vasa-Cre* transgene. To examine this possibility, we performed immunofluorescence on F2 testes in which the *LoxP* sites fail to recombine. We observe that CRE protein is expressed in spermatocytes and spermatids in the F2 testes that largely fail to undergo recombination (Figure 2). This suggests that the inhibition of recombination is likely caused by silencing of the *LoxP* sites themselves, rather than the lack of CRE expression from the *Vasa-Cre* transgene. This conclusion is identical what has previously been suggested for *Sycp1-Cre* mediated transvection (Rassoulzadegan et al., 2002).

Adding an extra generation alleviates *LoxP* inhibition

Little is known about the mechanism of transvection in mammals. However, based on the example of paramutation at the b1 locus in maize, transvection might be facilitated by a molecule able to diffuse between the two homologous chromosomes. During our crosses to conditionally delete *Kdm1a* in the germline, a *LoxP* targeted diffusible molecule could be generated in the F1 germline. This molecule could then be packaged into the F1 sperm, and direct the silencing machinery in the early embryo to the *LoxP* sites on the paternally inherited floxed chromosome. If transvection in our crosses occurred via this mechanism, then we could potentially alleviate the transvection event

by crossing our F1 mice to Wild Type for a generation before backcrossing to the *Kdm1a* floxed mice. In this case, the sperm would no longer contain the diffusible molecule generated in the F1 germline. To test this hypothesis, we added an additional cross to Wild Type after the F1 generation to generate F2 mice (hereafter referred to as extra cross F1 mice). These resulting extra cross F1 mice are genotypically identical to the F1 mice in our original cross, but with a different parental history. Compared to the original cross that resulted in only 33% recombination, the addition of this extra cross restored *LoxP* recombination to 100% efficiency (N=35) (Figure 3A). This result suggests that the *LoxP* sites in our original cross are being epigenetically silenced.

The alleviation of transvection with the extra cross is consistent with a model where a freely diffusible molecule can silence *LoxP* sequences *in trans*. Based on this model, crossing to a different floxed gene might result in *LoxP* silencing at this additional locus. To test this possibility, we crossed F1 mice, containing one deleted allele and one wild-type allele of *Kdm1a*, to mice that are homozygous for the floxed allele of *Arl13b.* In this cross (hereafter referred to as the heterologous cross), we find that the floxed allele of *Arl13b* recombines 100% of the time (Figure 3A,B), suggesting that transvection is confined to the *Kdm1a* locus. This indicates that the *LoxP* recognition sequence is not sufficient to initiate silencing, and that sequences flanking the *LoxP* may also be involved.

Sperm RNA does not target *LoxP* sites for inactivation.

The successful recombination in the F1 extra cross mice supports a transvection model involving a freely diffusible molecule. Based on the example of paramutation at the b1

locus in maize, we considered the possibility that this molecule could be an RNA. For example, if small RNAs targeting the *LoxP* site were generated in the germline as a response to the first recombination event, they could be deposited in F1 sperm and initiate silencing of the *LoxP* sites on the homologous chromosome in the early F2 embryo. The plausibility of such a model has been demonstrated at the *Kit* locus in mice, where sperm RNA mediates a trans-generational silencing event (Rassoulzadegan et al., 2006).

If the observed transvection were due to small RNAs targeting the floxed *Kdm1a* allele, we reasoned they should only be present, or at least be more abundant, in F1 sperm from the original cross. To examine this possibility, we produced small RNA libraries from multiple F1 sperm samples derived either from the original cross or the extra cross. However, we do not detect any RNA reads specifically overlapping with the *LoxP* recognition site. We also failed to detect any enrichment for F1 original cross small RNAs mapping to the regions flanking the *LoxP* sites (Figure 4A). This lack of small RNA enrichment at the *Kdm1* floxed locus was not due to a deficiency in our small RNA libraries, as we detect the normal high number of reads mapping to the 5' half of *tRNA-Gly-GCC-5-1* (Figure 4B). Furthermore, we also did not detect any consistent differences in micro RNAs (miRNA), piwi-RNAs (piRNA), repeats, ribosomoal RNAs (rRNA) or transfer RNAs (tRNAs) between replicates (Supplemental Figure 1). Taken together, these results seem to exclude the possibility that *LoxP* targeted small RNA molecules deposited in sperm are responsible for silencing of the *LoxP* site *in trans*.

LoxP sites are DNA methylated prior to _LoxP_ inhibition.

Previously, it was suggested that inhibition of *LoxP* recombination occurs via DNA methylation of two CpG dinucleotides within the 34bp *LoxP* site (Figure 1A)(Rassoulzadegan et al., 2002). This methylation was hypothesized to block the binding of the CRE recombinase to the *LoxP* recognition site (Rassoulzadegan et al., 2002). To determine if DNA methylation might also account for the decreased recombination efficiency in our F2 original cross mice, we used bisulfite DNA methylation analysis to determine the methylation status of the *LoxP* sites in our crosses. Consistent with the observations of Rassoulzadegan and colleagues, we found DNA methylation at two CpG dinucleotides within the LoxP recognition sites that were inhibited from recombining (Figure 5A,D). We also detect methylation at CpG dinucleotides immediately adjacent (1 CpG 11bp 5' and 2 CpG's 9bp 3' and 28bp 3') to the *LoxP* site (Figure 5D). However, we observed a similar methylation profile in F1 extra cross alleles that recombined with perfect efficiency (Figure 5C). Furthermore, the F0 floxed *Kdm1a* allele used to initiate these crosses was also fully methylated at these CpG dinucleotides, in the complete absence of any Cre transgene (Figure 5B). These data strongly suggest that DNA methylation is not sufficient to inhibit *LoxP* recombination in these mice.

In addition to CpG DNA methylation, we also observe non-CpG methylation in the *LoxP* recognition site (Supplemental Figure 2). This methylation occurs at one of the cytosine residues that was also previously reported to be methylated in *Sycp1-Cre* crosses (Rassoulzadegan et al., 2002). The observation of this non-CpG methylation in F1 original cross mice, where recombination occurs with full efficiency, indicates that

this non-CpG methylation also does not inhibit *LoxP* recombination (Supplemental Figure 2B).

We were surprised to find that *Kdm1a LoxP* sites were already methylated at CpG residues prior to the introduction of the *Cre* transgene. This suggests that *LoxP* sites may be stochastically targeted by DNA methylation. To determine if this is the case, we assayed the DNA methylation status of the *LoxP* recognition sequence in another floxed allele at the *Arl13b* locus(Su et al., 2012). These mice have been shown to undergo normal *LoxP* recombination with several different *Cre* transgenic lines(Higginbotham et al., 2013; Su et al., 2012). Similar to what we observed in *Kdm1a* mice, we find that the two CpG dinucleotides in the *Arl13b LoxP* recognition sequence are also largely methylated (Figure 5A). This result is consistent with our conclusion that DNA methylation is not sufficient to inhibit *LoxP* recombination.

CpG methylation does not inhibit CRE binding to *LoxP* sites.

Our observations that *LoxP* sites can recombine normally even when they are fully methylated suggests that the CRE recombinase must be able to bind to methylated *LoxP* recognition sequences. To test the ability of CRE to bind methylated *LoxP* sites, we performed electrophoresis mobility shift assays (EMSA). EMSAs were performed with radiolabeled 34bp *LoxP* probes that were either methylated or unmethylated at both CpG dinucleotides (Figure 1A). Recombinant CRE protein produced a strong retarded mobility complex with the unmethylated *LoxP* recognition sequence, indicating that CRE binds with high affinity to the *LoxP* site (Figure 6, lanes 1 and 2). This binding was specific, as *LoxP* sequences, but not an unrelated promoter sequence, could

compete for binding at 200-fold excess (Figure 6, lanes 3 and 4). Most importantly, CRE binding was also independent of methylation status, as the fully methylated *LoxP* probe produced an identical pattern of strongly retarded mobility (Figure 6, lanes 5-8)). This result, that CRE binds to the *LoxP* recognition sequence regardless of DNA methylation status, is consistent with our *in vivo* observations that DNA methylation does not inhibit *LoxP* recombination.

Discussion

To generate mice with *Kdm1a* deleted in the germline, we crossed floxed *Kdm1a* mice to *Vasa-Cre* transgenic mice (Gallardo et al., 2007; Wang et al., 2007). In the initial F1 cross, *LoxP* sites recombined with high efficiency. However, upon backcrossing to generate germline homozygous deleted mice, we found that the efficiency of *LoxP* recombination on the remaining floxed allele was dramatically reduced. This reduction was not caused by silencing of the *Vasa-Cre* transgene, as CRE remained robustly expressed in mice where the *LoxP* sites failed to recombine. This suggests that the *LoxP* sites themselves are becoming silenced. In addition, the decrease in recombination efficiency is specific to *Vasa-Cre,* as normal recombination is observed with both *Zp3-Cre* and *Gdf9-Cre* (Ancelin et al., 2016; Wasson et al., 2016). Since the inhibition of *LoxP* recombination in the F2 germline only occurs after initial exposure to VASA-CRE, we conclude that it is dependent upon germline exposure to CRE in the F1 animals. Thus, initial exposure to CRE must trigger an alteration, either in the chromatin itself or in the associated cellular environment, which can be propagated through sperm to the next generation. In the subsequent F2 animals, this alteration can then inhibit the

floxed *Kdm1a* allele on the homologous chromosome from efficient recombination. Therefore we conclude, as was previously concluded for *Sycp1*, that the inhibition of *LoxP* recombination occurs via a transvection event. This second example of *Cre*-initiated transvection reinforces the conclusion that certain meiotically expressed *Cre* alleles can initiate transvection in mammals.

Since transvection can be initiated by two different *Cre* transgenes that are expressed during meiosis, it is tempting to hypothesize that the phenomenon is triggered by *LoxP* recombination specifically during meiosis. However, in our crosses, recombination first occurs in the early embryo, rather than during meiosis, due to maternally-inherited CRE from the F0 mother. Therefore, we propose that transvection in our crosses may be triggered by CRE protein binding to the already deleted *LoxP* site during meiosis, rather than by meiotic *LoxP* recombination. It is possible that binding of ectopic CRE recombinase to DNA during meiosis, and/or the recombinase trying repeatedly to initiate a double stranded break, could trigger a surveillance mechanism targeted to DNA damage or foreign elements.

There are two prevailing models for the mechanism of transvection. The first theorizes that transvection occurs during via a physical interaction between the homologous chromosomes when they are paired during meiosis. The second invokes a molecule able to freely diffuse between the homologous chromosomes. Thus far, the only two examples of *Cre*-initiated transvection occur in animals expressing *Cre* during meiosis. These observations seem to be consistent with a model where that transvection requires a close physical interaction between chromosomes. However, the floxed *Kdm1a* allele in our F2 original cross mice is blocked from recombining via a

transvection event that must occur prior to the onset of *Vasa-Cre* expression. Otherwise, the floxed *Kdm1a* allele would presumably recombine with full efficiency. In male mice, expression of *Vasa-Cre* begins at embryonic day 18 with full deletion obtained before birth (Gallardo et al., 2007). Surprisingly, this expression is much earlier than the onset of meiosis in males, which occurs after birth (Bowles and Koopman, 2007). This suggests that the *Kdm1a* transvection occurs in germ cells before birth, arguing against a simple model where it occurs via physical interaction during meiosis.

If *Cre*-mediated transvection does not require the physical association of the floxed and deleted alleles, it is possible that a freely diffusible molecule allows for communication between chromosomes *in trans*. If such a molecule is generated during the initial *LoxP* recombination in the F1 germline, it could be packaged into sperm and target the remaining floxed allele on the homologous chromosome for silencing in the embryo following fertilization. To test this possibility, we performed the F1 extra cross. Remarkably, this extra cross completely restored recombination efficiency, raising the possibility that a diffusible molecule could be propagated through sperm in our crosses. Based on previous evidence from the *kit* locus in mice, we wondered whether this diffusible molecule could be a specific RNA (Rassoulzadegan et al., 2006). However, we fail to detect any RNAs selectively present in the original cross sperm that could specifically target the *LoxP* sites. Thus, our data fail to support a model in which transvection is initiated by an RNA corresponding to the *LoxP* recognition site.

Although we still do not know the mechanism of mammalian transvection, our data nevertheless provide significant insight. We propose that the binding of CRE recombinase protein to the *LoxP* recognition site during meiosis triggers an alteration

that can be propagated through sperm to initiate transvection in the resulting embryo. It is possible that this alteration could be a type of histone modification (Brykczynska et al.; Hammoud et al., 2009), or an unknown molecule. Regardless, the alteration must then be maintained throughout embryonic development into the germline, where it initiates the transvection event that blocks the recombination of the *LoxP* sites on the homologous chromosome. Furthermore, this silencing of the *LoxP* sites must occur in germ cells prior to the expression of *Vasa-Cre* at birth, well before the onset of meiosis. Intriguingly, the ICRs of imprinted loci have recently been shown to initiate a transvection event in pre-meiotic germ cells (Sandhu et al., 2009). Based on this example, we speculate that CRE initiated transvection may also occur in pre-meiotic germ cells, either via a physical interaction or a freely diffusible molecule. However, we find that adding an extra cross eliminates the *Kdm1a* transvection. This suggests that any alteration propagated through sperm to initiate transvection is not stable enough to be maintained through a subsequent generation. Thus, the alteration may be reprogrammed in the germline, to prevent it from being passed on to future generations.

Our data also provide mechanistic insight into the mechanism of *LoxP* silencing. In the previous case of meiotic *Cre*-initiated transvection, it was concluded that DNA methylation inhibits *LoxP* recombination (Rassoulzadegan et al., 2002). Our results, both *in vivo* and *in vitro,* directly contradict this conclusion. It is possible that these two observations are mechanistically unrelated. However, since both cases involve the silencing of *LoxP* recombination via a transvection event when *Cre* is meiotically expressed, we favor the idea that these phenomena are related. If this is the case, the

observed acquisition of DNA methylation in the case of *Sycp-1* may have been correlative rather than causative (Rassoulzadegan et al., 2002).

Importantly, we find that adding an extra generation between the F1 and F2 generations completely eliminates silencing, despite the fact that that both crosses were performed with animals that are genetically identical at the floxed locus. This finding leads to three new insights. First, the fact that parental history, rather than genotype, determines the outcome strongly suggests that inhibition of *LoxP* recombination is an epigenetic phenomenon. Second, our results provide a roadmap for the use of other meiotic *Cre* transgenes that may be associated with similar *LoxP* silencing. Although we are aware of only one additional published example of meiotic *Cre* initiated transvection (Rassoulzadegan et al., 2002), personal communications indicate other likely examples of meiotic *Cre*-initiated *LoxP* silencing. The data presented here suggest that the simple addition of an extra cross could enable efficient use of these meiotically expressed *Cre* transgenes. Finally, by uncovering a system where the simple addition of an extra cross completely eliminates transvection, we have established an important *in vivo* mouse model that can be used to elucidate the mechanism of transvection in mammals.

Materials and Methods

Animal husbandry and ethics statement

The following mouse strains were used: *Kdm1a/Lsd1* floxed allele (Wang et al., 2007), *Vasa-Cre* (Gallardo et al., 2007) and *Arl13b* floxed allele (Su et al., 2012). The strains were obtained directly from the Rosenfeld, Castrillon and Caspary labs. Genotyping primers are listed in Table 1. All mouse work was performed under protocols approved by the Emory University Institutional Animal Care and Use Committee.

Testis Immunostaining

Dissected testes were fixed for 105 minutes at 4°C in 4% paraformaldehyde, washed in 1x PBS for 2 hours, then transferred to a 30% sucrose solution overnight at 4°C. The tissue was then embedded in OCT compound (Tissue-Tek). 10µm sections were incubated in a humidified chamber with anti-mouse CRE antibody (Sigma Aldrich C7988) diluted to 1:500 in 1x PBS, 1% heat-inactivated goat serum (Invitrogen 16210072) and 0.5% Triton X-100 overnight at 4°C, and then in secondary goat anti-mouse antibody (Invitrogen A11001 used at 1:500) at room temperature for 2 hours. Slides were then washed in 1x PBS three times and mounted in ProLong antifade (Molecular Probes).

Bisulfite analysis

Bisulfite conversion was performed using 400ng of either tail or testis DNA using the EZ Methylation Kit (Zymogen). Following bisulfite conversion, the samples were amplified

using the primers listed in Table 1 and TA cloned (Invitrogen 450040) for sequencing. BiQ Analyzer was used to analyze bisulfite sequencing data (Bock et al., 2005).

Electropheretic mobility shift assay (EMSA)

34bp loxP oligonucleotides were ordered from Integrated DNA Technologies (either methylated or unmethylated at both CpG residues), labeled with T4 polynucleotide kinase (M0201S), and annealed. Probe sequences are listed in Table 1. All probes were purified in 5% acrylamide gels. Mobility shift reactions were carried out in 30ul at room temperature for 30 minutes in CRE buffer (NEB) with 20,000 cpm radiolabelled DNA, 0.15 ug/ul poly(dI:dC) and 1 unit of CRE protein (NEB). Reaction mixtures were analyzed without loading dye on 1.5mm thick 5% acrylamide gels in 1/4XTBE.

Next generation sequencing

Sperm from male mice was collected from the cauda epidydimis from both the original cross F1 or the extra cross F1. Four independent samples were collected (two for each cross). RNA was extracted from each sperm sample using Trizol and the samples were treated as biological replicates. Between 250 to 1500 ng of RNA were used to prepare small RNA libraries using the TruSeq Small RNA Sample Prep kit according to manufacturer's instructions (Illumina).

Small RNA libraries were clipped using FASTX Toolkit version 0.0.13, and reads longer than 18 nucleotides after clipping were mapped to the mouse genome (mm10) using Bowtie 1.1.2 (allowing up to one mismatch). Reads mapping to the genome were then mapped sequentially to a series of FASTA files containing rRNAs (Ensembl),

miRNAs (hairpin from miRBase), tRNAs (GtRNA db), repeats (Repbase), piRNA clusters (Li et al., 2013) and Refseq (NCBI). To identify potential small RNAs targeting the LoxP site or its immediate surroundings, all reads over 18 nucleotides after clipping were mapped using Bowtie (1 mismatch allowed) to the floxed *Kdm1a* allele. Coverage plots for the floxed *Kdm1a* and for tRNAs were then produced using BEDTools v2.24.0-33 (Quinlan and Hall, 2010)and plotted using R (R Core Team, 2013).

Data availability

All strains and reagents are available upon request. Gene expression data have been deposited into the Gene Expression Omnibus with accession number TBD. File S1 contains all supplemental figure legends. File S2 contains Supplemental Figure 1. File S3 contains Supplemental Figure 2. File S4 contains Table 1 with EMSA and bisulfite primer sequences.

Acknowledgements

We would like to thank S. Kerr, A. Simon and other members of the Katz lab for helpful discussions on the work and the manuscript. Thank you to T. Caspary for providing the *Arl13* floxed mice, M. Rosenfeld for providing the *Lsd1* floxed mice and D. Castrillon for providing the *Vasa-Cre* mice. D. Myrick and J. Rodriguez were members of the PREP post-baccalaureate program (5R25GM089615-04). M. Christopher was supported by the GMB training grant (T32GM008490-21). T. Lee is supported by the Fellowships in Research and Science Teaching IRACDA postdoctoral program (K12GM00680-16).

The work was supported by a grant to D. Katz from the National Science Foundation (IOS1354998).

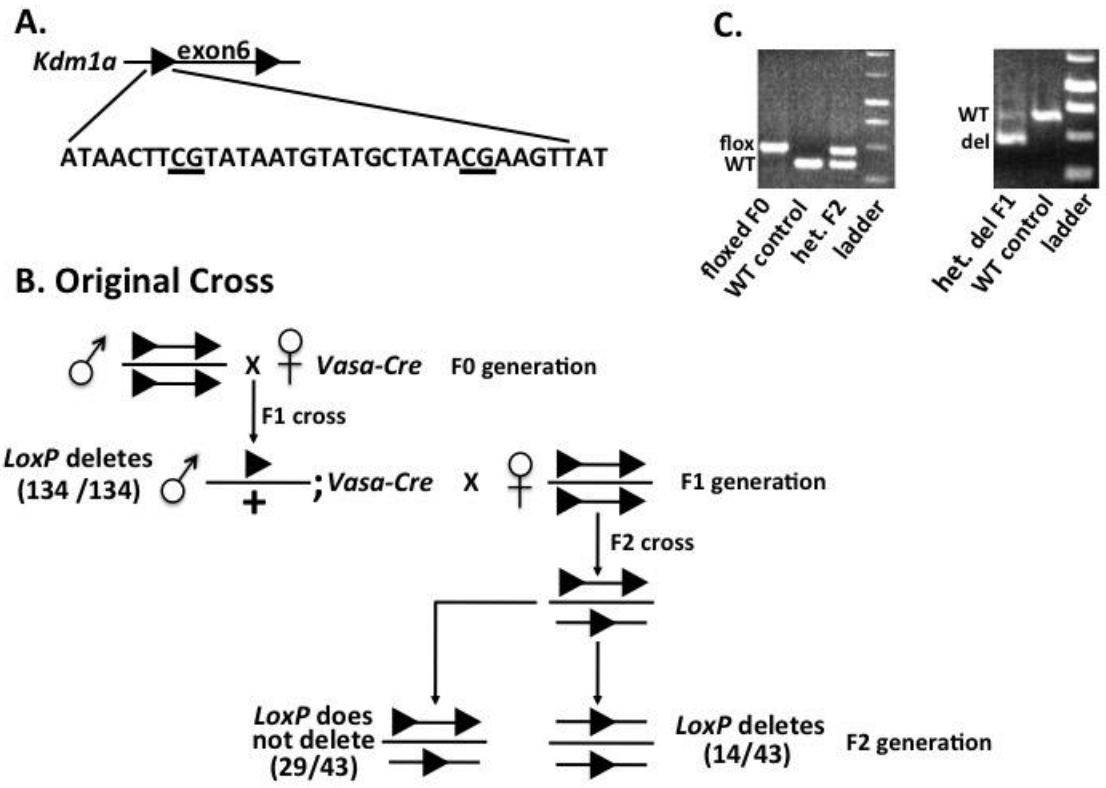

Figure 1. Inhibition of *LoxP* recombination during second passage through the germline. **(A)** Diagram of the floxed *Kdm1a* locus. The two CpG residues in the 34bp *LoxP* recognition sequence are underlined. **(B)** Diagram of the cross used to generate germline *Kdm1a* conditional knockout mice. In F1 mice the floxed *Kdm1a* locus deletes with 100% efficiency. However, in F2 mice the *LoxP* sites are largely inhibited from recombining. **(C)** Sample genotyping showing the ability to distinguish all possible genotypes during the crosses.

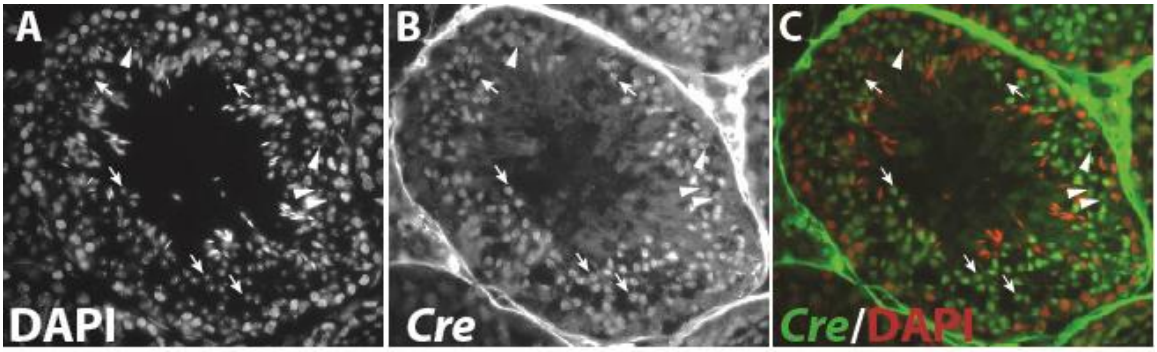

Figure 2. The expression of CRE in inhibited F2 testes. DAPI **(A)**, *Vasa-Cre* **(B)**, and merge **(C).** *Vasa-Cre* is still expressed in spermatocytes (arrowheads) and spermatids (arrows) of F2 testes that fail to recombine.

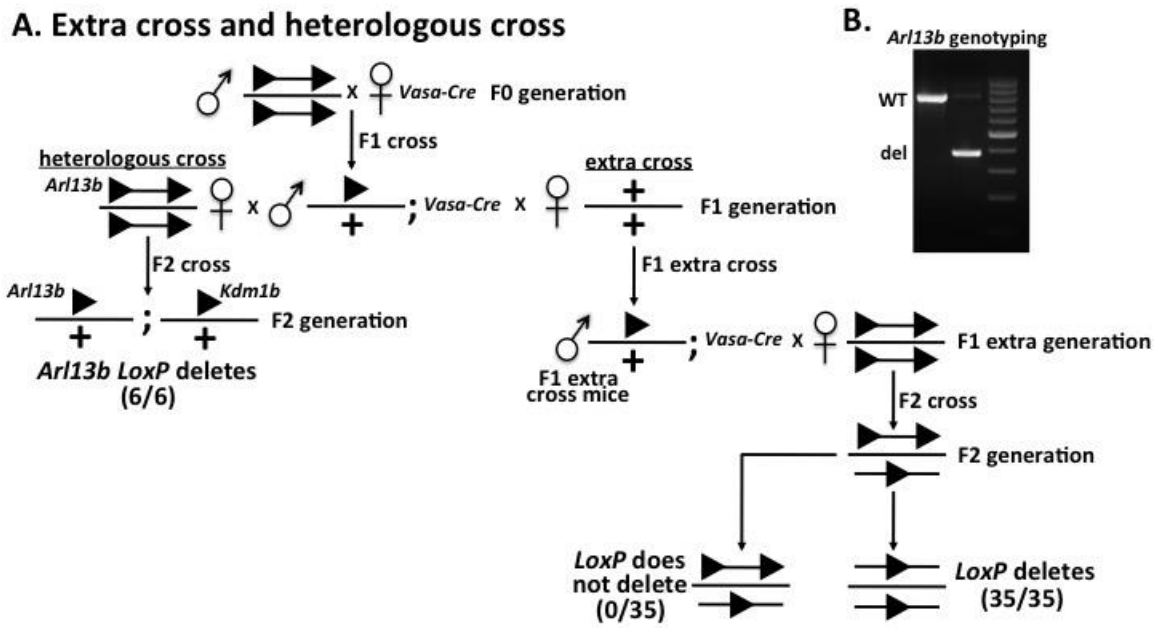

Figure 3. (A) Diagram of the extra cross and heterologous cross. As in the original cross (Figure 1), floxed *Kdm1a* mice are initially crossed to *Vasa-Cre* to generate F1 heterozygotes. However, unlike in the original cross, the F1 heterozygotes are subsequently crossed to WT to generate F1 extra cross mice. These mice are genotypically identical to the original cross F1 mice, but differ in their parental history. Upon backcrossing to the floxed mice, the F2 progeny of these extra cross F1 mice now recombine with 100% efficiency. Alternatively, F1 heterozygotes are crossed to floxed *Arl13b* mice (heterologous cross). In the heterologous cross, the *LoxP* sequences recombine with 100% efficiency. **(B)** Sample genotyping showing the ability to distinguish *Arl13b* genotypes.

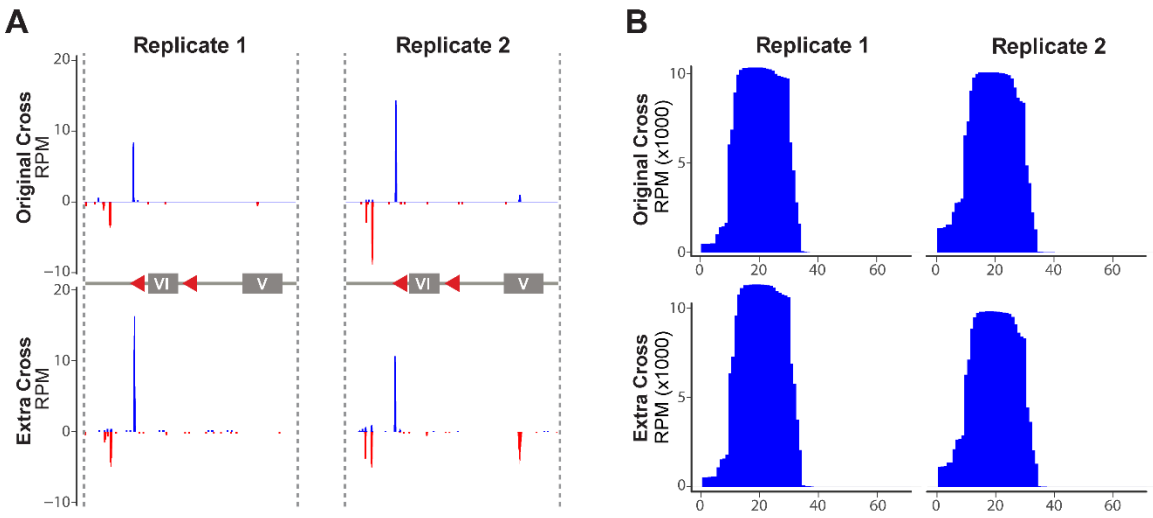

Figure 4. Sperm small RNAs do not target *LoxP* sites. **(A)** Coverage plots of *LoxP* sites (red arrows) flanking exon 6 in *Kdm1a*, showing very few reads mapping to the *Kdm1a* floxed locus and no difference between F1 original cross sperm (top) and F1 extra cross sperm (bottom) in two biological replicates. The *LoxP* sites are intended to show the relative position, and are not drawn to scale. Plus strand is shown in blue and minus strand is shown in red. **(B)** For comparison, coverage plots of the plus strand (blue) of *tRNA-Gly-GCC-5-1* are shown for the same libraries.

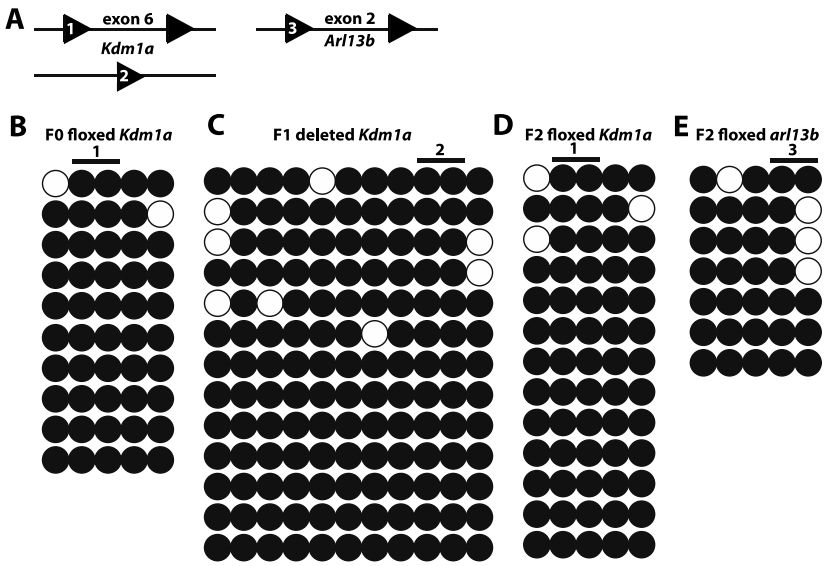

Figure 5. Bisulfite DNA methylation analysis of the *LoxP* recognition site. **(A)** Diagram depicting the *LoxP* site that was analyzed from the *Kdm1a* floxed allele (marked with 1), the *Kdm1a* deleted allele (marked with 2) and the *Arl13b* floxed allele (marked with 3). *In vivo* bisulfite analysis of the two CpG dinucleotides in the *LoxP* recognition sequence (denoted by the line above), as well as CpG residues from the flanking region, in the F0 floxed allele prior to recombination **(B)**, the F1 deleted allele after recombination **(C)**, the F2 floxed allele that does not recombine **(D)**, and the F2 *Arl13b* floxed allele **(E)**.

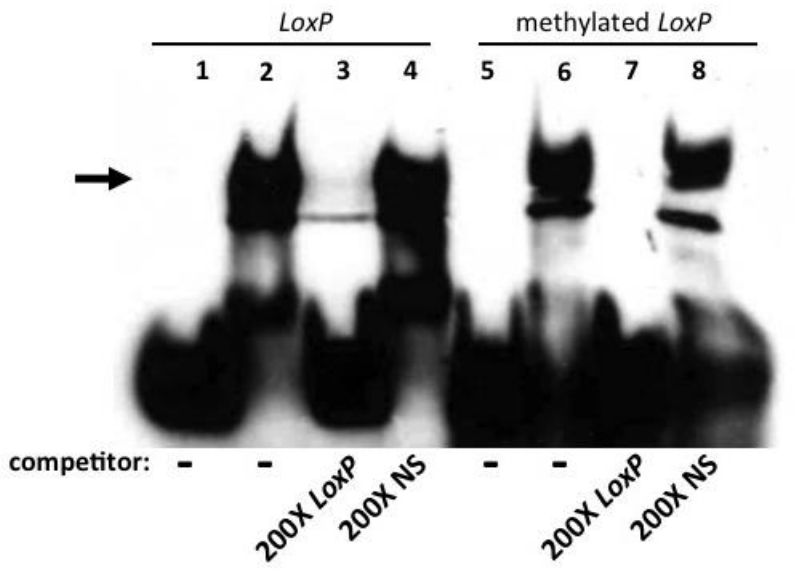

Figure 6. Binding of CRE to the *LoxP* recognition sequence. Electrophoresis mobility shift assays with the unmethylated *LoxP* recognition sequence (lanes 1-4) and the fully methylated *LoxP* site (lanes 5-8) bound to recombinant CRE protein (lanes 2-4 and 6-8) or with probe alone (lanes 1 and 5). The retarded mobility shift complex is indicated by the black arrow to the left. In lanes 3 and 7, the retarded mobility shift complex has been competed with 200-fold molar excess of specific *LoxP* competitor probe, while in lanes 4 and 8, the retarded mobility shift complex has been competed with non-specific (NS) competitor.

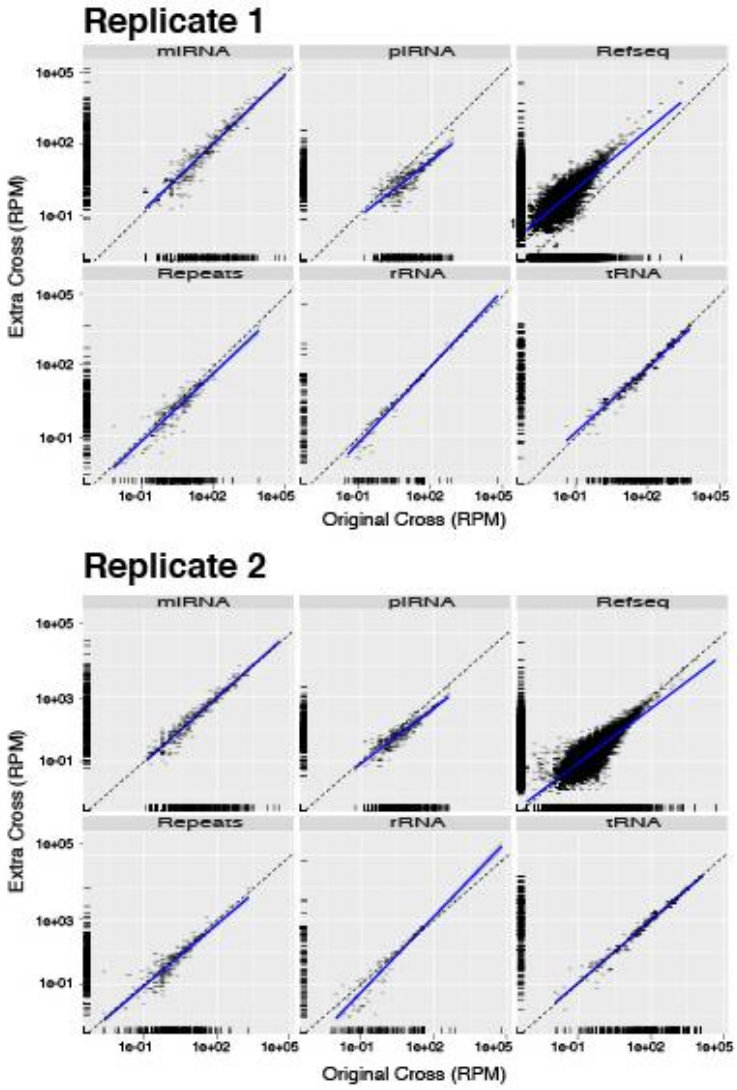

Supplemental Figure 1. No small RNA classes are enriched in either original cross or extra cross sperm. Scatter plots from two independent biological replicates comparing transcript levels in F1 extra cross sperm and F1 original cross sperm for the following small RNA gene classes: micro RNA, PIWI-interacting RNA, ribosomal RNA, tRNAs, repeats (transposons and other repetitive sequences), and Refseq (small RNAs that did not map to other categories).

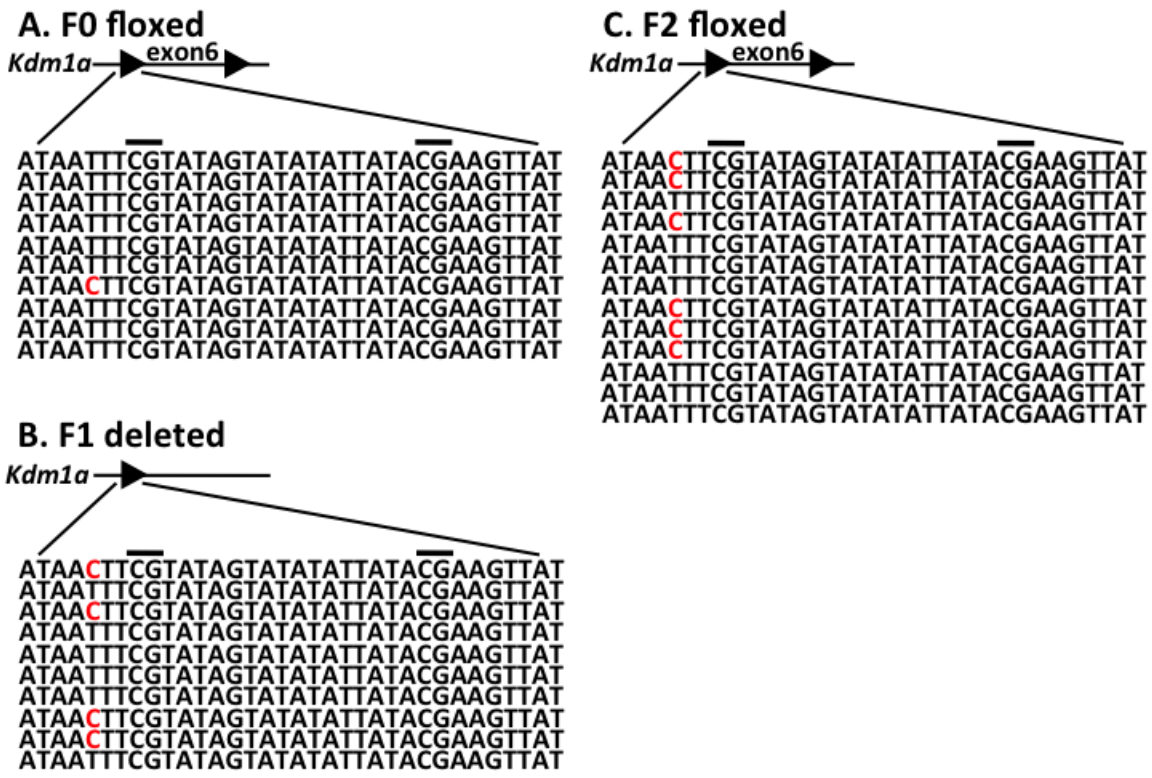

Supplemental Figure 2. Non-CpG methylation of the *LoxP* recognition site. Bisulfite converted sequence from **(A)** the F0 *Kdm1a* floxed allele prior to recombination, **(B)** the F1 *Kdm1a* deleted allele after recombination, and **(C)** the F2 *Kdm1a* floxed allele that does not recombine. The methylated non-CpG cytosine just 5' of the CpG (denoted by the line above) in the *LoxP* site is shown in red. The sequences are depicted in the same order as the lollipop representations in Figure 5.

Table 1

Primer	Sequence	Assay
LoxP sense	5’-ATAACT TCGTATAATGTATGCTATACGAAGTTAT-3’	EMSA
LoxP antisense	5’-ATAACTTCGTATAGCATACATTATACGAAGTTAT-3’	EMSA
LoxP sense methylated(CH3)	5’-ATAACTC(CHE)GTATAATGTATGCTATAC(CH3)GAAGTTAT-3’	EMSA
LoxP antisense methylated (CH3)	5’-ATAACTC(CH3)GTATAGCATACATTATAC(CH3)GAAGTTAT-3’	EMSA
archipelago (ago) promoter NS	5’GGAGGGTGGGAAGAGAATGAATACGAATATGGGAAAATGT 3’	EMSA
KDM1 Bisf Reverse	5’-ACAATTCAATTACTTTCAAACTATAAAAAC-3’	Bisulfite
KDM1 Bisf Forward	5’-AGGGGATTAGTTTGGGTTGT-3’	Bisulfite
KDM1 Del Right	5’-CCATAATTACTAACACCTCAAA-3’	Bisulfite
KDM1 Del Left	5’-TGGTTTATATTGGTATAGTTGTGAAGG-3’	Bisulfite
Arl13b loxp Left	5’-GGGAATTGTATAGGGTTATATTAGGA3’	Bisulfite
Arl13b loxp Right	5’-CAAAACTTTATCAATCCAAACAA-3’	Bisulfite

References

Ancelin, K., Syx, L., Borensztein, M., Ranisavljevic, N., Vassilev, I., Briseno-Roa, L., Liu, T., Metzger, E., Servant, N., Barillot, E.*, et al.* (2016). Maternal LSD1/KDM1A is an essential regulator of chromatin and transcription landscapes during zygotic genome activation. Elife *5*.

Aramayo, R., and Metzenberg, R.L. (1996). Meiotic transvection in fungi. Cell *86*, 103-113.

Arteaga-Vazquez, M.A., and Chandler, V.L. (2010). Paramutation in maize: RNA mediated trans-generational gene silencing. Curr Opin Genet Dev *20*, 156-163.

Bock, C., Reither, S., Mikeska, T., Paulsen, M., Walter, J., and Lengauer, T. (2005). BiQ Analyzer: visualization and quality control for DNA methylation data from bisulfite sequencing. Bioinformatics *21*, 4067-4068.

Bowles, J., and Koopman, P. (2007). Retinoic acid, meiosis and germ cell fate in mammals. Development *134*, 3401-3411.

Brykczynska, U., Hisano, M., Erkek, S., Ramos, L., Oakeley, E.J., Roloff, T.C., Beisel, C., Schubeler, D., Stadler, M.B., and Peters, A.H. Repressive and active histone methylation mark distinct promoters in human and mouse spermatozoa. Nat Struct Mol Biol *17*, 679-687.

Chandler, V.L. (2007). Paramutation: from maize to mice. Cell *128*, 641-645.

Coe, E.H. (1966). The properties, origin, and mechanism of conversion-type inheritance at the B locus in maize. Genetics *53*, 1035-1063.

Gallardo, T., Shirley, L., John, G.B., and Castrillon, D.H. (2007). Generation of a germ cell-specific mouse transgenic Cre line, Vasa-Cre. Genesis *45*, 413-417.

Hammoud, S.S., Nix, D.A., Zhang, H., Purwar, J., Carrell, D.T., and Cairns, B.R. (2009). Distinctive chromatin in human sperm packages genes for embryo development. Nature.

Higginbotham, H., Guo, J., Yokota, Y., Umberger, N.L., Su, C.Y., Li, J., Verma, N., Hirt, J., Ghukasyan, V., Caspary, T.*, et al.* (2013). Arl13b-regulated cilia activities are essential for polarized radial glial scaffold formation. Nat Neurosci *16*, 1000-1007.

Lewis, E.B. (1954). The Theory and Application of a New Method of Detecting Chromosomal Rearrangements in Drosophila-Melanogaster. Am Nat *88*, 225-239.

Li, X.Z., Roy, C.K., Dong, X., Bolcun-Filas, E., Wang, J., Han, B.W., Xu, J., Moore, M.J., Schimenti, J.C., Weng, Z.*, et al.* (2013). An ancient transcription factor initiates the burst of piRNA production during early meiosis in mouse testes. Mol Cell *50*, 67-81.

Quinlan, A.R., and Hall, I.M. (2010). BEDTools: a flexible suite of utilities for comparing genomic features. Bioinformatics *26*, 841-842.

R Core Team (2013). R: A language and environment for statistical computing (Vienna, Austria: R Foundation for Statistical Computing).

Rassoulzadegan, M., Grandjean, V., Gounon, P., Vincent, S., Gillot, I., and Cuzin, F. (2006). RNA-mediated non-mendelian inheritance of an epigenetic change in the mouse. Nature *441*, 469-474.

Rassoulzadegan, M., Magliano, M., and Cuzin, F. (2002). Transvection effects involving DNA methylation during meiosis in the mouse. Embo J *21*, 440-450.

Sandhu, K.S., Shi, C., Sjolinder, M., Zhao, Z., Gondor, A., Liu, L., Tiwari, V.K., Guibert, S., Emilsson, L., Imreh, M.P.*, et al.* (2009). Nonallelic transvection of multiple imprinted

loci is organized by the H19 imprinting control region during germline development. Genes Dev *23*, 2598-2603.
Sauer, B. (1998). Inducible gene targeting in mice using the Cre/lox system. Methods (San Diego, Calif *14*, 381-392.
Su, C.Y., Bay, S.N., Mariani, L.E., Hillman, M.J., and Caspary, T. (2012). Temporal deletion of Arl13b reveals that a mispatterned neural tube corrects cell fate over time. Development *139*, 4062-4071.
Wang, J., Scully, K., Zhu, X., Cai, L., Zhang, J., Prefontaine, G.G., Krones, A., Ohgi, K.A., Zhu, P., Garcia-Bassets, I.*, et al.* (2007). Opposing LSD1 complexes function in developmental gene activation and repression programmes. Nature *446*, 882-887.
Wasson, J.A., Simon, A.K., Myrick, D.A., Wolf, G., Driscoll, S., Pfaff, S.L., Macfarlan, T.S., and Katz, D.J. (2016). Maternally provided LSD1/KDM1A enables the maternal-to-zygotic transition and prevents defects that manifest postnatally. Elife *5*.
Woodhouse, M.R., Freeling, M., and Lisch, D. (2006). Initiation, establishment, and maintenance of heritable MuDR transposon silencing in maize are mediated by distinct factors. PLoS Biol *4*, e339.